Volume Perfussion Index (VPI): Developing a New Tool for Measuring Fetal Blood Flow by using Four Dimensional Ultrasound and Power Doppler Signal

Mathematical modelling of Fetal Cardiac Output in an Experimental Animal model.

Candidate: Juan Carlos Bello Muñoz

DOCTORAL THESIS

UNIVERSITAT AUTONOMA DE BARCELONA

2012

THESIS CO-DIRECTORS

Professor Dr Lluis Cabero Roura.

Professor Dr. Elena Carreras Moratonas

A mis padres
A Alejandra y Andrea, por el sacrificio mas grande

To my parents
To Alejandra and Andrea, for their unsurmontable sacrifice.

Acknoledgements

Author wish to acknowledge :

Mister Mauricio Ayala Sánchez for his continuous teaching on mathematics and physics of the fluids, and also for developing part of the software for image analysis.

Doctor José Luis Peiró for his teaching and help in animal surgery and for generously providing the experimental subjects.

Doctors Francesc Soldado and Francisco Garcia-Fontecha for generously providing experimental subjects from their own projects.

Doctor Marta Rosales from the Animal Warehouse of the Research Institute in Vall d'Hebron Hospital for her support in accessing the facilities.
Doctors Marielle Estevez and Carla Mendes from the Animal Warehouse of the Research Institute in Vall d'Hebron Hospital for her thorough care of the animals involved in the experiment.

Doctor Raul Cruz-Hidalgo from the Applied Physics and Mathematics Dept of the University of Navarra for his help in developing the algorithms

Mister Mariano Sanchez and Mistress Dolores Cantelli from the technical and scientific department of Philips Medizin System for their initial support and for providing us with a iU22 US machine for this experiment

Mister Sun Ho Ko and Miss July Bartholomew from the technical and scientific department of Samsung Medical Co for their irrestrict support and for providing us with a Medison Accuvix V20 Prestige. Mister Juan Carlos Elias and Carme Perramon from the applications development center of Samsung Medical for providing us with unreleased versions of their Sonoview software.

Doctors Paula Oliveros, Nazareth Campo , Gabriel Villagómez, Mauricio Orozco, Francisco Villanueva and John Freddy Plata, for their cooperation in collecting the first normal fetuses.

Mister George Chilton for his thorough review of the english version of this work.

Abstract

Aims

Primary aim: To develop a tool for measuring fetal flow and perfussion by Spatio- time correlation (4D) and power Doppler signal.

Secondary aim: To test and calibrate the designed tool in a well controled animal (sheep) model

Methods: Mathematical modelling of a vectorial velocity color signal displacement algorithm. Experimental measurement of the algorithm by comparing it to known flow profiles in vitro by designing a phantom model of pulsatile flow and in-vivo by comparing obtained values to actual measurements obtained, by invasive methods, from fetal aortic arch in eight term pregnant sheep. Acquisition of 4D volume datasets with offline analysis of color signal by using the already validated Vascularization Flow Index (VFI)® and the newly designed Volume Perfusion Index (VPI). Comparison of both methods in terms of repeatability and accuracy, in-vitro as well as in-vivo.

Results: When tested in-vitro, both techniques showed a good repeatability. Intra-Observer Intraclass Correlation Coefficient (ICC; 95% CI) was similar for VPI (0.95; 0.91-0.99) and VFI (0.9; 0.88-0.92). Inter-Observer ICC was also alike for VPI (0.90; 0.87-0.99) and VFI (0.88; 0.84-0.91). When plotting VPI against actual flow calculation the Pearson's correlation Index (95% CI) was 0.88 (0.58-0.97) for VPI and 0.34 (0.31-0.44) for VFI. When tested in-vivo the VPI exhibited an Intra-Observer ICC(95% CI) of 0.9(0.88-0.99) and the VFI 0.79(0.75-0.92); and an Inter-Observer ICC (955 CI) of 0.88 (0.87-0.99) for VPI and 0.78 (0.74-0.91) for VFI.

The flow measurement in the animal model correlated significantly better in VPI than in VFI with a Perason's Correlation Index (95% CI) of 0.88(0.58-0.97) Vs -0.34 (-0.31-0.44). $p < 0.001$

Conclusion The Volume Perfusion Index exhibits a more robust correlation with actual flow than the currently used Vazcularization Flow Index and further work and investment in this direction is clearly justified

Resumen

Objetivos

Objetivo principal: Desarrollar una herramienta para medir el flujo y perfusión fetales, mediante el uso de ecografía tridimensional en tiempo real por correlación espacio-tiempo (4D) y el uso de la señal power-Doppler.

Objetivo secundario: evaluar y calibrar la herramienta diseñada en un modelo animal bien controlado (ovino).

Métodos: Modelación matemática de un algoritmo de la velocidad de desplazamiento de color vectorial de la señal de color. Medida experimental del algoritmo al compararlo con los perfiles de flujo conocidos in vitro mediante el diseño de un modelo fantasma de flujo pulsátil e in vivo, mediante la comparación de los valores obtenidos con las mediciones reales obtenidas por métodos invasivos, desde el arco aórtico fetal en ocho ovejas gestantes plazo. La adquisición de bases de datos 4D de volumen en línea con el análisis de la señal de color mediante el índice de vascularización de flujo ya validado (VFI), ® y el Índice de Volumen de perfusión, diseñado por nuestro equipo (VPI). La comparación de ambos métodos en términos de replicabilidad y precisión, in vitro, así como in vivo.

Resultados: Durante el ensayo in vitro, ambas técnicas mostraron una buena capacidad de repetición. Intra-observador coeficiente de correlación intraclase (ICC, IC 95%) fue similar para VPI (0,95; 0,91 a 0.99) y VFI (0,9; 0,88 a 0.92). Inter-observador CCI también fue igual para VPI (0,90; 0,87 a 0,99) y VFI (0,88; 0,84 a 0,91). Al trazar VPI contra la corriente real de cálculo Índice de correlación de Pearson (95% IC) fue de 0,88 (.58 a .97) para VPI y 0,34 (0,31-0,44) para la VFI. Cuando la prueba in vivo el VPI exhibió una Corte Penal Internacional intra-observador (95% IC) de 0.9 (0.88-0.99) y la VFI 0,79 (0,75 a 0,92), y una Corte Penal Inter-observador (955 CI) de 0,88 (0,87- 0,99) para VPI y 0.78 (0.74 a 0.91) para la VFI.

La medición de flujo en el modelo animal se correlacionó significativamente mejor en VPI que en VFI con un índice de correlación de Pearson (95% IC) de 0.88 (0.58-0.97) vs -0,34 (-0,31 hasta 0,44). p <0,001.

Conclusión El VPI muestra una correlación más fuerte con el flujo sanguíneo fetal real que el VFI, actualmente en uso, y futuros trabajos e inversión en este sentido están claramente justificados.

Prologue

Measuring Fetal Blood flow has been always an elusive matter. Diverse attempts to represent this physiological phenomenon have been done in the last thirty years without achieving an acceptable accuracy. The weakest point in the previous assays relies on the limited clinical utility of the techniques employed. When using pulsed Doppler and two dimension ultrasound, the repeatability of the measurement was low indeed and the technical skills required from the expert taking the measurements were extremely high,

Previous reports have pointed to the potential of two dimensional power Doppler signal and some research teams developed the so-called Fractional Moving Blood Volume (FMBV) algorithm. Its representation of moving particles and its quite acceptable repeatability made this tool a promising opportunity for approaching to circulatory changes in the fetus, at least in the regional vascularity during a given situation. Nevertheless, the limited information provided by two dimensional still images made the limitations of the tool prohibitive as for being considered as a clinical application. Similar limitations were found when using three-dimensional ultrasound and power Doppler. Several Indexes were designed and validated as true representations of both, vascularization and flow. However, any attempt to give a clinical meaning to these measurements has been unsuccessful.

The main limitation to al those previous uses of the power Doppler signal ahs been the impossibility of a signal normalization process. In the case of FMBV, it has been described something alike, but the essential limitations under the image caption made the process inefficient and the individual variability of the registers an insurmountable boundary for this tool. In the case of 3D indexes, there is simply no way for a signal

normalization. Therefore the individual variability is so wide than even few seconds between one caption and the next in the same patient can vary dramatically. Also, as we have tested and mentioned in the present thesis, these indexes vary in a remarkable way, when using different machines in the same patient and clinical conditions.

This is a new attempt focused mainly in using a frame sequence as the base for a normalization process, assuring that small variations in the signal process become less important and true variations in the signal intensity could be reliably registered. In the next pages, the author pretends to probe how this variation in the register and interpretation of the signal might be a breakthrough in the non invasive study of physiological and pathological conditions of the fetal circulation.

Index

Pàg.

List of figures

List of equations

List of tables

Chapter 1. Background of the tool

1.1 Three Dimensional Ultrasound and Power Doppler

Three-dimensional Ultrasound (3DUS) has grown quick and constantly for the last fifteen years. These notwithstanding, some of their clinical uses remain, in best of cases, to define. Three-dimensional Power Doppler (PD) is based in both, its ability for registering the signal amplitude of the ultrasound wave, which allows depicting most of moving particles in a given Region of Interest (ROI) and the three-dimensional US principles, which allow collecting signal from such particles in a given Volume of Interest (VOI). The addition of a time sequence or a Space-Time Image correlation (STIC) algorithm developed and made available by some US machines add the additional possibility of following the signal evolution during a pre-established lap. At the beginning, this promising tool was used to evaluate vascularisation and perfusion in a series of foetal organs, finding neither adequate accuracy nor repeatability. Nowadays, its use is seriously restricted to certain foetal conditions but new research on this topic is ongoing and further uses for this technology are being unveiled.

As largely known (Burns 1992), there are compelling scientific and medical reasons to seek measuring the volumetric flow rate, which means to estimate the volume of flow delivered per minute to a tissue bed. No

doubt, the success in delivering oxygen and nutrients to the tissues depends, mainly, on the amount of blood delivered to such tissues per unit of time. At the beginning of the Doppler ultrasound era, a number of attempts for achieving this calculation were done (Gill 1979; Eik-Nes et al. 1982; Sauders et al. 1980). The standard method for estimating volume flow using sonography consisted of multiplying the mean spatial velocity by the luminal cross-sectional area. However, it is well known that this technique has many problems. These include inherent variability of vessel geometry, assumptions about flow profile, 1-dimensional sampling, and other important technical limitations derived from the way pulsed and spectral Doppler signal are registered, and an unsustainable amount of human interaction in the final estimation (J M Rubin 1999). All of that made those efforts to fail and lead this pretension to be forsaken for two decades.

Then, it was described the experimental analysis of the Doppler Effect altogether –taking into account the amplitude of the wave- and tracking the acoustic speckle pattern produced by the echoes from moving blood (J M Rubin et al. 1994; Forsberg et al. 1995; Harrington et al. 1996; J M Rubin 1999). From those initial approaches, it was developed the concept of Fractional Moving Blood Volume (FMBV) (J M Rubin et al. 1997) which was mainly a mathematical normalization process of the colour pattern

obtained from the power Doppler signal acquisition (Tomas Jansson et al. 2003; A Welsh 2004). Preliminary publications established a direct relationship between the data from FMBV acquired by registering the power Doppler signal in a given Region of Interest (ROI) and actual perfusion of the tissue as measured by invasive methods in animal models (E Hernandez-Andrade, T Jansson, et al. 2004; E Hernandez-Andrade, Thuring-Jönsson, et al. 2004). Recently, it has described how, in certain pathological fetal conditions such as fetal growth restriction, some perfusion patterns are objectively altered and significantly differ from "normal" patterns established by the authors (E Hernandez-Andrade et al. 2008; Rogelio Cruz-Martinez et al. 2009; R Cruz-Martinez, F Figueras, E Hernandez-Andrade, et al. 2011).

Nonetheless, there are still enormous gaps between the information obtained by FMBV and real estimations of either flow or perfusion (A Welsh 2004; Lai et al. 2010). Frontiers that will limit insurmountably the utility of this technique, such as the low repeatability when comparing one patient with the same in a better acquisition setting or one patient with difficulties for exploration like obese or anxious mothers to a normal one. Additionally, it will be impossible to relate such magnitudes with flow when there is no time frame considered in the image quantification process (A. W. Welsh et al. 2005; Aw Welsh et al. 2012).

No additional experience in this technique has been published and very likely it will not in the future. The next logical step would be to evaluate the possibilities of three dimensional ultrasound and power Doppler as an alternative approach to this phenomenon(Lai et al. 2010; Heck et al. 2012).

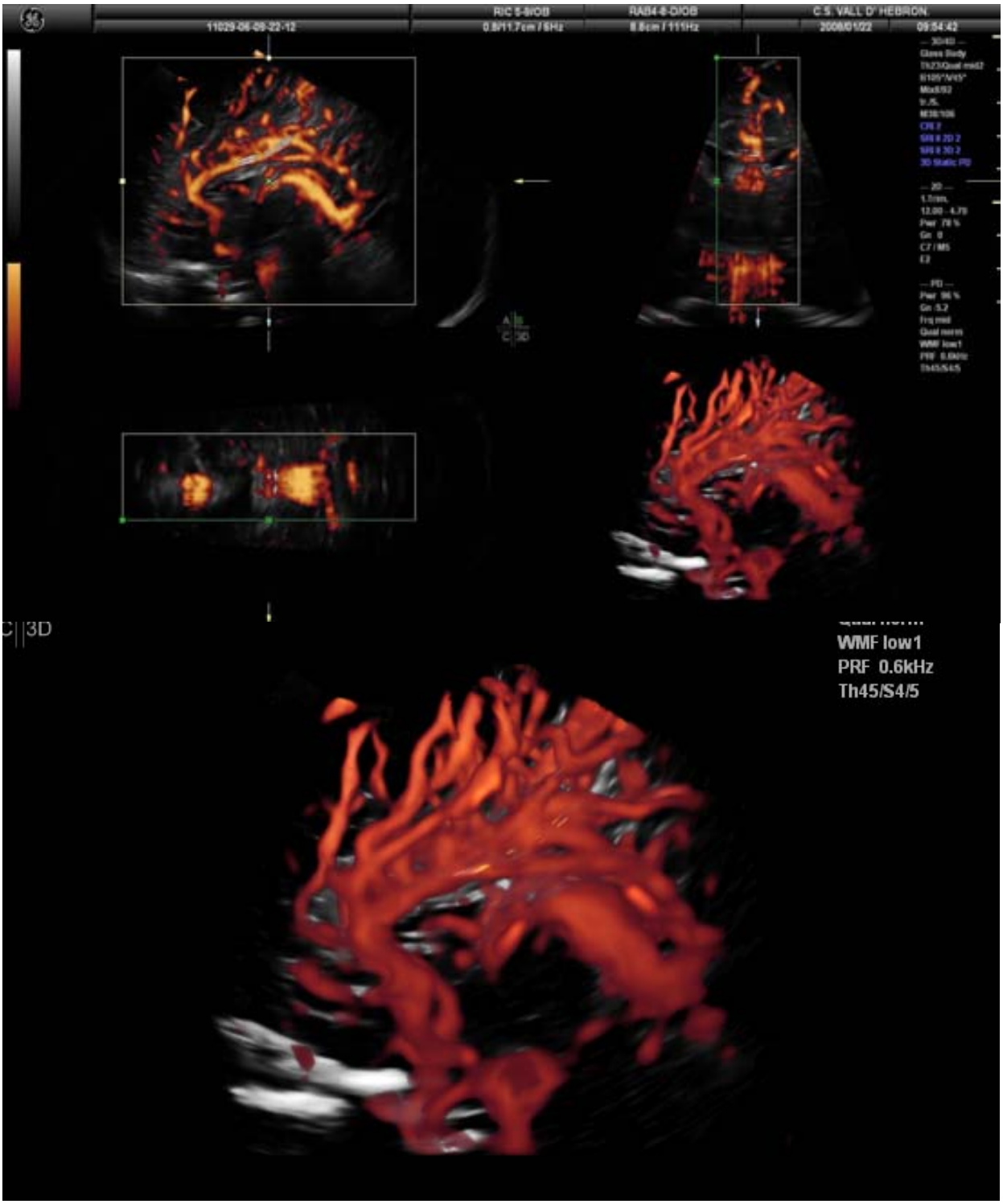

Fig. 1. Three dimensional PD angio mode rendering of intracranial blood vascularisation in a term fetus

1.2. Three-dimensional power Doppler signal and the vascular indexes

Three-dimensional power Doppler (PD) became available for medical purposes towards the end of the last century (Fenster et al. 1998; Z. Guo et al. 1998). Its advantages, considering the higher sensitivity of the PD for detecting, and therefore depicting, moving particles, its first use was to evaluate vascularisation in compromised regions, trying to elucidate whether there was an obstruction or not in a given vessel (Z. Guo & Fenster 1996). Considering its potential for depicting accurately vascular structure, it was employed as a tool for measuring potentially angiogenic structures as tumours (Bendick et al. 1998; Kupesic & Kurjak 2000). Also its potential for depicting vascular architecture and potential anomalies has been considered as promising (Fig 1) (Heling et al. 2000; Chaoui & Kalache 2001)

Nevertheless, the information given by this technique was rather limited, considering there was no quantification of the signal and no objective measurements would be done. Then, it was developed a mathematical algorithm, firstly used in gynecology, by the way(J M Rubin 1999; Pairleitner et al. 1999); based on the possibility of a direct correlation between PD signal intensity and, somehow, the velocity of the particles

and the possible quantification of moving particles in a Volume of Interest (VOI) over the amount of grayscale, B-mode, particles in the same VOI. It were developed three indexes which, indirectly, could give a mathematical expression of vascularisation and flow:

*Vascularization index (VI) = color voxels/(total voxels − background voxels)

$$VI = \frac{\sum_{c=1}^{100} hc(c)}{\sum_{g=1}^{100} hg(g) + \sum_{c=1}^{100} hc(c)} \quad (1)$$

Where g= gray-scale value in the US image, normalized to 0-100: lowest intensity= 1; highest = 100

c= color value in the US image from power Doppler signal representation. Normalized to 0-100: lowest intensity= 1; highest = 100

hg(x) = frequency of gray-value x in US image

hc(x) = frequency of color value x in US image

*Flow index (FI) = weighted color voxels/color voxels

$$FI = \frac{\sum_{c=1}^{100} c \cdot hc(c)}{\sum_{c=1}^{100} hc(c)} \quad (2)$$

*Vascularization–flow index 1 (VFI) = weighted color voxels/(total voxels ˜ background voxels)

$$VFI = \frac{\sum_{c=1}^{100} c \cdot hc(c)}{\sum_{g=1}^{100} hg(g) + \sum_{c=1}^{100} hc(c)} \quad (3)$$

Based on the above mentioned indexes, a number of research communications have been produced, evaluating the vascularity of benign versus malign ovarian (Kurjak et al. 1998; Juan Luis Alcázar & Jurado 2011) and prostatic (Moskalik et al. 2001) masses. Regarding the feto-placental unit, several attempts to correlate those indexes with regional perfusion of brain (Hayashi et al. 1998; Nardozza et al. 2009), liver (C.-H. Chang et al. 2003), lungs in normal (Dubiel et al. 2005) as well as pathologic conditions (Ruano et al. 2006). However, the clinical efficacy of this method remains unsupported by the evidence. No clinical estimations can be done from those values so far. (Fig 2)

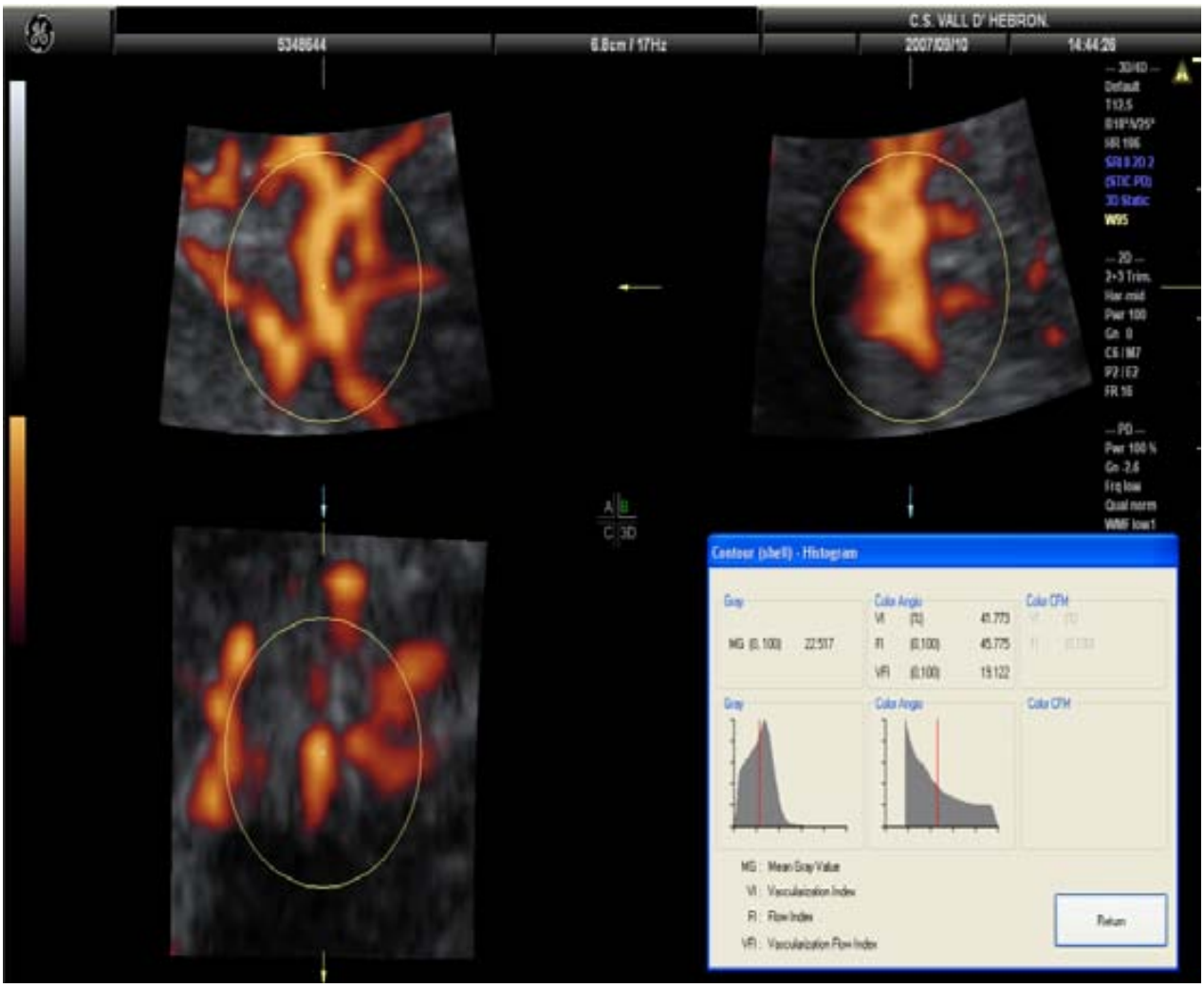

Fig. 2. Three dimensional PD angio mode rendering of intracranial blood vascularisation in a mid-trimester fetus with suspected brain sparing. In the right lower corner it is possible to visualize the histogram with the indexes obtained from the spehere-VOI

A promising field, still open to research is the analysis of placental vasculature and its potential relationship to placental dysfunction (Nia W Jones et al. 2011). Some authors have found a positive correlation between low vascularisation indexes in early pregnancy and Fetal Growth Restriction (FGR) (Bozkurt et al. 2010; Dar et al. 2010; Guimarães Filho et al. 2011; Morel et al. 2010; Negrini et al. 2011; A. O. Odibo et al. 2011; Pomorski et al. 2011; Rizzo et al. 2009). It seems that the evaluation of first trimester placental vascularisation correlates, somehow, with a compromised placentation and therefore could predict some adverse perinatal outcomes of placental origin. Besides, the technique exhibits quite a good repeatability and accuracy (Tuuli et al. 2010; Martins & N J Raine-Fenning 2010; Yigiter et al. 2011).

The challenges for the future go through overcoming some of the technical problems three dimensional PD is plagued with and to establish an adequate normalisation protocol, which is lacking nowadays. (Figure 3)

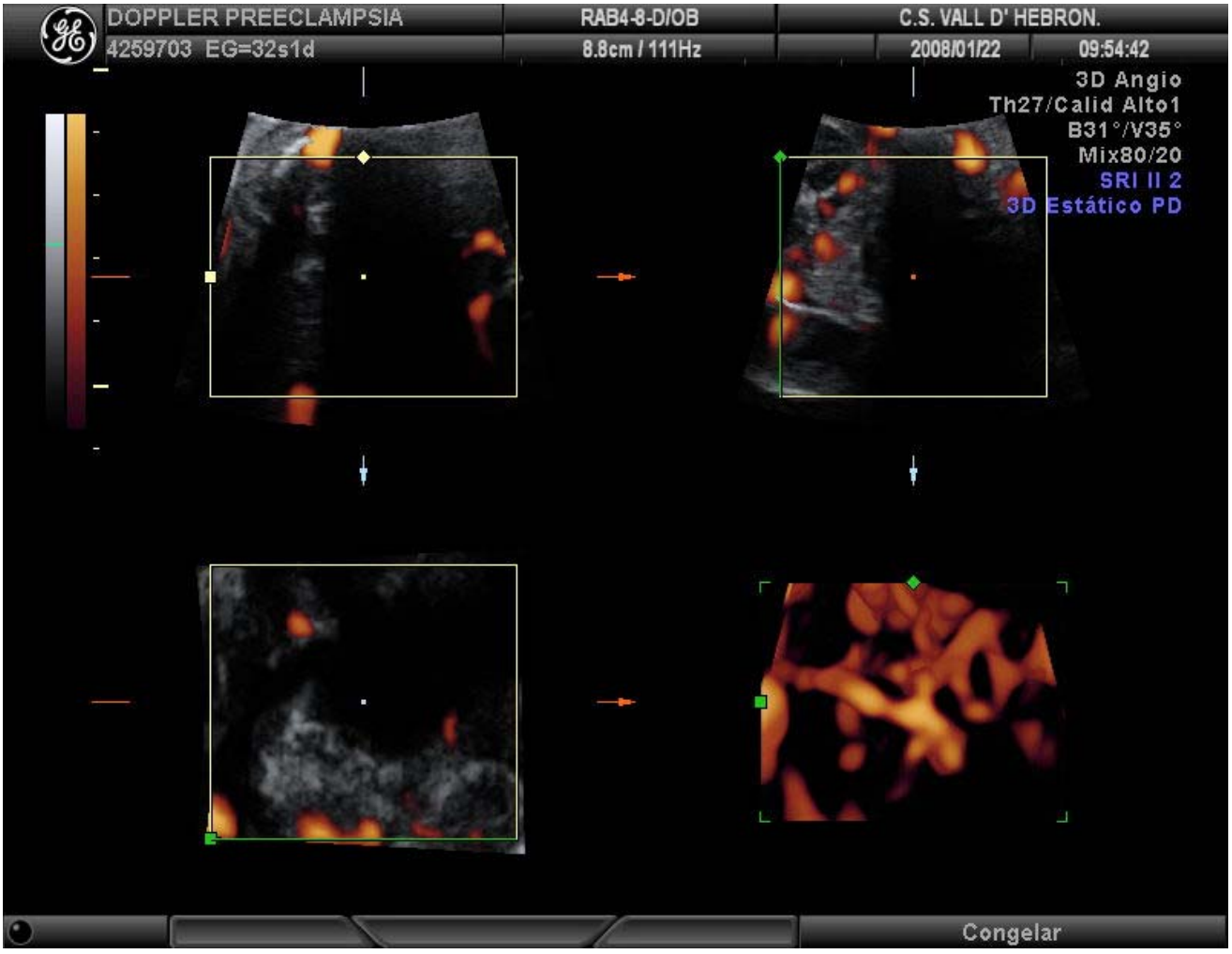

Fig. 3. Three dimensional angio mode rendering of placental vascularisation in a pre-eclampsia patient. Quantificaction of vascular branches suggest a lower flow in the corial plate when compared to volumes taken at the same gestational age from normal gestations.

Another promising approach, recently attempted, is to use 3D PD for the evaluation of progressive fetal conditions such as fetal goitrous hypothyroidism (Marín et al. 2010): In a given patient, under well controlled conditions, it should be possible evaluating the progression of ,either, an inflammatory response or the success of the treatment, which was thyroid hormone supplementation in this case. (Fig 4).

Despite being rather promising, the 3D PD still has important limitations, some related to the power Doppler signal itself and some derived by acoustic impedance and mechanical interference. Some of these aspects are going to be discussed further in the next section.

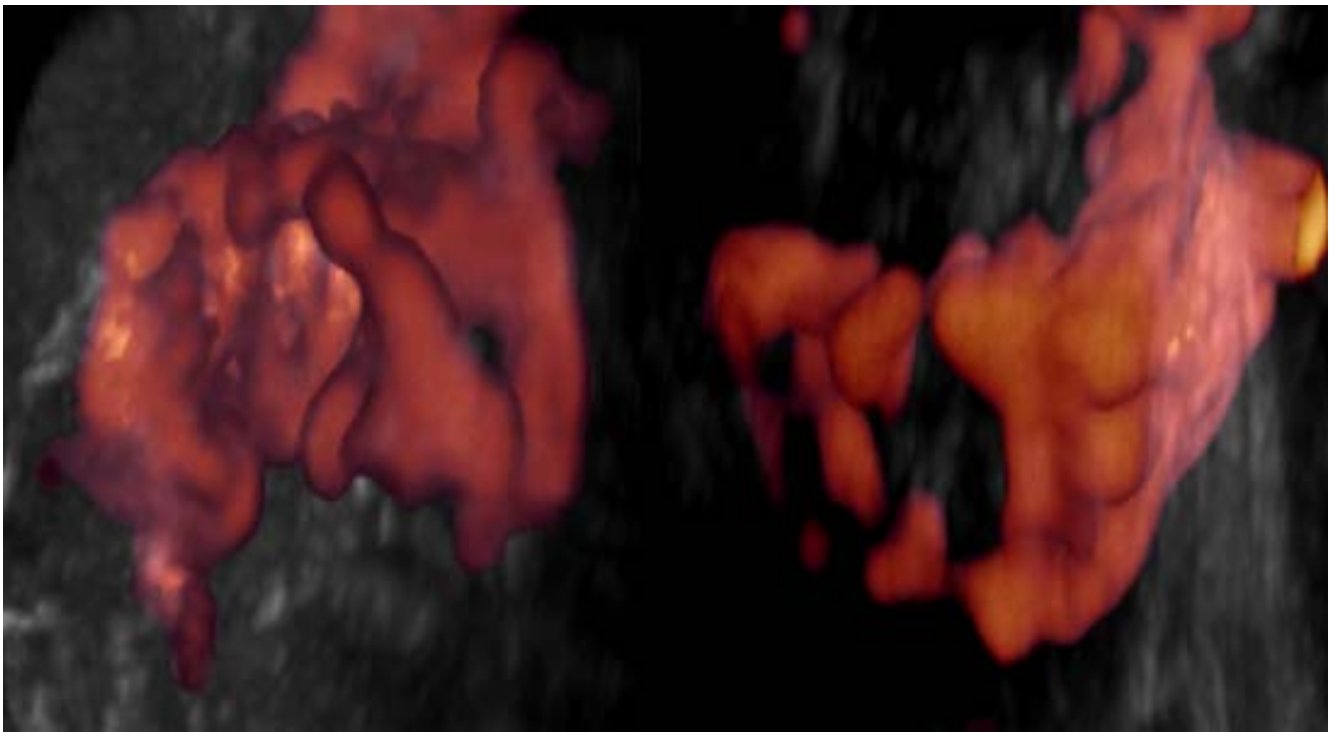

Fig. 4. Three dimensional PD angio mode rendered image of Thyroid gland of the same human fetus, before (left side) and after four weeks of intra-amniotic thyroid hormone supplementation (right side). Actual volume of the gland changed according to fetal growth, but vascularisation decreased markedly after treatment.

1.3 The signal normalization problem and its consequences

To normalize the 3D PD signal, it is necessary to take into account three paramount boundaries:

- The signal can be altered by tissue impedance, which means that a low velocity flow in a deep vessel will produce completely different PD patterns depending on the mother's abdominal wall thickness, the amount of amniotic fluid and the position of the fetus (Schulten-Wijman et al. 2011).
- The settings of the machine can modify sensibly the amount of signal registered by the processor, and therefore, the amount of color voxels inside the VOI: the algorithms for refining the B-mode signal like the speckle reduction or the cross beam reduction post-process algorithms mask the signal processed and "erase" a significant amount of moving particles. (N J Raine-Fenning et al. 2008b)
- The post-processing software provided by the developers of the Volume Measurement software: 4DView and virtual organ computer-aided analysis (VOCAL®) by General Electric Medical division. Q-lab® by Philips Medical Division, as well as Sonoview® and Histogram by Samsung-Medison Co show no correlation in their measurements. Therefore, the same structure, under similar circumstances, draw off

different results once measurement of the VOI is performed. (J L Alcázar 2008)

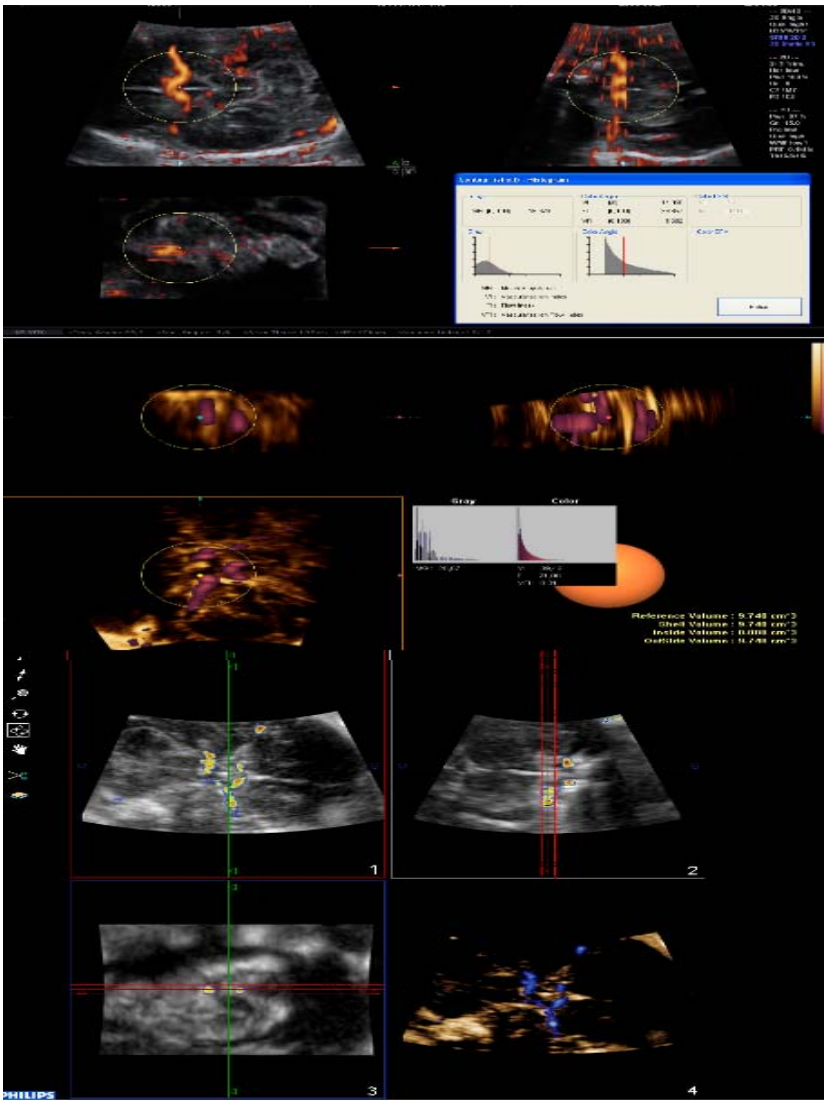

Fig. 5. Images obtained from a single fetus in cephalic presentation, from three different machines: General Electric Voluson E8 (Upper); Medison Accivix V20 Prestige (Middle); Philips iU22 (Lower).

1.3.1. The biases behind the algorithm

Based on previous observations, we conducted a preliminary study, on five healthy fetuses on their 20th week of gestation, comparing the values obtained in the same fetus with different machines and adjusting settings as main gain in 600 Hz, medium wall filter in 60 Hz, cross beam reduction off and persistence of color signal in 0. In all of them the structure was the Willis' polygon at the cranial base. Figure 5 shows the images obtained from the machines and the histograms.

The results, summarized in the table 1, show how different the measurements are, depending on the brand, and also how they differ among themselves, despite the same gestational age and similar maternal characteristics.

Fetus	GE Voluson E8			Philips iU22			Medison Accuvix V20		
	VI	FI	VFI	VI	FI	VFI	VI	FI	VFI
1	44.9	46.1	20.7	32.3	25..1	33.5	48.6	16.9	5.5
2	14.1	39.8	5.6	16.6	28.3	9.5	39.4	21.1	8.3
3	23.6	51.1	17.3	36.2	17.3	19.5	42.5	28.1	4.7
4	36.3	38.9	21.3	27.3	32.8	11.1	25.8	40.3	19.2
5	37.3	44.0	9.5	48.1	27.3	13.1	35.8	39.9	6.9

Table 1. Results from comparing similar ROI in three different machines when using the PD quantification application included in their software.

In conclusion, normalizing the data from 3D PD signal is currently not possible and reference ranges to discriminate normality from pathologic conditions are not available. Therefore, no feasibility for these indexes in obstetric clinical practice could be foreseen at short term. (Aw Welsh et al. 2012)

1.4 The regional normalization solution

Given that, no decisions can be made from direct measurement of the abovementioned indexes, a possible approach could be to use two

Regions of Interest (ROI) inside the same volume. The more reliable possibility after *in-vitro* testing was the VFI (N J Raine-Fenning et al. 2008a). And the easier and more repeatable formula was a simple VFI index

$$VFI_1 / VFI_2 \quad (5)$$

1,4.1 The ductus venosus shunting as an example

In phisiological conditions, few regions of fetal circulation could offer enough regional differences as fro being considered clinically relevant. But the most important of them is, no doubt, the physiological shunt in the ductus venosus which is not only a reliable indicator of preload, but also a sensitive mechanism of circulatory re-distribution in adverse circulatory conditions such as placental insufficiency (M Bellotti et al. 2000; T Kiserud 2001) .

The original description of Ductus Venosus Shunting (DVS) measurement was published by Belloti (Maria Bellotti et al. 2004), and was, simplifying, an index of estimated flow through Ductus Venosus (DV) over the one through Umbilical Vein (UV)

The classical way for estimating the flow through th UV is

$$Q_{UV} = 0.5 \times (V_{\max})_{UV} \times \pi \times (D_{UV}^2/4) \quad (6)$$

Also, the calculation of DV flow, made by Belloti et al, is

$$Q_{DV} = (-0.03 \times DR^2 + 0.189 \times DR + 0.43) \times (V_{\max})_{DV} \times \pi \times (D_{DV}^2/4) \quad (7)$$

Therefore, the DVS could be expressed as

$$Q_{DV}/Q_{UV} \cdot 100 \quad (8)$$

Description of the ideal technique for measuring blodd flow in both UV and DV has been precisely described (M Tchirikov et al. 2006). For UV blood volume flow measurement, a straight segment of the intra-abdominal part of the UV upstream of any hepatic branches should be selected, with the Doppler gate positioned so as to completely cover the vessel's diameter. The UV flow volume can also be measured in the umbilical cord. Authors suggest measuring blood flow volume following the 'maximum principle',

which aims to determine the maximum diameter of the vessel, the maximum intensity weighted mean velocity (or time-averaged mean velocity, TAV) at the maximum vessel length in a straight longitudinal section. The inner vessel diameter is determined to the nearest tenth of a millimeter by placing the calipers at right angles to the vessel axis on a frozen B-mode image (without color). This is followed by the TAV measurement at the same vessel portion with a small angle of insonation (less than 30◦). The blood volume flow rate is calculated from diameter (D) and TAV as flow rate = TAV × ð × *(*D*/*2*)*2 mL/min. Regarding the DV, The inner diameter of the DV should be measured by insonation perpendicular to the vessel wall at the isthmus. In order to reduce random error, the procedure must be repeated four or more times and the calculated mean diameter entered into the statistics (T Kiserud et al. 2006). Doppler evaluations must be carried out in the absence of fetal breathing and body movements.

As evident, the skills needed for achieving such measurements are prohibitively high; the time needed for every exploration is too long for a usual clinical exploration and the medical scope of this practice is quite reduced. Our proposal to address this issue is a far simpler, faster and repeatable approach, by using 3D PD.(Bello□Muñoz et al. 2009)

By taking a single volume of the fetal abdomen in Angio 3D PD mode, it was possible to measure the UV VFI by calculating it into a 1 cc sphere. After navigating through the volume, same measurement (DV VFI) was done in the DV, employing the same 1 cc sphere (Figure 6 summarizes both measurements)

Our study compared 162 volumes from normal fetuses and 36 from Fetal Growth Restriction (FGR) cases. In all of them we measured the DVS as described classically by Belloti et al (M Bellotti et al. 2007), and collected a volume of the fetal abdomen with 3D PD angio mode signal, always adjusting the same settings in the machine (General Electric Voluson E 8 GE Medical Systems Milwaukee USA) with a 3D RNA5-9-D Volume Convex Array Transducer Probe.

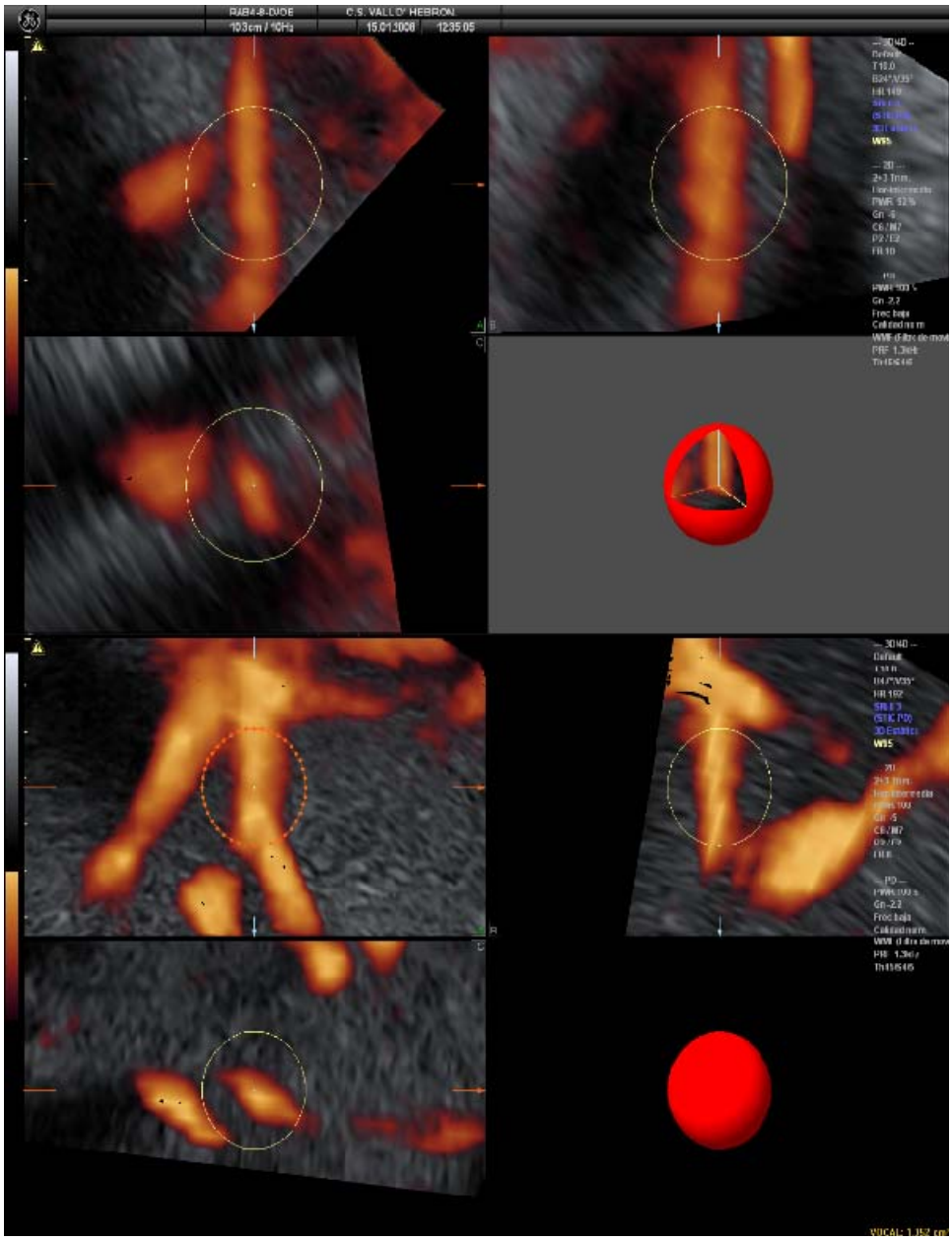

Fig. 6. VFI measurement in abdominal umbilical vein (upper) and in ductus venosus (lower). As the size of the sphere is exactly the same, the VOI remains unchanged.

The calculation of the DV/UV VFI ratio was as simple as:

$$DV\ VFI/UV\ VFI. \cdot 100 \quad (9)$$

We found a significant positive correlation between DVS measured as described by Belloti et al and DVS measured as a ratio of DV/UV VFI (Figure 7)

Also, as previously described, we found a significant difference in DV/UV VFI ratio between normal and FGR fetuses. Comparing results in growth restricted fetuses showed difference as plotted by gestational age mean (SD):39 (11,5) and 53(16,8) ($p = 0,03$). (Figure 8)

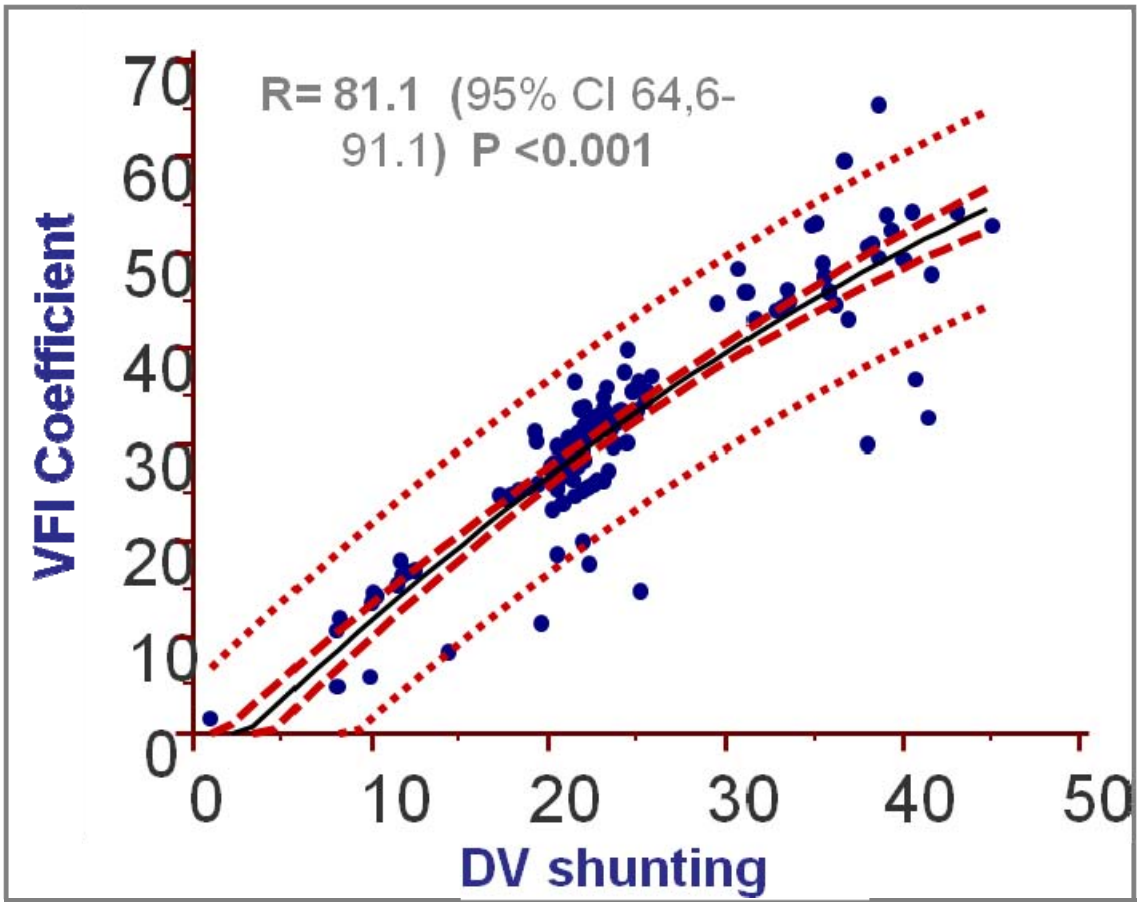

Fig. 7 Lineal regression plot comparing the DVS measured as classically described and the DV/UV VFI ratio r value = 0.81 P<0.001

Reference ranks equation $y = 0{,}6766 + 1{,}6542\ x + -0{,}007813\ x^2$

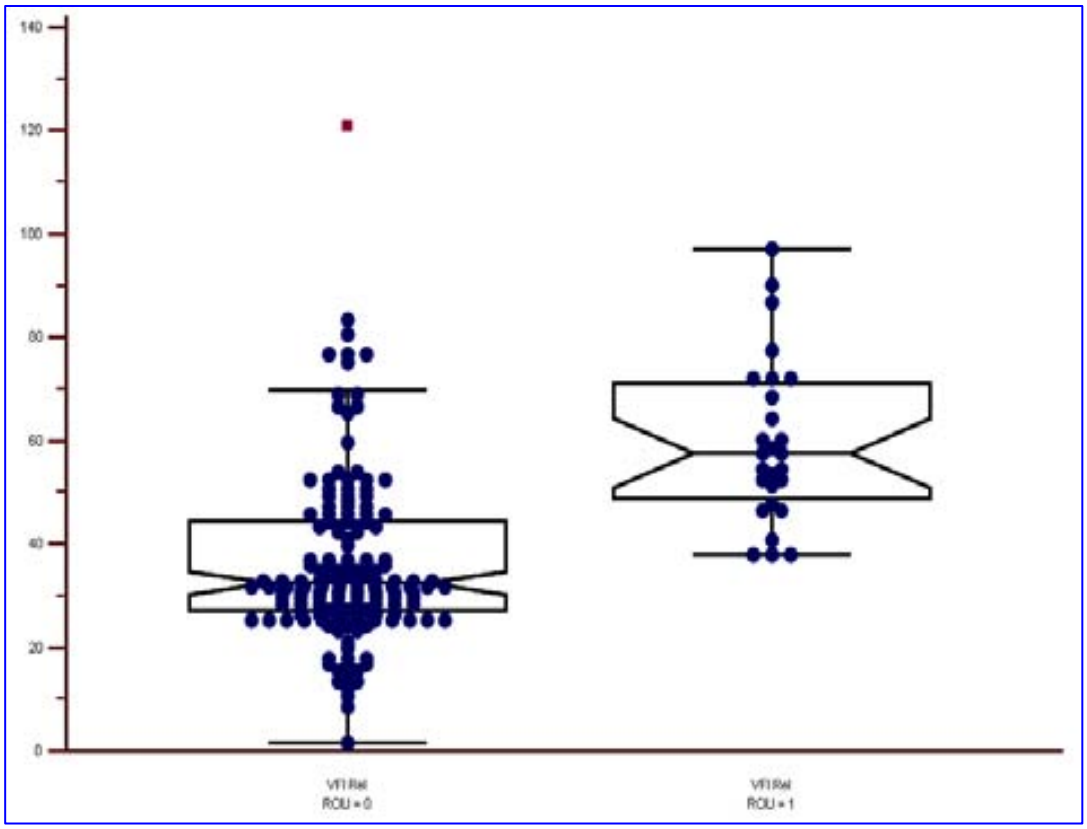

Fig. 8 Box Whisker plot of DV/UV VFI ratio comparing normal (left) to IUGR fetuses (right)

1.5. Four-dimensional power Doppler signal and the estimation of flow

1.5.1 The addition of a time sequence

Since the solution provided is already limited and only allows to estimate some regional changes in vascularity, applicable perhaps to the abovementioned DVS and to placenta (Odeh et al. 2011), but is still far away from depicting the flow phenomenon; it is necessary to move forward, towards two recently opened gates:

First is the integration of power signal derived velocities profile, which most reliable approach is the Surface Integration of Velocity Vectors ,(Sun et al. 1995; J M Rubin et al. 2001; S. Berg et al. 2000) a clarifying concept which was developed for Color Dopler signal analysis, but has the handicap of the angle effect (Pemberton et al. 2005; X. Li et al. 2005), reason why it was left aside. Until the algorithms for calculating velocity of particles from power Doppler signals were developed (M. G. Jones et al. 2003; Kripfgans et al. 2006; Petersch & Hönigmann 2007)

Surface integration of velocity vectors is based on Gauss' theorem, which relates the divergence of the quantity (*v)* in an enclosed volume (*V)* to the flux through the surface (*S)* covering (*V)*. In other words, a surface integral of *v* over the enclosing boundary *S* will yield the volume flow *Q*:

$$Q = \int_S \vec{v} \cdot d\vec{A} \,. \qquad (10)$$

The easiest way to implement SIVV is to choose a surface that is locally perpendicular to each Doppler beam. For this case, the right side dot product in Equation 1 will be replaced by a regular multiplication of the Doppler velocity and the size of the surface element. In other words, this surface has a constant depth geometry with respect to the Doppler beams. (Kripfgans et al. 2006)

The most general scanning geometry is the surface of a torus because the center of rotation for the axial-lateral and axial-elevational beams can differ). Volume flow can be computed by integrating all Doppler acquisitions on the defined surface, as expressed by Kripfgans et al:

$$Q = \sum_{i \in S} v_i \cdot a_i \ . \qquad (11)$$

Where, *Q* is the total flux through the surface *S*, which equals volume flow; *vi* is the local Doppler

velocity; *ai* is the associated cross-sectional area on *S* for this voxel, and · is the dot product between the local velocity vector and the local surface normal. In this case, the detected velocity is parallel to the surface normal.

In Kripfgans et al experiment, for the depicted type of tube-to-transducer orientation, the left-/right-most Doppler beam has the smallest/largest Doppler angle, respectively. This causes the velocity maximum to shift toward the left. However, warping of velocity values does not affect the measured SIVV value. Inherent compensation of this warping is due to nonuniform distribution of surface elements over the tube cross section.

A very important matter, mainly derived from biophysical characteristics of blood is the Rouleaoux' effect (J M Rubin et al. 1997; A. W. Welsh et al. 2005; N J Raine-Fenning et al. 2008a). The local Doppler power is largest inside the vessel and smallest outside because of the effect of partial volume averaging and the Doppler wall filter effect, which gives the pixels inside the vessel a higher power. All Doppler data is wall filter processed

internally in the scanner by the smallest setting possible on the machine. Therefore, it is mandatory to minimize filtering for the selected Doppler frequency range.

Authors define a solution for surface integration of velocity vectors, which was weighted on the basis of the Doppler power in the respective voxels. A velocity masking algorithm which was generated, using the Doppler power value *pT* to weight the velocity values of the integration surface.

Therefore, the modified SIVV method that was used by the authors was

$$Q = \sum_{i \in S} (v_i \cdot a_i)\, p_i \,. \tag{12}$$

Where, *pi* is a scaling factor based on the local Doppler power. Power weighting factors *pi* were set to 1 for all Doppler powers larger then *pT*. Values between 0 and *pT* were scaled between 0 and 1 on the basis of their Doppler power value. The justification for the selection/scaling process is that voxels near the wall, which partially contain flow and soft tissue, will show lower than- maximum Doppler power. Fractional power is therefore weighted by fractional scaling factors. So far, the threshold *pTwas* set empirically by developers. However, it was set constant for all

measurements, and it could be shown that the *pT* contour fills the lumen. User-selected Doppler gain was adjusted as needed to compensate for signal reduction due to large angles between flow and Doppler beams.

Next addition to the conceptual framework was the estimation of pulsatile conditions by Richards and Kripfgans (Richards et al. 2009), by adding to the model the potential signal fluctuations derived from the wall movements and the local velocity profile changes derived from particles acceleration. As a first issue, authors defined the possibility of collecting not one, but *N* number of velocity profiles according to the local variations in time and position. Such local velocities were expressed as:

$$\widehat{v_i}=E\left(v_i\left(X_i\right)\right)=\frac{\sum_{j=1}^{N} v\left(X_i,t_j\right)}{N}, \tag{13}$$

Where *E*(*vi*(X*i*)) is the expected value of the local velocity estimates. *v*(*Xi*,t*j*) are the local velocity estimates that are measured at randomly selected time increments defined by t*j* asfollows:

$$t_{j+1}=t_j+t_s+t_r, \tag{14}$$

Authors defined an experiment to obtain the average volume flow in the presence of pulsatility: 50 random time points distributed across the equivalent of a cardiac cycle were collected and averaged at each location. Power Doppler data were then used to correct for partial volume effects as described in the previous paragraph. Then, using seven previously defined surfaces for flow estimate, the equation for the modified SIVV method, became:

$$Q=\frac{1}{M}\sum_{i\in S_M} s_i \bullet w_i \bullet \widehat{v_i}, \qquad (15)$$

where *M* is the number of integration surfaces and the surface of integration *(S)* has been
modified to include the *M* surfaces *(SM)*.

In our opinion, Richards & Kripfgans' works have achieved a breakthrough in this matter, and the experiment we have developed is nothing but a logical consequence of their postulates.

Before describing the experiment, next consequent step was to add a regular time frame to the algorithm. Fortunately, the tool for getting the initial data was already developed and seated on the machine: The Spatio

Temporal Image Correlation (STIC) is an automated volume acquisition in which the array inside the transducer housing performs a slow, single sweep, recording one single 3D data set. This volume consists of a high number of 2D frames, one behind the other. Due to the small region of interest required to image the fetal heart, the B-mode frame rate during the acquisition of the volume scan is very high, in the range of 150 frames/s. Assuming a volume acquisition time of 10 s and sweeping over an area of 25◦ (both parameters can be adjusted), there are 1500 B-mode images in the volume memory. During this acquisition time the fetal heart beats 20–25 times, which means there are 20–25 images showing a systolic peak contained within these 1500 B-mode frames (DeVore et al. 2003; Chaoui & Heling 2005). Concerning this application, further studies have shown how, the mere analysis of intra-ventricular stroke volume in left and right heart gave information reliable enough for calculating the cardiac output in fetuses from 16 to 32 weeks (Molina et al. 2008a).

Basis of volume calculation in VOCAL are performed by integration of

$$Vol = \frac{\pi}{N} \cdot [\sum_{i=1}^{2 \cdot N} TA_i \cdot ds_i] \qquad (16)$$

polygon areas marked in parallel planes. The method used for the integration of the polygon areas is given by the formula

Where N = number of marked polygon areas Ai = polygon area in plane i di,j = distance between plane i and plane j the sort order of planes 1,..., N is given by d1,2 £ d1,3 £... £ d1,N. (Sohn 1993; Robb et al. 1997).

And the basis for stroke volume calculation and cardiac output calculation were (Molina et al. 2008b):

$$CO = \lim_{n\to\infty}\left(1+\frac{1}{n}\right)^{n} \cdot Vs \; \vdots - \vdots \lim_{n\to\infty}\left(1+\frac{1}{n}\right)^{n} \cdot VD \qquad (17)$$

Where CO = Cardiac Output, VS is Systolic Volume and VD is Diastolic Volume.

The abovementioned approach provides some additional information on cardiac output and has proven to be repeatible and more accurate than previous methods (Messing et al. 2007; Hamill et al. 2011; Simioni, Nardozza, Araujo Júnior, Líliam Cristine Rolo, et al. 2011). Notwithstanding, it still has a substantial amount of human interaction, and is rather time-consuming as for being used in an actual clinical setting.

x

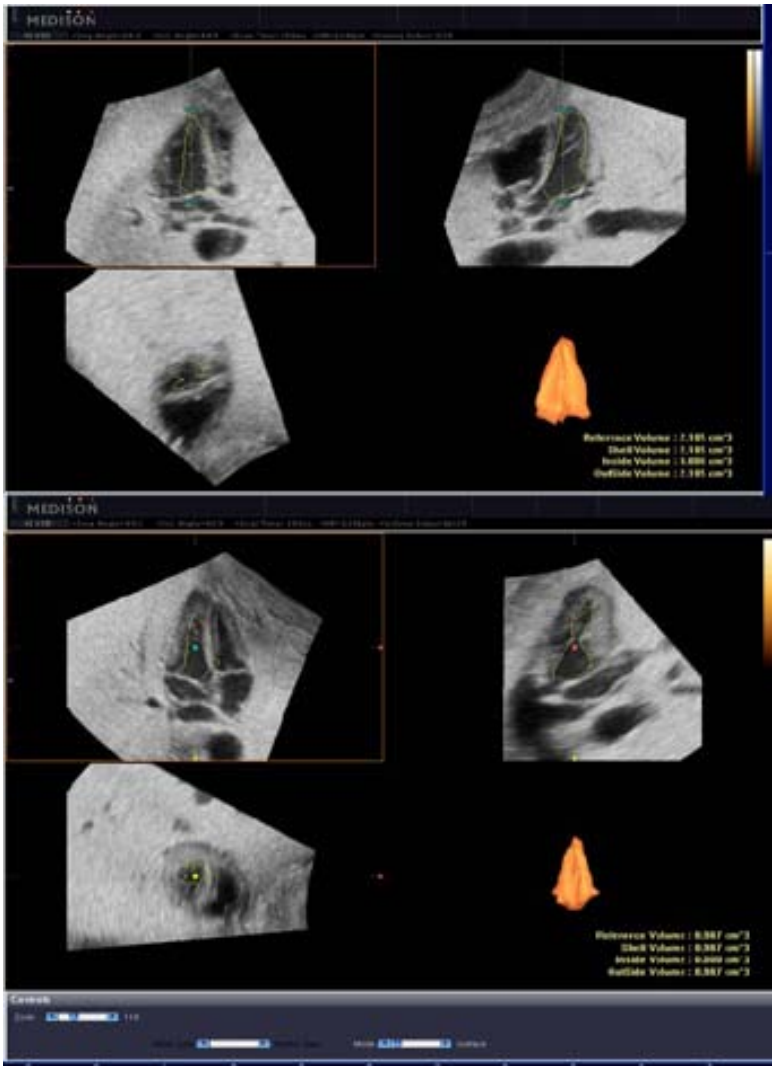

Fig. 9. Reproduction of STIC and VOCAL model for left ventricle output calculation in a term ovine fetus, taken by the authors during their experiment (Bello□Muñoz et al. 2010); as proposed by Molina et al.

1.5.2. The Dynamic Tissue Perfussion Model

The foetal perfusion has to meet the needs of the rapidly growing organism, to deliver oxygen and nutrients in order to permit a normal intrauterine growth. Among other causes placental insufficiency is an important reason for disturbed intrauterine growth, resulting in intrauterine growth retardation (IUGR) and postnatal complications. The evaluation of foetal perfusion today is based in daily practice on the calculation of RI and PI in large arteries, mainly the umbilical, the cerebral arteries and the aorta, sometimes supplemented by flow pattern evaluations in the venous duct attempts tried to quantify the umbilical venous flow volume with the aim to evaluate the foetal perfusion in quantitative terms . These studies were not continued because of limited reproducibility . Nevertheless, these studies targeted at a parameter – volumen flow –, which has a much better rationale than the popular and easy to measure RI and PI.

The early studies were flawed mainly by two limitations, which could not be overcome with two-dimensional sonographic techniques. First the angle correction of flow velocity in space and second the non-circular shape of the transection of the umbilical vein (UV).

Spatial angle correction is but pivotal in this setting, because the UV is continuously winding around the umbilical arteries and the whole cord is

irregularly bent within the amniotic cavity. Two-dimensional images thus may allow an angle correction within the frontal plane but this can be vastly misleading. Depending on the sagittal angle the true and only relevant spatial angle can differ substantially thus leading to unpredictable errors of the volume flow calculation, when unknown. The second source of error was the universal assumption, that the UV is a round tube. The investigators tried to depict a straight running venous segment with parallel borders to apply the formula for circular area calculation in order to multiply this area with the mean flow velocity which was traced with a pulsedwave- Doppler instrument in the centre of the vein.

These sources of error combined in an unpredictable manner and caused the refusal of this approach.

The technique of DTPM combined with the modern three-dimensional imaging techniques can resolve all of these imponderabilities. We developed the three-dimensional, spatial angle corrected umbilical vein flow volume measurement, which is outlined below.

In this plane both velocity as displayed by a certain colour hue and shape of the vessel's cross section are distorted by a stretching factor which is equal to the cosine of the spatial angle between vessel's course and the ultrasound waves' propagation line – the so called Doppler angle α. While the area is stretched by the reciprocal of cos α the velocity is virtually reduced by the by multiplication with cos α

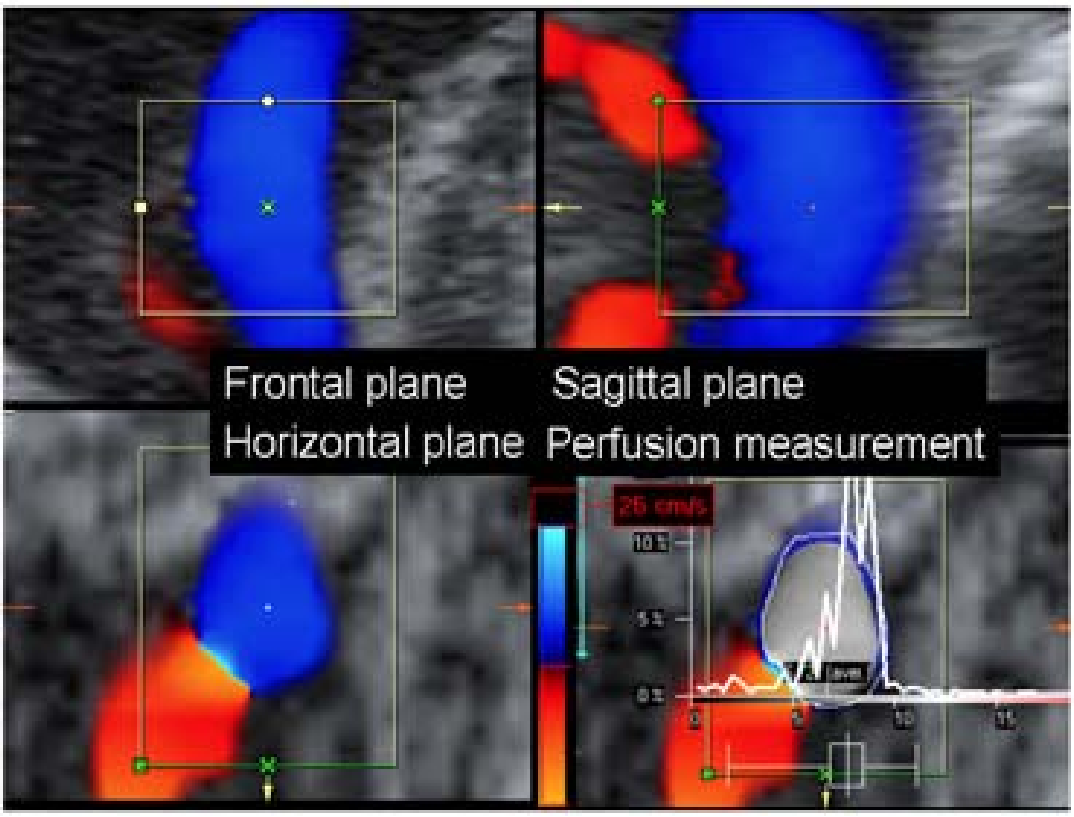

Fig. 10. Example of a spatially angle corrected fetal volume flow measurement in the umbilical vein. A 3D-dataset is shown displaying three perpendicular imaging planes. The horizontal plane is used for DTPM (right lower quarter): False color map of the venous flow.

Therefore, direct calculation of true flow volumes directly from measurements within the horizontal plane is possible.. The reproducibility of these measurements in a clinical situation lies in the range of around 6 % and less, if exclusively data with steep spatial Doppler angles are allowed

A significant correlation of such volume flow measurements with fetal weight could be demonstrated that was the better the steeper the spatial angle could be arranged. Moreover, in a preliminary study a significantly diminished flow volume per gram fetal weight could be shown

DTPM offers a universally applicable approach to tissue perfusion measurement as far as sonographic depiction of tissues is possible. So far, inaccessible details of perfusion intensity, perfusion distribution, perfusion gradients within a certain vasculature open a widow to an individualized evaluation of the specific pathophysiological situation. Treatment efforts can be evaluated according to their effect on perfusion. Besides these intrinsic advantages, the technique requires no additional hardware, is non-invasive, needs no specific preparation of the patient and thus can be recommended for a broad array of clinical applications.

True volume flow calculation becomes feasible with three-dimensional colour Doppler data. True volume flow calculation means the exact calculation of the blood flow volume running through any vessel which is cut perpendicularly.

The method of true volume perfusion measurement in vessels cut by the horizontal plane in any spatial angle is described and proven below. The

spatial angle, which is the angle between the vessel and the ultrasound propagation line, influences simultaneously the stretching of the shape of the vessels' cross-sectional area as well as the change of the recorded flow velocity. towards the ultrasound propagation line (blue line). The horizontal imaging plane, which is calculated during the three-dimensional ultrasound imaging, cuts the vessel. Line *a′* is the stretched vessel's diameter as it can be seen in the horizontal plane. Vector b is the original flow velocity within the vessel. Due to the Doppler angle á the recorded velocity is displayed with the value for vector b'. This means, the color hue of b' is darker, representing a lower velocity as if vector b would be displayed in its appropriate color. This is the well known Doppler effect ($fd = 2 * fo * vt\ c\ * \cos \alpha$) , which reduces the recorded velocity according to the cosine of á.

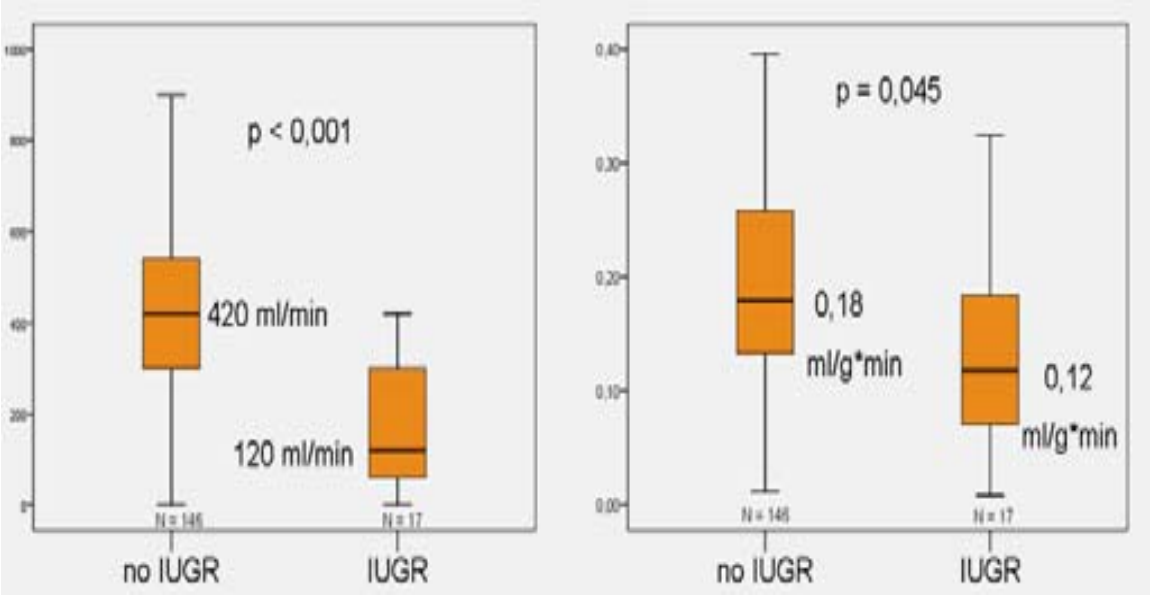

Fig. 11. A significant reduction of fetal perfusion per gram fetal weight could be demonstrated by DTPM in fetuses with intrauterine growth retardation (IUGR) compared to normal children

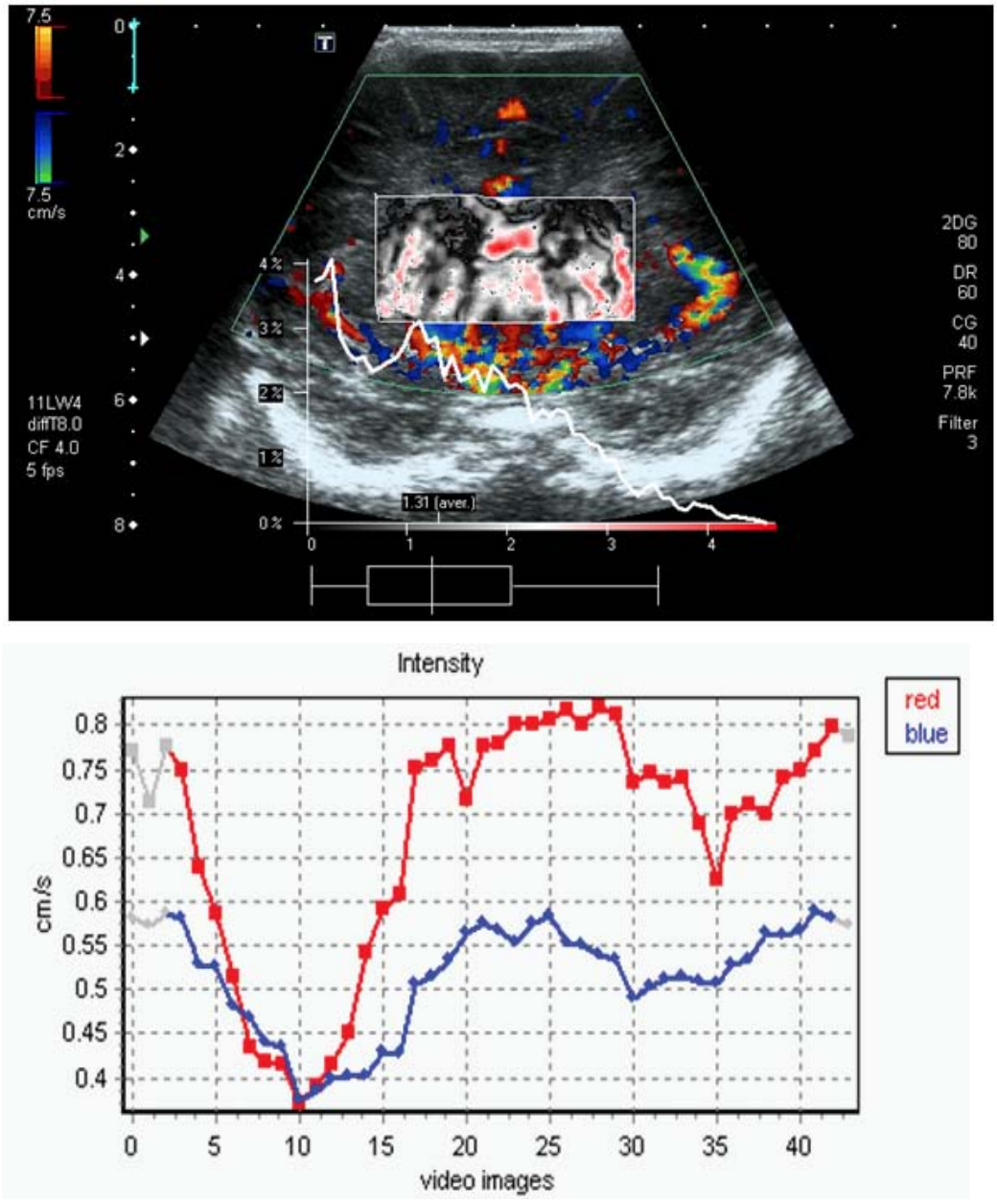

Fig. 12. Example of a DTPM of basal ganglia in a newborn. Upper part: false color map of the basal ganglia and distribution curve. Lower part: Perfusion intensity course during one examination. (Image and measurement courtesy of Dr. Ricardo Faingold, Montreal)

The real flow volume per time (V) of a circular vessel is calculated as calculates the circular area of the perpendicularly cut vessel

$$V\,t = \text{ð}\ 4 \ast a \ast a \ast b$$

$$// \ \text{ð}\ 4 \ast a \ast a$$

The oblique transsection of a round vessel, a vessel running not perpendicularly towards the horizontal plane, results in stretching of the circular vessel's round cross-sectional area in the direction of the projection vector of the spatial angle of this vessel with the horizontal plane. This results in an ellipse which longer axis is represented by a' , the stretched projection of a onto the horizontal plane (Fig. 30). The shorter axis is equal to the original diameter of the vessel. It remains unstretched since no angulation occurs. It is therefore possible to consider the change of diameter a towards a' , the long axis of the ellipse in order to describe the change of the horizontally projected cross-sectional area of the vessel. The change of the circular area towards the elliptical area is thus equal to the stretching factor $a' \, a$.

The other relevant change is the reduction on the displayed flow velocity compared to the original velocity b, the reduction factor is $b' \, b$.

It is now claimed, that the flow volume V’ per time, which is passing through the horizontal

plane in direction of the vessel, calculated by multiplying the elliptical area

(A=ð 4∗a∗a') (17)

with the flow velocity b’ of the vessel in the horizontal plane is equal to V per time, the flow volume passing through the perpendicularly cut vessel in

$$V' = V$$

Proof:

$$V'/t = \pi/4 * a * a' * \vec{b'}$$

// $\pi/4 * a * a'$ calculates the elliptic area of the horizontally cut vessel
a : short axis of the ellipse
a' : long axis of the ellipse

the same time. (18)

The depiction of the horizontally cut vessel shows the velocity b'

and a stretched Wessel diameter a' .

The triangle ABC is rectangular, since the blood vessel is a rectangle, a perpendicularly cut circular straight vessel. Doppler angle á is complemented to 90° by the angles DAB and FAC since the ultrasound propagation line (blue line running through F) runs perpendicular to the transducer's surface and thus the horizontal imaging plane. Both angles are thus equal and named â. Angles FAC and CAB add to 90° since again the ultrasound propagation line runs perpendicular to the horizontal imaging plane. Thus angle CAB is á again, the Doppler angle.

$$a' = a / \cos\alpha$$

$$\vec{b'} = \vec{b} * \cos\alpha$$

by inserting (3) and (4) into (2) results (5)

$$V' = \pi/4 * a * a/\cos\alpha * \vec{b} * \cos\alpha$$

which is (6) after cancelling cos α

$$V' = \pi/4 * a * a * \vec{b} = V \text{ see (1)}$$

thus

$$V' = V$$

(19)

This means, that it is possible to calculate the true flow volume of all vessels cut horizontally from the depicted flow velocities1 and the pixelwise calculated cross-sectional areas2 directly, thus compensating

any spatial angle. Both measurements (1 and 2), are carried out automatically by the PixelFlux-software, which delivers thus true flow volumes of all vessels in any tissue section cut horizontally in three-dimensional color Doppler ultrasound data

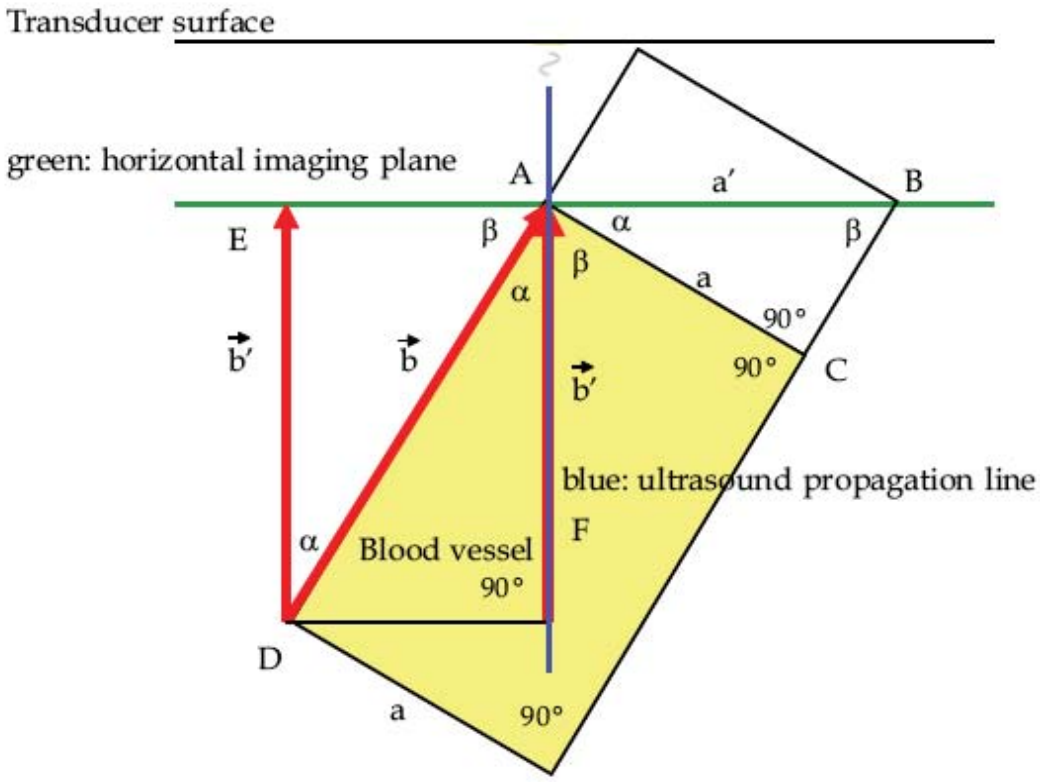

Fig. 13. Schematical depiction of a horizontally cut vessel in a 3D-color Doppler sonographic dataset

Chapter 2. The Fetal Circulation

2.1 Subtle changes with huge consequences

2.1.1. The normal patterns

Many of the mechanisms described in animal experiments also occur in the human fetus, but with differences. The reasons for variation are many, e.g. a sheep fetus has a different anatomy compared with a human fetus, with a longer intrathoracic inferior vena cava (IVC), a smaller brain, the fetal liver is positioned differently, two umbilical veins, a higher temperature, a lower Haemoglobin (Hgb), a higher growth rate and a shorter pregnancy. Ultrasound in obstetrics has been used increasingly to provide physiological data from human fetuses, and this is reflected in the present review.(Torvid Kiserud & Ganesh Acharya 2004).

The blood volume in the human fetus is estimated to be 10–12% of the body weight, compared with 7–8% in adults (G. C. S. Smith & A. D. Cameron 2003) The main reason for this difference is the large pool of blood contained within the placenta; a volume that reduces as gestation progresses. The calculated blood volume of 90–105 ml/kg in fetuses undergoing blood transfusion during the second half of pregnancy is probably an underestimate (P. Johnson 2000). Other studies have

indicated a volume of 110–115 ml/kg, which is more in line with experimental sheep studies. (Yamamura et al. 2012). The estimated volume of 80 ml/kg contained within the fetal body is marginally more than that in adults. Compared with adults, the fetus is capable of much faster regulation and restoration of the blood volume due to high diffusion rates between fetal compartments.

Arterial and venous blood pressure

The mean arterial pressure in human fetuses was measured to be 15 mmHg during cordocentesis at gestational weeks 19–21(T. Kiserud et al. 1994). Intra-uterine recording of the intraventricular pressure in the human fetus suggests that the systemic systolic pressure increases from 15–20 mmHg at 16 weeks to 30–40 mmHg at 28 weeks.(P. Johnson 2000). There was no obvious difference between the left and right ventricles. This increase was also seen for diastolic pressure, which was ≤5 mmHg at 16–18 weeks and 5–15 mmHg at 19–26 weeks.

Umbilical venous pressure, recorded during cordocentesis and corrected for amniotic pressure, increased from 4.5 mmHg at 18 weeks to 6 mmHg at term (K Flo, T Wilsgaard & G Acharya 2010).

Cardiac performance

Structural details of the heart are organized during the embryonic period but are dependent on the physical environment, including blood flow, in

order to develop normally. The myocardium grows by cell division until birth, and growth beyond birth is due to cell enlargement. The density of myofibrils increases particularly in early pregnancy and the contractility continues to improve during the second half of pregnancy (H. Li et al. 2006). The two ventricles perform differently in pressure/volume curves and when tested with intact peripheral vasculature (Reller et al. 1987) .The fetal heart has limited capacity to increase stroke volume by increasing diastolic filling pressure, the right ventricle even less than the left, as they are already operating at the top of their function curves. The Frank–Starling mechanism does operate in the fetal heart, which is apparent during arrhythmias(Grosse-Wortmann et al. 2006). Adrenergic drive also shifts the function curve to increase stroke volume. However, increased heart rate may be the single most prominent means of increasing cardiac output in the fetus (Hamill et al. 2011; Simioni, Nardozza, Araujo Júnior, Líliam Cristine Rolo, et al. 2011).

The two ventricles pump in parallel and the pressure difference between them is minimal compared with postnatal life(Reller et al. 1987). However, experimental studies show some variation in pressure and velocity waves between the two sides, ascribed to the difference in compliance of the great arteries and downstream impedance (upper body vs lower body and placenta) (Ganesh Acharya et al. 2004) . Some of the ‘stiffness’ of the fetal myocardium is attributed to the constraint of the pericardium, lungs and

chest wall (Torvid Kiserud & Ganesh Acharya 2004; R Cruz-Martinez, F Figueras, Benavides-Serralde, et al. 2011) ,all of which have low compliance before air is introduced. However, with the shunts in operation and a metabolism capable of extracting oxygen at low saturation levels, the fetal heart appears to be a very flexible, responsive and adaptive structure. Figure 14 represents schematically the major features of fetal circulation

Cardiac output and distribution

The fetal systemic circulation is fed from the left and right ventricles in parallel. The left ventricle is predominantly dedicated to the coronary circulation and upper body, while the right ventricle is the main distributor to the lower part of the body, the placenta and the lungs. When using outer-inner diameter measurements of the vessels, the combined cardiac output (CCO) is reported to be 210 ml/min at mid-gestation and 1900 ml/min at 38 weeks (Hamill et al. 2011) . A summary of these measurements could be seen in table 2 (J.-C. Fouron et al. 2009). When using inner diameters, these numbers are lower. The right ventricular output is slightly larger than that of the left ventricle, and pulmonary flow in the human fetus is larger (mean 13–25%) than in the classical fetal lamb studies (≤10%). Interestingly, a developmental transition in fetal haemodynamics seems to occur at 28–32 weeks when the pulmonary blood flow reaches a maximum with a simultaneous change in oxygen

sensitivity in the pulmonary vasculature (Ruano et al. 2006; Dong et al. 2011) . Another study found that less blood was distributed to the fetal lungs (11%) (Mess & Ferner 2010) ,which is more in line with previous experimental studies.

The three shunts (ductus venosus, ductus arteriosus and foramen ovale) are essential distributional arrangements that make the fetal circulation a flexible and adaptive system for intra-uterine life. A classical concept describes the pathway of oxygenated blood as the via sinistra, leaving the umbilical vein through the ductus venosus to reach the foramen ovale, left ventricle and aorta, thus feeding the coronary and cerebral circuits. Conversely, a via dextra directs de-oxygenated blood from the caval veins through the tricuspid valve, pulmonary trunk and ductus arteriosus to reach the descending aorta, largely bypassing the pulmonary circuit.

Oxygen saturation gives a picture of distribution and blending of flows in the central fetal circulation. The lowest saturation is found in the abdominal IVC, and the highest saturation is found in the umbilical vein (Ganesh Acharya & Sitras 2009) . Interestingly, the difference between the left and right ventricles is only 10%, and this increases to 12% during hypoxaemia. The small difference between the left and right ventricles is due to the abundant volume of oxygenated blood presented to the foramen ovale. In addition to the ductus venosus blood flow, the umbilical blood passing

through the liver has had a modest reduction in saturation and represents another sizeable volume of oxygenated blood flowing in much the same direction as the ductus venosus towards the foramen ovale. In addition to some blending, the abundance of oxygenated blood will cause a spillover to the right side when reaching the foramen ovale with its crista dividens (limbus) .

Ductus venosus and liver circulation

In the human fetus, the ductus venosus is a slender trumpet-like shunt connecting the intra-abdominal umbilical vein to the IVC at its inlet to the heart. The inlet of the ductus venosus, the isthmus, is the restrictive area with a mean diameter of 0.5 mm at mid-gestation and hardly exceeds 2 mm for the rest of a normal pregnancy (T. Kiserud et al. 1994; Bello□Muñoz et al. 2009; M Tchirikov et al. 2006) .The umbilical venous pressure ranges from 2 to 9 mmHg (Maria Bellotti et al. 2004; Kaji et al. 2012) (the portocaval pressure gradient), and causes the blood to accelerate from a mean of 10–22 cm/s in the umbilical vein to 60–85 cm/s as it enters the ductus venosus and flows towards the IVC and foramen ovale (M Bellotti et al. 2000; Torvid Kiserud & Ganesh Acharya 2004; G Acharya et al. 2005) . The blood flow with the highest oxygenation, coming from the ductus venosus, also has the highest kinetic energy in the IVC and predominantly presses open the foramen ovale valve to enter the left

atrium, i.e. the ‘preferential streaming’ described in animal studies(M Tchirikov et al. 2006).

While 30% of the umbilical blood is shunted through the ductus venosus at mid-gestation, this fraction is reduced to 20% at 30 weeks and remains so for the rest of the pregnancy, but with wide variations. These results are similar to those of another study (Kaji et al. 2012) ,but are at variance with experimental animal studies, admittedly using a different technique, which showed that approximately 50% was shunted through the ductus venosus(M Tchirikov et al. 2006; M Bellotti et al. 2007; Bello□Muñoz et al. 2009) The redistributional mechanisms of increased shunting during hypoxaemia described in animal experiments also seem to operate in the human fetus (Edelstone & Rudolph 1979; Rudolph 1985; van Cappellen et al. 1999)

The ductus venosus is under tonic adrenergic control, and distends under the influence of nitroxide and prostaglandins (P. Vallance et al. 1989; D. J. Williams et al. 1997) .The most extensive dilatation is seen during hypoxaemia, leading to a 60% increase of the diameter in fetal sheep. However, the changes in diameter are not restricted to the isthmus but also include the entire length of the vessel, which has a far greater impact on resistance (Maria Bellotti et al. 2004). The shunt obliterates within 1–3 weeks of birth in term infants, although this takes longer in premature

births and in cases with persistent pulmonary hypertension or cardiac malformations (Baez et al. 2005; Borrell et al. 2003) . In contrast to the ductus arteriosus where increased oxygen tension triggers the closure, no trigger has been found for the ductus venosus (Fugelseth et al. 1998; Loberant et al. 1999; Ishida et al. 2011)

Equally important to the active regulatory mechanism is the passive regulation based on fluid dynamics, i.e. viscosity and pressure (C Ebbing et al. 2011; Erkinaro et al. 2009). Blood velocity in the ductus venosus is high and has Newtonian properties with low viscosity (similar to water). In contrast, liver tissue represents a huge capillary cross-section with a low blood velocity. At low velocities, the blood is non-Newtonian with an accordingly high viscosity (and resistance) and a closing pressure of 1–4 mmHg. It follows that an increase in haematocrit leads to increased viscous resistance in the low-velocity venous liver flow and has little effect on the high-velocity flow in the ductus venosus. Thus, the change in haematocrit alone leads to a shift of umbilical venous flow from the liver to the ductus venosus.

Along the same lines, variation in the umbilical venous pressure affects the two pathways differently. A reduction in venous pressure reduces liver perfusion more than ductus venosus flow, as a further reduction in an already low velocity in the large cross-section of the portal vasculature

implies a considerable increase in viscous resistance. The result is a higher degree of shunting (T Kiserud et al. 2006).

In addition to these fluid dynamic determinants, the neural and endocrine regulation of the hepatic vascular bed also play a role (T Kiserud 2001; Jörg Kessler et al. 2009) .The portal vasculature shows a more pronounced constricting response to adrenergic stimulation compared with the ductus venosus (Kilavuz et al. 2003; Jörg Kessler et al. 2008) .It all combines to make a distribution system that is extremely sensitive to both active and passive regulation, which is in line with the substantial normal variation of shunting seen in human fetuses (Coceani & Olley 1988; M Tchirikov et al. 2006; T Kiserud et al. 2006)

The physiological role of the ductus venosus is not well understood. The shunting seems more prominent in early pregnancy than after 30 weeks of gestation. The low degree of shunting through the ductus venosus during the last 8–10 weeks of pregnancy implies that approximately 80% of the umbilical blood perfuses the liver, signifying a very high developmental priority of the umbilical liver perfusion compared with the ductus venosus (Torvid Kiserud & Ganesh Acharya 2004) . However, during hypoxic challenges, the priority seems to be different. Fetuses maintain a higher degree of ductus venosus shunting, probably as a redistributional adaptation to hypoxic pressure, ensuring oxygenation of the heart and brain (A. A. Baschat et al. 2002; G. Haugen et al. 2005) . It should be

borne in mind that oxygen extraction in the liver is rather modest (10–15% reduction in oxygen saturation) (C.-H. Chang et al. 2003; G. Haugen et al. 2005) ,which means that blood coming from the median and left hepatic vein are important contributors of oxygenated blood. Actually, the position and direction of the left hepatic venous blood under the Eustachian valve (IVC valve) favour this blood to be delivered at the foramen ovale (Mikhail Tchirikov et al. 2005; Kaji et al. 2012)

Although agenesis of the ductus venosus has been linked to abnormalities and fetal demise (P. Volpe et al. 2002), agenesis is also found in fetuses that have exhibited normal growth (Wald et al. 2012; Thomas et al. 2012; P. Volpe et al. 2002; P. Volpe et al. 2011; Staboulidou et al. 2011). Experimental obliteration of the vessel seems to have little haemodynamic effect, but causes an increase in insulin-like growth factor 2 and increases the growth of fetal organs (Mikhail Tchirikov et al. 2005). Recent studies have indicated that the fetal umbilical flow to the liver towards the end of pregnancy is influenced by the maternal nutritional state and diet (Cerf et al. 2010). Umbilical venous flow constitutes 75% of the venous supply to the liver, with the remaining 25% coming from the main portal stem (Kilavuz et al. 2003).In human fetuses, the arterial supply to the liver is not known but it seems to have a more prominent role during compromise (Cathrine Ebbing et al. 2009; C Ebbing et al. 2011)

Doppler examination of the ductus venosus is increasingly used to identify hypoxaemia, acidosis, cardiac decompensation and placental compromise, and is a promising tool for timing the delivery of critically ill fetuses (S Yagel et al. 2006; Fasouliotis et al. 2002) .Increased pulsatility, mainly caused by the augmented atrial contraction wave, signifies increased atrial contraction due to adrenergic drive, or increased venous filling pressure, or both.

In early pregnancy, the augmented a-wave in the ductus venosus is associated with an increased risk of chromosomal aberration and has been suggested as a secondary screening test (Borrell et al. 2003; Wald et al. 2012)

Foramen ovale

A defect in the atrial septum is commonly associated with left-right or right-left shunting in postnatal life. It is conceivable that this concept is carried over to describe the function of the foramen ovale in the fetus (T Kiserud et al. 1992; R. L. Lewis & Gutmann 2002) ,but this is not a fair representation of the actual haemodynamics. Rather, the inferior venous inlet to the heart should be viewed as a column of blood that ascends between the two atria from below .This column hits the interatrial ridge, the crista dividens, and is divided into a left and right arm . The left arm fills the ‘windsock’, formed between the foramen ovale valve and the atrial septum, to enter the left atrium. The right arm is directed towards the

tricuspid valve and joins the flow from the superior vena cava and coronary sinus to form the via dextra.

This is an equilibrium easily influenced by changes in pressure on the two sides. Increased resistance and pressure of the left side is instantaneously reflected in increased diversion of blood to the right side. In contrast to the hypertrophy of the left ventricle seen in aortic stenosis in adults, fetal stenosis commonly leads to a shift of blood volume from left to right at the level of the foramen ovale, with corresponding development of left-sided hypoplasia and compensatory growth of the right ventricle.

The developing ventricle responds to the demands of the afterload and is stimulated by the blood volume of the preload. However, for the left side of the heart, the foramen ovale is an important limiting factor, particularly in cases of a maldeveloped foramen or a premature closure. Under physiological conditions, it is not the oval-shaped hole of the septum that constitutes the restricting area for the flow to the left atrium, but the horizontal area between the foramen ovale valve and the atrial septum above the foramen ovale. Interestingly, the growth of this area is somehow blunted after 28–30 weeks of gestation compared with the cross-section of the IVC. This effect coincides with changes in fetal lung perfusion and ductus venosus shunting, and may signify a transition into a more mature circulatory physiology (Torvid Kiserud & Ganesh Acharya 2004; Bartha et al. 2009).

Ductus arteriosus and pulmonary circulation

The ductus arteriosus constitutes a wide muscular vessel connecting the pulmonary arterial trunk to the descending aorta (Fig. 14). During the second trimester, the velocity in the ductus arteriosus increases more than that in the pulmonary trunk, reflecting the development of the wind-kessel function of the pulmonary trunk (Dong et al. 2011). During the second half of pregnancy, 40% or less of the CCO is directed through the ductus arteriosus (Ishida et al. 2011). The lungs receive 13% of the CCO at mid-gestation and 20–25% after 30 weeks, which is more than that reported in fetal sheep experiments and a more recent human study (Mess & Ferner 2010). Normally, the shunt closes 2 days after birth, but a patent duct is a common clinical problem. An increase in oxygen tension is regarded as the main trigger for its closure. The vessel is under the general influence of circulating substances, particularly prostaglandin E_2, which is crucial in maintaining patency (Smolich et al. 2012; Wei et al. 2011). Sensitivity to prostaglandin antagonists is at its highest in the third trimester and is enhanced by glucocorticoids and fetal stress. Nitric oxide has a relaxing effect prior to the third trimester. The increased reactivity of the ductus arteriosus in the third trimester makes it vulnerable to prostaglandin synthase inhibitors, such as indomethacin, which may cause severe and longlasting constriction (Momma & Takao 1989; Smolich et al. 2012; Weichert et al. 2010)

The ductus arteriosus bypasses the pulmonary circuit, but the distribution between these two pathways depends heavily on the impedance of the pulmonary vasculature, which is under the control of prostaglandin I_2 and modified by a series of substances. In an elegant study, Rasanen et al. showed how reactivity in the pulmonary vascular bed increased in the third trimester (J Rasanen et al. 1996). While fetuses at gestational age 20–26 weeks showed no changes during maternal hyperoxygenation, fetuses at 31–36 weeks had lower impedance in the pulmonary arteries assessed by the pulsatility index, and increased pulmonary blood flow. Correspondingly, the blood flow in the ductus arteriosus was reduced (Lim et al. 2012).

Brain circulation

Differences in circulation physiology between animal experiments and human fetuses are likely to be greatest when concerning the brain, as the human brain is relatively larger than in other species. In a study of human previable fetuses weighing 12–272 g (probably corresponding to 10–20 weeks of gestation), it was found that the brain received approximately 15% of the systemic venous return (equal to the CCO less the pulmonary circuit). The proportion directed to the brain increased with low arterial pH, increased pCO_2 and reduced placental perfusion. A study of the primate *Macaca mulatta* at an advanced stage of gestation found that 16% of the

CCO was distributed to the brain, and this fraction increased to 31% during hypoxic challenge (Edelstone & Rudolph 1979; Bracci et al. 2006; Limperopoulos 2009) Both of these studies reflect redistributional preferences to the brain during hypoxaemia and acidosis. Clinical obstetrics has taken advantage of such 'brain-sparing' mechanisms, and uses the increased diastolic blood velocity recorded in the middle cerebral artery as a marker of compensatory redistribution of blood to the brain (Nathanielsz & M. A. Hanson 2003; Kok et al. 2002; Licht et al. 2009)

	% of combined cardiac output at gestational age		
	20 weeks	**30 weeks**	**38 weeks**
Combined cardiac output	210 (ml/min)	960 (ml/min)	1900 (ml/min)
Left ventricle	47	43	40
Right ventricle	53	57	60
Foramen ovale	34	18	19
Lungs	13	25	21
Ductus arteriosus	40	32	39

Table 2. Combined cardiac output and distribution in human fetuses during the second half of pregnancy according to Rasanen et al.

Fetoplacental circulation

In the fetal sheep, 45% of the CCO is directed to the umbilical arteries and placenta (T Kiserud 2001; Torvid Kiserud & Ganesh Acharya 2004) .This percentage is less in exteriorized human fetuses, but it increases from 17% at 10 weeks to 33% at 20 weeks of gestation. These results overestimate the placental fraction as the CCO calculation was based on systemic venous return, not including the pulmonary venous return. Secondly, the measurements were not performed under strict physiological conditions. Doppler studies of low-risk pregnancies have found similar results; one-third of the fetal CCO is directed to the placenta at 20–32 weeks of gestation, (Erkinaro et al. 2009; Yigiter et al. 2011; A. O. Odibo et al. 2011) but this decreases to approximately one-fifth beyond 32 weeks of gestation (Negrini et al. 2011).

The introduction of Doppler ultrasound made it possible to assess umbilical venous blood flow (Maria Bellotti et al. 2004; Jörg Kessler et al. 2008), in the human fetus in-utero. Recent longitudinal observations in low-risk pregnancies have found that the umbilical blood flow increases from a mean of 36 ml/min at 20 weeks to 265 ml/min at 40 weeks of gestation (K Flo, T Wilsgaard & G Acharya 2010) Umbilical flow normalized for fetal weight is at its highest (117 ml/min/kg) at 25 weeks and at its lowest at 41 weeks (63 ml/min/kg) of gestation. The fact that human umbilical flow is considerably lower than that in the fetal sheep is

not disconcerting as fetal sheep have a higher growth rate, a higher temperature and a lower Haemoglobin.

Resistance to flow is mainly determined by the peripheral vascular bed of the placenta. This vasculature has no neural regulation and catecholamines have little effect on the vasculature. Endothelin and prostanoid have a constricting effect and nitric oxide has a vasodilatory effect (P. Vallance et al. 1989), but the exact role of humoral regulation is not fully understood. Placental blood flow has been found to be fairly stable and chiefly determined by arterial blood pressure (Odeh et al. 2011) The substantial increase in the vascular cross-section during late gestation accounts for a reduction in impedance and the corresponding fall in umbilical artery pulsatility seen in longitudinal studies. Placental vasculature is believed to account for 55% of the umbilical resistance. The waveform recorded by Doppler measurement in the umbilical artery reflects this downstream impedance and is used extensively to identify placental compromise.

Watershed areas and the compromised circulation

The watershed area in the brain circulation has long been used to explain certain lesions of neonates, and a concept of a watershed at the isthmus of the aorta, the left portal vein and the foramen ovale with its crista dividens has been proposed recently.

It has long been known that fetuses with critical aorta stenosis or hypoplastic left heart syndrome direct ductus arteriosus blood in a retrograde direction through the isthmus aortae to feed the aortic arch. Recent studies have highlighted the isthmus aortae as a watershed between the aortic arch and the ductus arteriosus in anatomically normal fetuses. Since this watershed also reflects the difference in impedance between the cerebral circuit and that of the placenta and lower fetal body, the blood velocity pattern across the isthmus with various degrees of reversed flow was suggested to be an indicator of placental compromise.

Similarly, the direction of flow in the left portal vein is suggested to reflect compromised venous return demanding a compensatory increase of blood from the main portal stem to maintain portal and umbilical pressure, with the result being a cessation of umbilical venous flow to the left portal branch, and, at a more advanced stage of compromise, reversed flow that permits splanchnic blood to enter the ductus venosus.

A third watershed, the foramen ovale, differs from the two former watersheds. It distributes blood to the left and right atria by dividing the ascending venous blood into two arms at the crista dividens. The horizontal area between the foramen ovale valve and the atrial septum is thought to be the restricting area for flow to the left atrium. In cases with increased venous return (e.g. arteriovenous malformation), an increased volume of blood is diverted to the right side, leading to increased growth of

the right ventricle. In cases of abnormally small foramen ovale, the left side of the heart develops less in size (one of the possible mechanisms leading to hypoplastic left heart syndrome).

These concepts are in need of detailed studies to make them clinically relevant.

Circulatory regulation

Circulatory responses to hypoxaemia and hypovolaemia have been particularly well studied in animals during the last trimester of pregnancy, but even during mid-gestation and earlier, there seem to be neural and endocrine responses in addition to the prominent direct effect on cardiac function caused by hypoxic insults. A hypoxic insult in late pregnancy activates a chemoreflex mediated by the carotid bodies (and, to a lesser extent, the aortic bodies), causing an immediate vagal effect with reduced heart rate and a sympathetic vasoconstriction. This is followed by endocrine responses (e.g. adrenaline and noradrenaline) maintaining vasoconstriction (α-adrenergic), increasing heart rate (β-adrenergic) and reducing blood volume with renin release and increased angiotensin II concentration. The responses involve angiotensin–vasopressin mechanisms, and increased concentrations of adrenocorticotrophic hormone, cortisol, atrial natriuretic peptide, neuropeptide Y and adrenomedullin orchestrate a circulatory redistributional pattern that

maintains placental circulation and gives priority to the adrenal glands, myocardium and brain. In clinical medicine, this translates into a frequently visualized coronary circulation, a shift in left–right ventricular distribution, a cerebral circulation with high diastolic flow, and increased impedance in the pulmonary circulation during circulatory compromise.

Sustained hypoxia forces an adaptational shift to less oxygen demand, reduced DNA synthesis and growth, with a gradual return towards normal concentrations of blood gases and endocrine status, although with a residual deviation that may have a longlasting effect on fetal and newborn life. There is an increasing awareness that even subtle differences in the development of autocrine, paracrine, endocrine and metabolic functions induced by nutritional or circulatory variations during pregnancy could have lasting effects with increased risks of cardiovascular and endocrine diseases in adult life. This concept is currently known as fetal programming (J. Robinson et al. 1995; Myatt 2006; Murphy et al. 2006; Thomas Jansson & Powell 2007; K. M. Godfrey 2002; E Angiolini et al. 2006; C. P. Sibley et al. 2010; Ionel Sandovici et al. 2012).

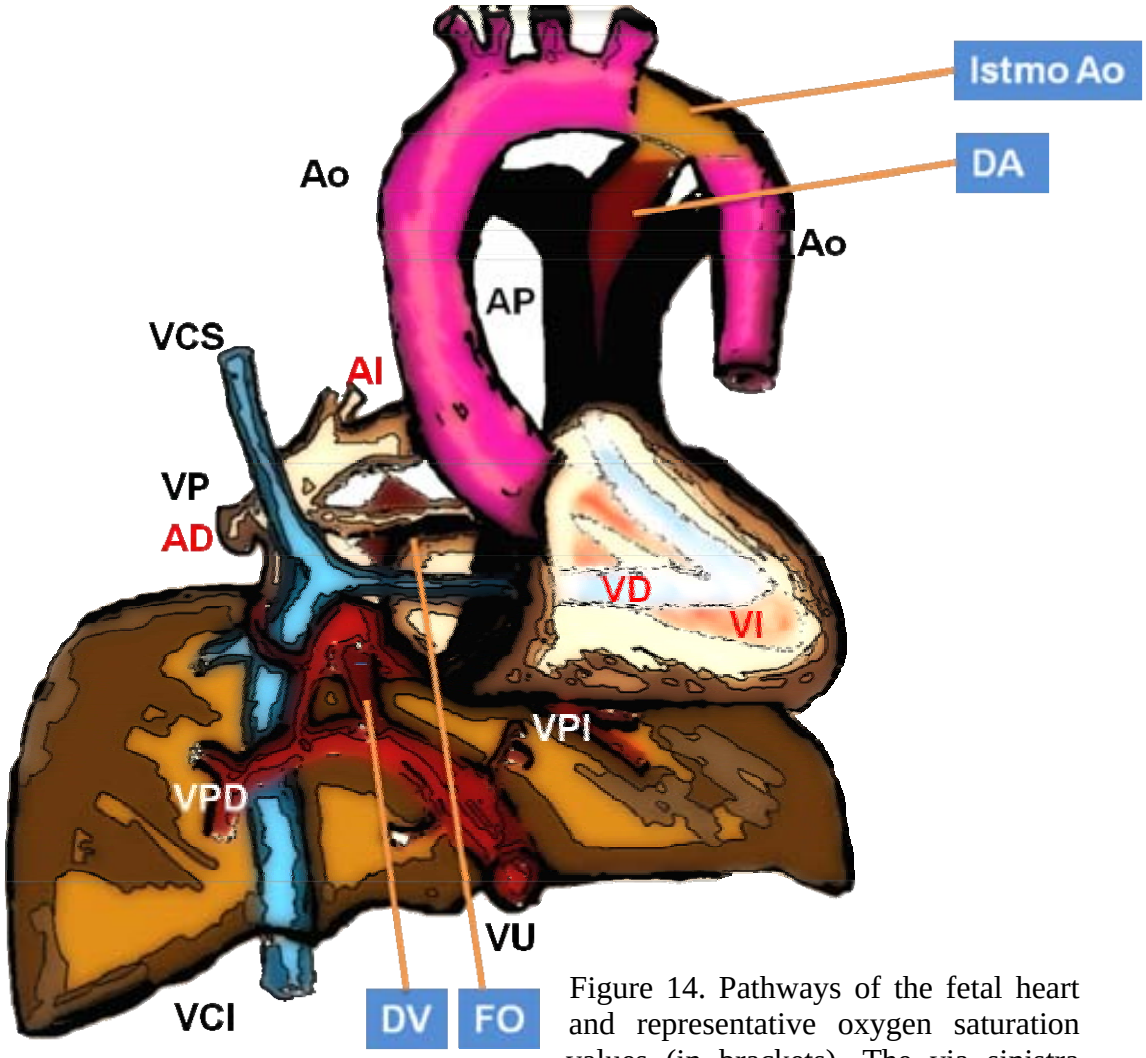

Figure 14. Pathways of the fetal heart and representative oxygen saturation values (in brackets). The via sinistra (red) directs well-oxygenated blood from the umbilical vein (VU) through the ductus venosus (DV) (or left half of the liver) across the inferior vena cava (VCI), through the foramen ovale (FO), left atrium (AI) and ventricle (VI) and up the ascending aorta (AO) to reach the descending AO through the isthmus aortae. De-oxygenated blood from the superior vena cava (VCS) and VCI forms the via dextra (blue) through the right atrium (AD) and ventricle (VD), pulmonary trunk (AP) and ductus arteriosus (DA). CCA, common carotid arteries; FOV, foramen ovale valve; LHV, left hepatic vein; LP, left portal branch; MHV, medial hepatic vein; MP, portal main stem; PV, pulmonary vein, RHV, right hepatic vein; RP, right portal branch. Copied and modified with permission from ref

2.1.2. The suspected changes

Redistribution has been defined as a shift in the proportional contribution of individual ventricles to the total cardiac output (A A Baschat 2006). When the relative contribution of the left ventricle rises, a higher proportion of nutrient-rich blood is channeled towards the myocardium and the upper body and brain through the brachiocephalic circulation. This concept could be considered as an oversimplification. Firstly, the physiological distribution of nutrients from the placenta places essential organs in a serial order (liver, myocardium, brain and placenta). Secondly, partitioning of nutrients also occurs at successive levels in the circulation (ductus venosus, foramen ovale, aortic isthmus, umbilical arteries). Finally, individual essential organs serve different roles in the human fetus and autoregulatory adjustments of organ perfusion have been reported for the liver, heart, and brain, and postulated for the placenta (al-Ghazali et al. 1989; Michael Tchirikov et al. 2010). These organ-sparing effects are also invoked in a sequential manner with advancing fetal compromise. It therefore appears worth considering the fetal circulation as a serial unit distinguishing between venous redistribution, arterial redistribution and individual organ-sparing effects.

Venous redistribution

The shunt dynamics in the ductus venosus–left portal vein system are responsive to umbilical venous nutritional content, decreased umbilical venous volume flow and marked elevations in placental blood-flow resistance (M Tchirikov et al. 2006). An unbalanced maternal diet in women with low body-fat content is associated with a decrease in ductus venosus diameter and increased umbilical venous diversion to the liver. On the other hand, a reduction in umbilical venous volume flow results in ductal dilation and increased umbilical venous diversion, maintaining overall ductus venosus contribution to the heart. The exact mechanisms that regulate these adjustments in ductus venosus diameter are under investigation (Mikhail Tchirikov et al. 2005; Bello□Muñoz et al. 2009; A A Baschat et al. 2012). With increased ductus venosus shunting towards the heart, marked reversal of flow in the left portal vein towards the ductus venosus may be observed. This suggests that the ductus venosus may receive a variable admixture of depleted splanchnic blood due to left portal shunting.

To summarize, venous redistribution potentially affects the nutritional supply of all downstream organs. If diversion to the liver is increased, ductus venosus contribution of nutrient-rich blood to the left ventricle decreases. If diversion towards the heart increases, volume flow may be

maintained, or increased. The proportion of portal shunting towards the ductus potentially alters the nutritional content of this bloodstream. Assessment for venous redistribution could therefore prove critical in the study of fetal programming and to refine our assessment of arterial redistribution.

Arterial redistribution

Arterial redistribution occurs at the level of the foramen ovale and the aortic isthmus. An increase in pulmonary vascular resistance, as may be observed in fetal growth restriction, increases intracardiac right-to-left shunting through the foramen ovale into the left ventricle. Therefore, there is a rise in the contribution of blood with higher nutritional content from the ductus venosus to left ventricular filling. Elevation of blood-flow resistance in subdiaphragmatic and placental vascular beds or a decline in brachiocephalic impedance impact at a cardiac level and in the aortic isthmus (J.-C. Fouron et al. 2009; R Cruz-Martinez, F Figueras, Benavides-Serralde, et al. 2011). This relative rise in right ventricular afterload promotes right-to-left shunting through the foramen ovale. At the aortic isthmus, diastolic reversal of blood flow indicates increased diastolic diversion of blood originating from the right ventricle towards the brachiocephalic circulation. The overall effect of these central adjustments in shunting is additive. The relative increase in left ventricular output

enhances myocardial and brachiocephalic perfusion, while aortic isthmus shunting supplements cephalic diversion of blood as long as the net flow of systolic and diastolic forward velocities is forward. When the net flow in the aortic isthmus becomes retrograde, the central shift of cardiac output towards the left ventricle is no longer observed. It has been suggested that the nutrient and oxygen content of the left ventricle drops under these circumstances; this is supported by the increased risk for adverse childhood neurodevelopment in fetuses that exhibit net reversal of aortic isthmus blood flow (J. C. Fouron et al. 2001). Distal to the confluence of the ductus arteriosus and aorta, ongoing perfusion of the placenta is critical to maintain adequate nutrient exchange. Marked elevation in blood-flow resistance in the pelvis and lower extremities favors diversion of blood flow towards the umbilical vessels. This mechanism may play a role in preserving placental perfusion in severe placental insufficiency (K. Mäkikallio et al. 2003; Uerpairojkit et al. 2012).

Venous and arterial redistribution can only be effective as long as adequate forward cardiac function can be maintained. In severe placental insufficiency with marked elevations of placental afterload and/or myocardial dysfunction, central venous pressure becomes elevated as forward cardiac function declines(Michael Tchirikov et al. 2010; Simioni, Nardozza, Araujo Júnior, Liliam Cristine Rolo, et al. 2011; Uerpairojkit et al. 2012). Facilitated retrograde transmission of the atrial pressure pulse

through a dilated ductus venosus, with a subsequent decline in the a-wave, is observed under these circumstances. The contribution of the ductus venosus to left ventricular filling may decrease under these conditions. On the arterial side of the circulation, forward cardiac function may become insufficient to maintain net antegrade flow in the aortic isthmus. Under these circumstances, intracardiac right-to-left shunting becomes inefficient and arterial redistribution does not occur. Individual organ-sparing effects may therefore be invoked at any time when local organ perfusion becomes insufficient.

Organ-sparing effects

Local autoregulatory vascular adjustments that control organ perfusion are of three principal types. The first type acts synergistically with venous and arterial redistribution to augment organ blood flow. The second type counteracts an 'organ-steal effect' that may occur as a result of redistribution. The third type is relatively independent of redistribution, because the vascular beds supplying the organs arise distal to the ductus arteriosus and therefore are little affected by redistribution. Of the local organ-sparing effects, brain sparing is the longest recognized in the human fetus, while heart, liver and adrenal sparing (A. A. Baschat et al. 2002; G. Haugen et al. 2005) were described more recently.

Heart and brain sparing act synergistically with venous and arterial redistribution

The heart is the driving force of the fetal circulation and also has a unique metabolic role, since myocardium can metabolize lactate and may remove up to 80% of circulating lactate under certain conditions(Wolfberg et al. 2007). The brain has similar metabolic capacities, as it can switch its major fuel source from glucose to ketone bodies, which is advantageous during fetal starvation (Cerf et al. 2010). Both of these organs derive their blood supply from the left ventricle. Venous redistribution towards the heart and arterial redistribution through the foramen ovale and aortic isthmus lead to increased diversion of blood towards these organs. Vasodilatation at the organ level acts synergistically to increase organ blood flow.

Heart sparing may be acute, chronic, or acute-on-chronic. Acute coronary vasodilatation in response to myocardial ischemia may recruit a myocardial flow reserve of approximately four times the basal flow. Chronic heart sparing is due primarily to redistribution. Acute-on-chronic heart sparing occurs with advanced cardiovascular deterioration. As chronic hypoxia induces coronary angiogenesis, massive augmentation of the coronary blood flow (up to 12-fold greater than the basal flow rate) can be triggered if acute myocardial hypoxia supervenes.

Brain sparing as a result of cerebral vasodilatation results in a decrease in the Doppler index. However, similar Doppler changes are observed with the development of fetal hypertension (Galan et al. 2005). Concurrent examination of the aortic isthmus may be helpful to refine the assessment of the cerebral arterial Doppler changes.

Liver sparing is triggered by 'hepatic steal' due to excessive venous redistribution

The liver is unique because it derives its blood supply from venous and arterial sources. These include the umbilical vein, the splanchnic portal system and the hepatic artery. In prolonged venous redistribution, diversion of umbilical venous blood away from the liver sets up a state of chronic hepatic insufficiency. When placental insufficiency deteriorates further and baseline arterial supply becomes insufficient, hepatic artery vasodilatation is invoked to recruit additional hepatic blood-flow reserve from the arterial circulation. This vascular state is typically associated with hepatic dysfunction in the fetus and a marked deterioration of the acid–base balance. Liver sparing is therefore unique, since, unlike brain and heart sparing, it does not act synergistically with venous and arterial redistribution (G. Haugen et al. 2005) .

Adrenal sparing is less dependent on redistribution

Because the blood supply to the adrenal glands arises after the confluence of the ductus arteriosus and the aorta, redistribution should have little impact on overall adrenal perfusion. It is therefore more likely that the augmentation of blood flow in this organ is due primarily to local autoregulation. (Fatima Crispi & Gratacós 2012)

Experience from the sheep model

Prior observations made in the animal model are increasingly being replaced by human data. However, because our ability for simultaneous assessment of several fetal vascular beds is limited, we still have to rely on animal experiment data. Experience from the sheep model verifies that decreased oxygen delivery through the umbilical vein results in increased diversion of cardiac output to the brain, heart and adrenal glands at the expense of the carcass, skin and scalp. This is achieved through venous and arterial redistribution as described above, and most likely auto-regulatory mechanisms that have not been evaluated concurrently. In this setting, adrenal artery blood flow increases by almost 300%, while myocardial and brain blood flow increase by 120% and 80%, respectively (Michael Tchirikov et al. 2010; Erkinaro et al. 2009; Bello□Muñoz et al. 2010; Morel et al. 2010).

2.2 How do we know what we know?

2.1.1. The experimental models

The vast majority of the physiological data we have, regarding cardiac function and circulatory events has been obtained from animal models (Pemberton et al. 2005; Yamamura et al. 2012). One of the most widely used methods has been to compare the ultrasound obtained data with invasive methods such as direct catheterization or radio-isotopes quantification (E Hernandez-Andrade, T Jansson, et al. 2004; Pardi & Cetin 2006). The chronic as well as the acute changes in such a function have been evaluated by invasive methods, and compared to certain US obtained indexes (Ram et al. 2011; Hashima et al. 2010). The more suitable models for these purposes are primates (Behrman et al. 1970; Hashima et al. 2010) and ovine models, such as the one employed by our group (Ganesh Acharya et al. 2004; Michael Tchirikov et al. 2010; Erkinaro et al. 2009; Bello□Muñoz et al. 2010).

The information obtained from these experimental models is reliable enough as for establishing certain parallelisms with actual fetal cardiac function in human subjects. Nonetheless, these data must be taken carefully as there are substantial differences in the cardiac anatomy of the two species: first of all, the heart of a sheep is bigger than humans and is positioned slightly different in the body. Also, instead of having pulmonary

arteries and veins they have what's called a pulmonary trunk and the top middle of the heart. Also there are two independent umbilical veins draining directly into the inferior vena cava, hence, there is no ductus venosus or something alike draining into the atrial bloodstream. The aortic arch is flat when compared with the hook shape it has in the human and, very likely, some of the shunting functions already described in the human are not that evident among the fetal sheep adaptive mechanisms. (Fatima Crispi & Gratacós 2012; Ganesh Acharya et al. 2008; Michael Tchirikov et al. 2010)

However, the information gathered from invasive tests in these animal models, renders a body of knowledge far more reliable than the data obtained from repeated observations in, either, healthy or compromised human subjects. Its utility remains in the possibility of assuring the researcher that, the findings in a physiological situation are sustained by reliable measurements and, hence, the changes witnessed under artificially generated adverse conditions are true (Staboulidou et al. 2007; Michael Tchirikov et al. 2010; N W Jones et al. 2009; Uerpairojkit et al. 2012).

Chapter 3. The Experiment

3.1 Materials and Methods

3.1.1. The Cardiac Output Model

Based on previous studies and encouraged by the works of Richards & Kripfgans, we decided to develop an algorithm of flow calculation, based on surface integration of velocity vectors and time frame sequences from STIC volumes. Volume datasets as obtained by the ultrasound machine Medison Accuvix V-20 prestige with a Medison 3D4-8ET 3D volumetric probe (Samsung Medical Co, Hoofddorp, Nz).

A total of eight fetuses from near term pregnant sheeps (125-140 days) were exteriorized through a cesarean section and a modified central catheter inserted via umbilical cord and under direct echographic vision. An arterial line was also inserted in one of the umbilical arteries. Both transducers from the catheters were connected to a PICCO monitor for invasive testing (PULSION Medical Inc. Irving TX, USA). Continuous measurement of combined cardiac output was the registered as long as the experiment was carried out, meanwhile one of the authors (JB-M), recorded several volume datasets synchronizing the register of the data

set with data obtained by monitorization. Analysis of all the data was made offline.

A complete spreadsheet of physiologic registers from the experimental subject was recorded for comparison and external validation of calculations. All images were processed by using the Mathematica ® software (Wolfram Research Europe Ltd., Oxfordshire, UK). All data from VOI analysis was addded to the calculation spreadsheet and a polinomial regression fit model was designed for testing the smoothness of the numeric register.

3.1.2. Mathematical Approach to the Phenomena

The mathematical background of this study was based on flow calculation:

$$Q = \sum_{ie\,S} (v_i \cdot a_i)\ p_i\ . \tag{20}$$

And the concept of vector velocity profile described above. But with the adittion of a time frame provided by the STIC algorithm, which means a continuous sum of velocity profiles, giving us a new profile of the area, represented as:

$$(1+A)^n = 1 + \frac{Ax}{1!} + \frac{A(n-1)x^2}{2!} + \cdots \tag{21}$$

And to the velocity profile, expressed also as

$$\sum\ vi(t1) + vi(t2) \ldots \ldots vi()tn \tag{22}$$

Where N is the entire amount of frames included in a cardiac cycle.

Once collected the sequences, information of velocity vector profile (VVP) form the VOI was collected in a series of frames, from the starting of the cardiac cycle (early start of diastole), denominated as t_0 until the end of same cycle (end of systole) hence called t_n. Information of VVP was then modified according to area variation in every frame. Therefore, the mathematical expression of this phenomenon could be expressed as a matrix of data: (23)

$$\sum_{t=1}^{N} Qn = \Big((A1.vi1)t1 \vdots (A2.vi2)t1 \vdots \cdots \vdots (Ax.vix)t1 \vdots (A1.vi1)t2 \vdots (A2.vi2)t2$$
$$(Ax.vix)t2 \vdots (A1.vi1)tn \vdots (A2.vi2)tn \vdots \cdots \vdots (Ax.vix)tn\Big)$$

Where A_x is an estimated area obtained by adding all the regional areas in the VOI and vi_x is the velocity vector profile in each sub-area, according to, previously described, sectorial variations in velocity. And t is the timeline described above.

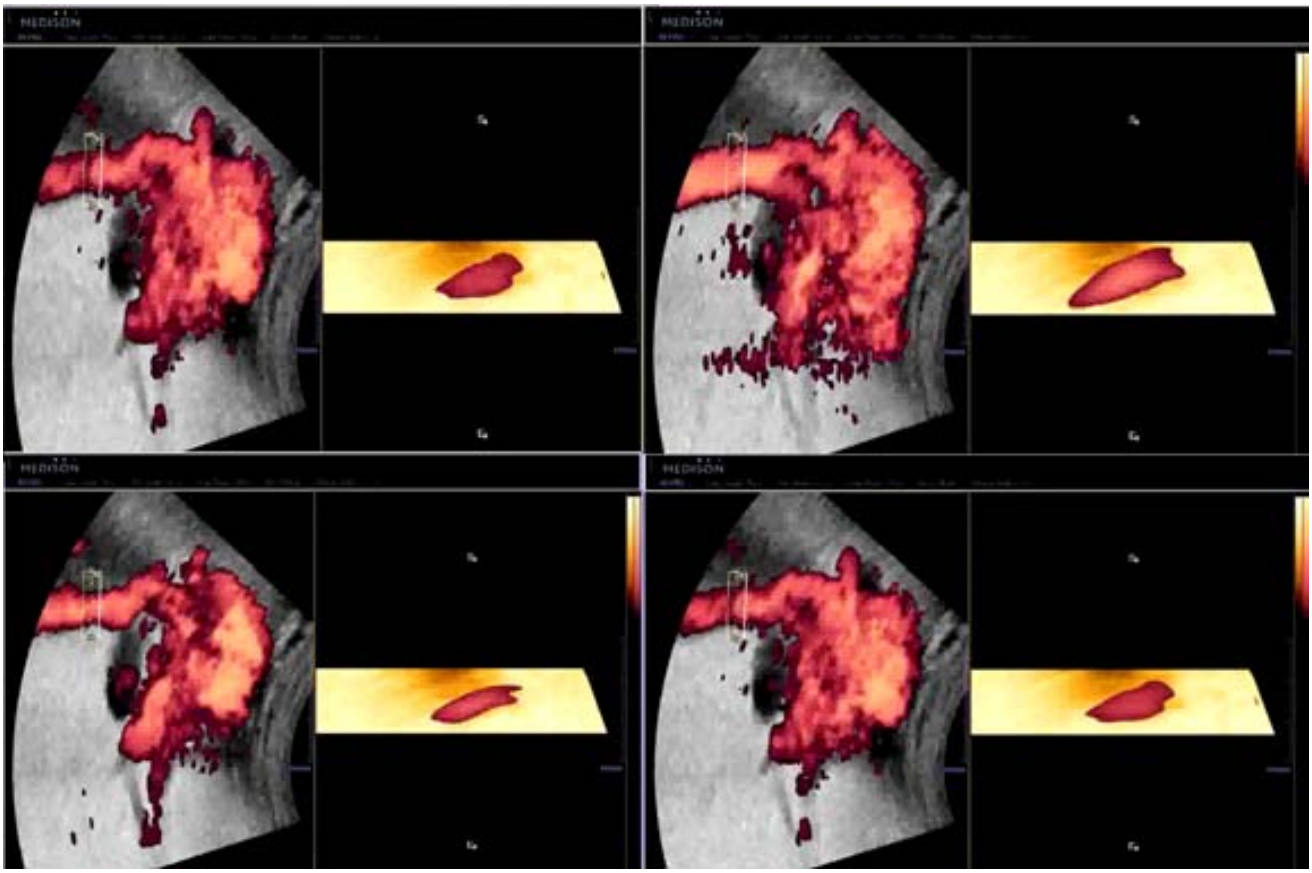

Fig. 15. Screen snapshot of descending aorta plane with selected volume of evaluation. Right side of the image is the VOI containing the $v_1 \ldots . v_n$ information. A set of voxels like this one was added to the matrix, since t_1 till t_n where n=end of the cardiac cycle. (Actual experiment added measurements from the aortic isthmus, this image is for illustrative purposes).

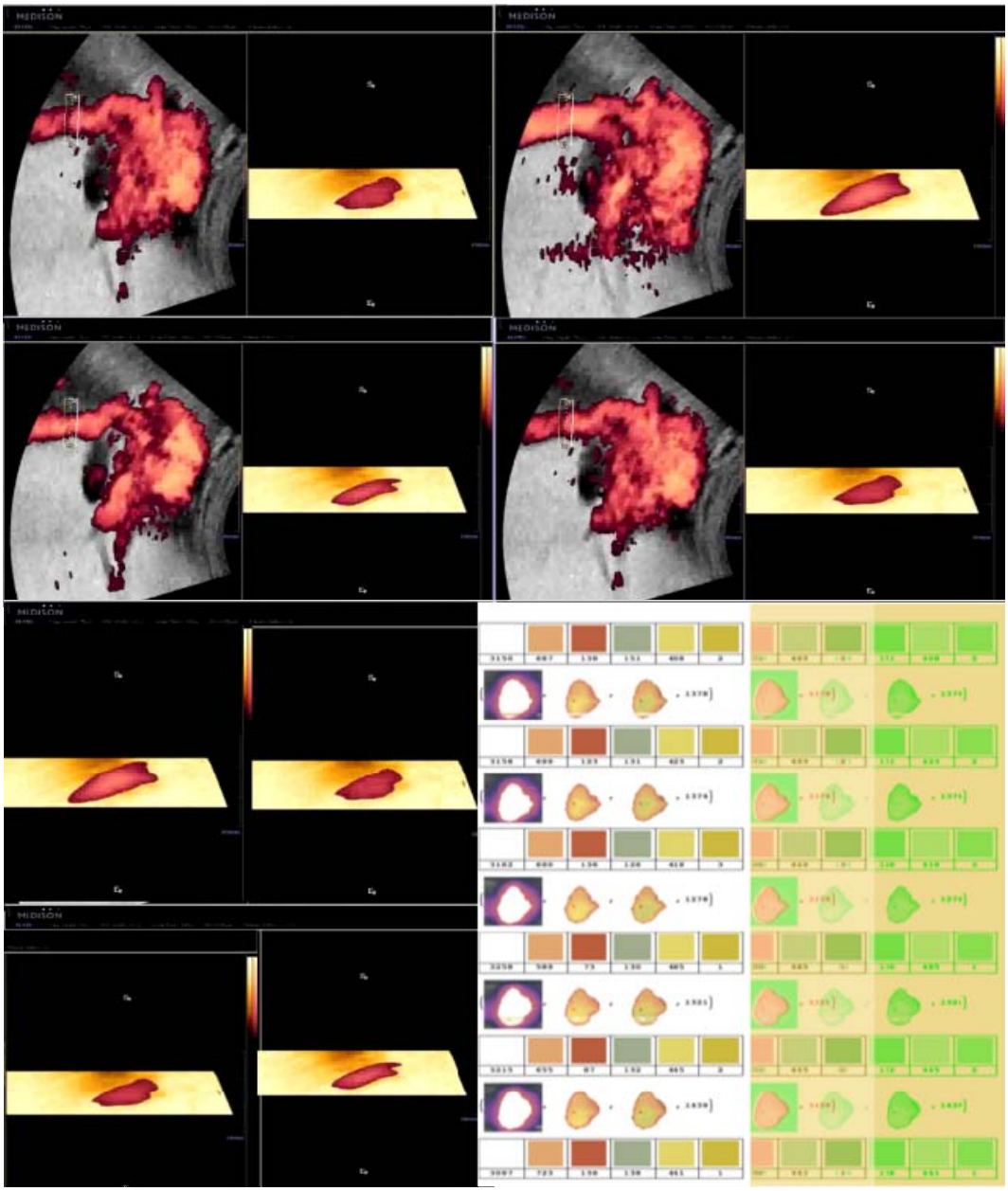

Fig. 16. Color deconvolution algorithm as delivered by the Mathematica software ®

The mathematical background of this study was based on flow calculation:

$$Q = \sum_{i \in S} (v_i \cdot a_i)\, p_i \,. \qquad (24)$$

And the concept of vector velocity profile described above. But with the addition of a time frame provided by the STIC algorithm, which means a continuous sum of velocity profiles, giving us a new profile of the area, represented as a Fourier sequence:

(25)

$$Q(t) = Q_M + \sum M_n sen(n\omega t + \phi_n)$$

Our aim is to represent the fetal blood flow dynamics by using STIC, which gives us a sequence of progressive stages during the cardiac cycle. Thus, every image with a Ω(t) value with a t=1,2,3,….,n carries a set of color intensity values that correlate somehow with the actual velocity of the fluid at the exact moment the image is acquired.

As a first step, it was necessary to draw a ROI and to segment the color voxels by decomposing the RGB signal into binaries and rendering again the deconvoluted color information. This process delivers two channels of information:

- The number of voxels included in the width of the ROI,which permits to extrapolate the value of the cross sectional area of the vessel $A_t(t)$ in every image of the sequence i= 1,2,…,m.
- An approach to the time average mean velocity $V_t(t)$ (area under the curve of the signal), extrapolated from the color signal scales

These data lead to the next proposition

$$\sum_{i=1}^{m} C * A_i(t) * v_i(t) = C * A_T(t) * \bar{v}(t), \tag{26}$$

Being A_i (t) the total Area for every (t), and $v_i(t)$ the velocity profile information for every (t)

Where C represents a constant derived from the signal insonation angle, flow density constants (to be experimentally established, but meaningless for the application).

The equations' system could be simplified as:

$$\mathbf{A} * \vec{v} = \vec{Q}_M$$

(27)

Where $\vec{v}$ = is the velocity vector

$\mathbf{A}$ Is a *n*m* matrix that contains the area information for the *m* streams evaluated in a *n* number of sequenced volumes

and $\vec{Q}_M$

Is a composed vector where every component represents the mean average flow calculated for every sequenced volume.

Thus, for achieving a solution for this matrix it is necessary to fulfil two conditions:

1. That the A matrix could be reduced to an inverted matrix A' with n'*m' components

$$\vec{v} = (\mathbf{A}')^{-1}\vec{Q}'_M. \quad (28)$$

2. That the number of streams (*m*) and the number of sequenced volumes (*n*), fulfil the condition n>*m.*

So, as a part of the validation experiment, and having as known the actual value of Q and V in the aortic isthmus, we developed a mathematical model for simulating the cardiac output by using the values obtained from

the matrix of equations previously described. Figure 12 shows the way we integrate a Medison predefined function in our protocol (to “cut” a 2mm length cylinder in the ROI). And figure 13 shows the application as we have developed it in a Mathematica ® platform.

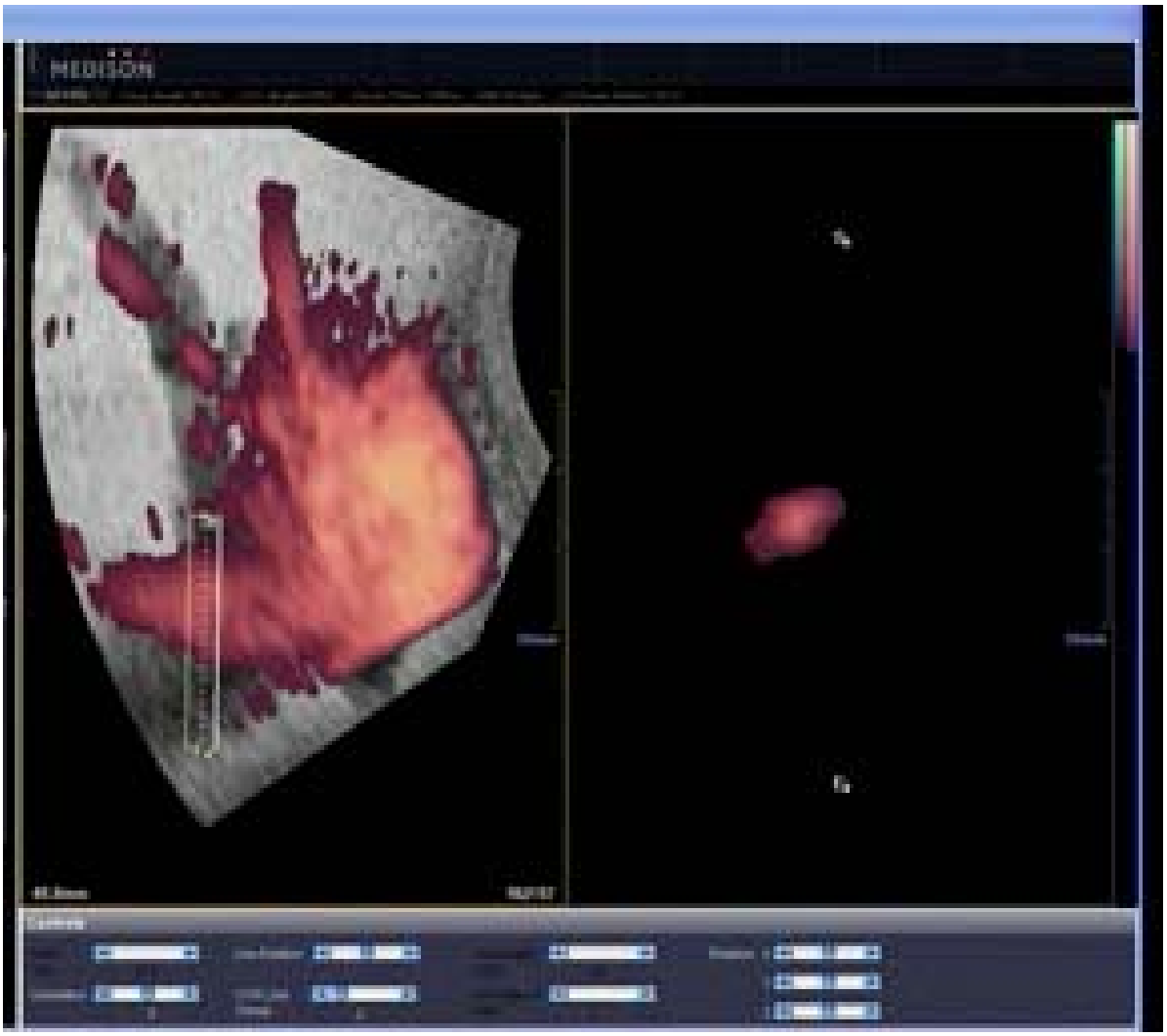

Fig. 17. Screen snapshot of descending aorta plane with selected volume of evaluation. Right side of the image is the VOI containing the $v_1 \ldots v_n$ information. A set of voxels like this one was added to the matrix, since t_1 till t_n where n=end of the cardiac cycle. (Actual experiment added measurements from the aortic isthmus, this image is for illustrative purposes).

Fig. 18. Colour deconvolution algorithm as delivered by the Mathematica software ®

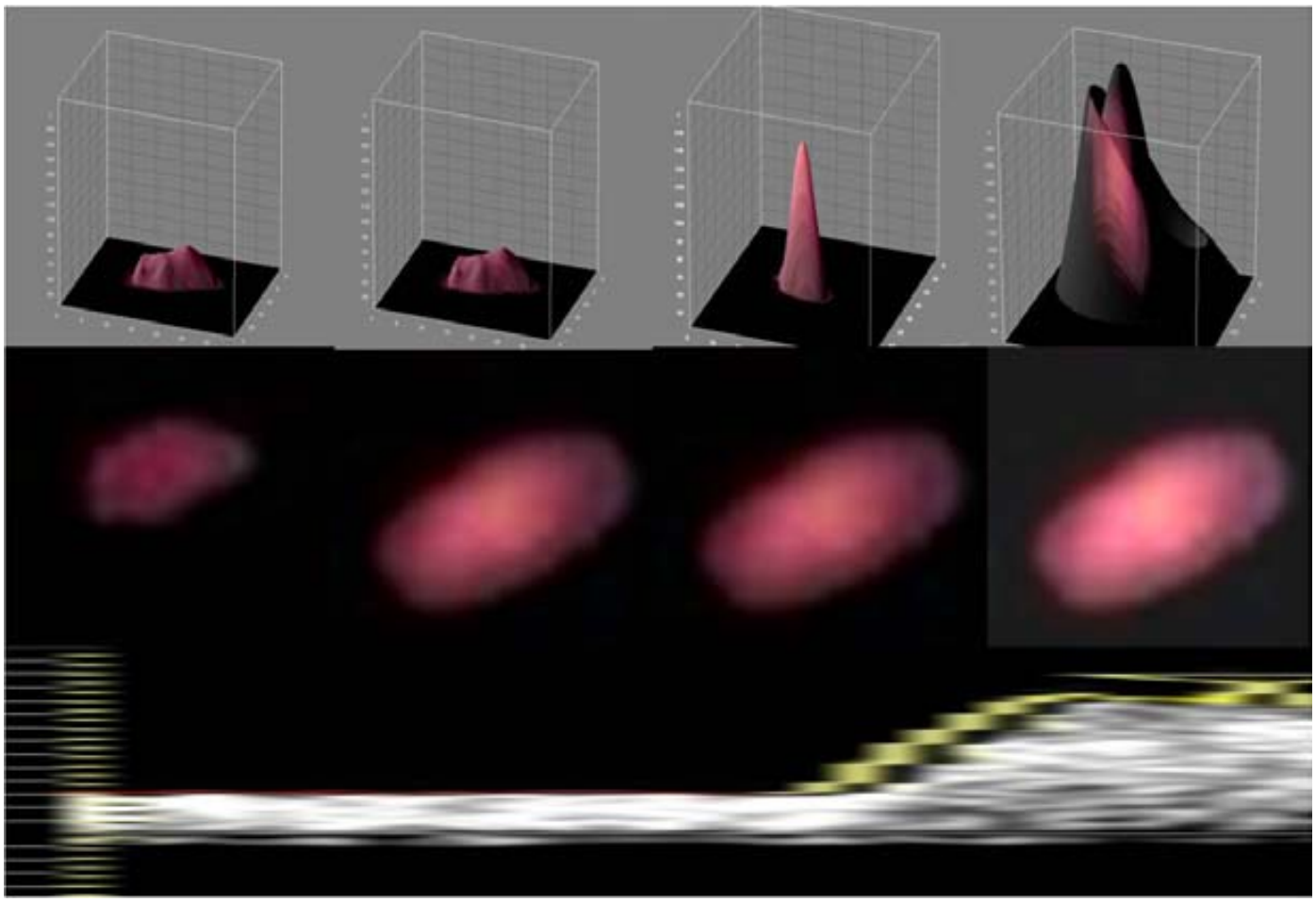

Fig 19. Cardiac cycle values as obtained from the different sequences, CCO was traced as an Area Under the Curve

The next step, which has become already the body of this thesis, was to develop a mathematical modelling process, based on simulations for random processes, to “draw” a pulsatile flow whose values could correlate with the actual flow in the ROI. This process has been pre-registered as VOLUME PERFUSION INDEX (VPI) as a potential for a patent by the Institut de Recerca Vall d’Hebron. (Appendix 2)

3.1.3 The In Vitro Test

The test device consisted of a flow phantom and gear pump, blood-mimicking fluid (BMF), and one ultrasound test tank system designed specifically for the experiment. The ultrasound test tank, containing tissue-mimicking material (TMM), and a variety of vessel orientations and arrangements, was insonated using power Doppler ultrasound and 3D-STIC datasets which were acquired over a range of flow rates, erythrocyte mimic concentrations and different depths in a series of experiments. All ultrasound settings were kept constant throughout the experiment to eliminate their effect on the power Doppler signal, and to ensure that any variation in the vascular indices related to differences between the test systems and experimental designs.

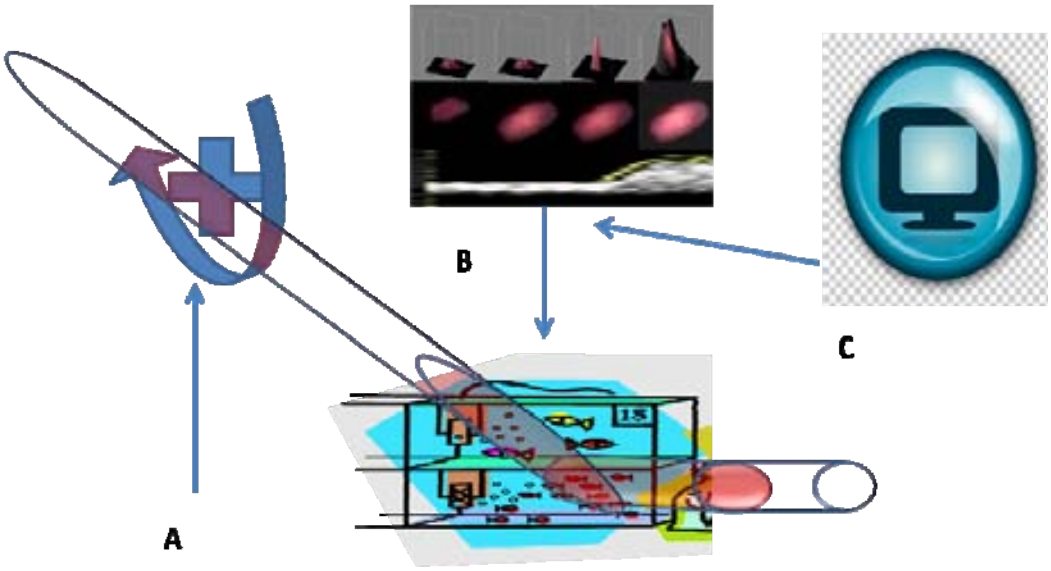

Figure 20. The 'flow phantom' and associated test device components: A) computer-controlled gear pump was used to circulate the blood-mimicking fluid through a closed circuit, incorporating a Windkessel, and through a test tank. B) A test tank filled with tissue mimicking material and vessel mimicking siliconized tubes. C) An ultrasound machine registering the movement generated information

Flow phantom test device components

A computer-controlled gear pump was connected to each ultrasound test tank via a series of connecting tubes, incorporating a Windkessel, to create a closed circuit The gear pump was used to circulate a BMF through this system in a continuous loop.

The motor used was a geared pump with electromagnetic coupling that produced flow which varied according to the voltage applied (Integra series micropump (EG130-0036), Micropump Corporation, Vancouver, WA, USA). Both continuous and pulsatile flow patterns may be achieved, with the latter varying between relatively simplistic square waves and waves that mimic flow seen within the carotid artery. For the purpose of these studies a pulsatile flow rate was used throughout. The true flow rate of the BMF was calculated by breaking the circuit and collection of the BMF into a measuring cylinder of known weight over a set amount of time.. The cylinder and collected fluid were then measured and the initial weight subtracted to calculate the weight of the collected fluid (with a well known density of 1.037 g/cc). This was repeated five times for each flow rate over the complete range of rates used in the study and the mean value used.

Reservoir and circulatory system : A 1-L capacity bell jar was filled with BMF, which was then pumped through the flow phantom to the test tank before returning to the jar. The system was closed with the BMF being

returned into, and beneath the surface of, the BMF within the reservoir to prevent the formation of air bubbles. Before each experiment the pump was activated and the BMF allowed to flow through the system for 30 seconds to expel any air bubbles that had formed and allow an even distribution of the fluid. Silicone rubber tubing was used to connect the system, which contained two independent limbs in parallel. One limb led to the test tank to be insonated and the other acted as a bypass limb, which returned directly to the reservoir. The overall flow rate was controlled in this limb through the application of a clamp. A Windkessel was included before the division into the two limbs. This smoothed the action of the pump and allowed the maintenance of a constant pulsatile flow within the system.

The tank used for the experiments consisted of a perspex box (25 × 30 × 12 cm) with a 0.8-mm thick C-flex™ tube of 4 mm in diameter (Cole-Palmer, Vernon Hills, IL, USA) running horizontally through the center of the tank and fixed at a constant depth. This test tank was used for assessment of the effect of velocity, erythrocyte mimic concentration and change in ultrasound settings. The tank was filled with an agar-based TMM and were constantly sealed from the atmosphere when not in use. The composition (% weight) of the TMM was 82.97% water, 11.21% glycerol, 0.46% benzalkonium chloride, 0.53% 400-grain silicon carbide (SiC) powder (Logitech Ltd, Glasgow, UK), 0.88% 0.3 μm aluminum oxide

(Al_2O_3) powder (Logitech Ltd), 0.94% 3 μm Al_2O_3 powder (Logitech Ltd) and 3.00% Struers agar (Merck Eurolab, Roskildevej, Denmark). These components were prepared, mixed in a double boiler, heated to 96 °C and then maintained at 96 °C (± 3 °C) for 1 h, mixing continuously with a stirring rod. The solution was allowed to cool to 42 °C, while being stirred continuously, and finally poured into the test tank. All the procedures mentioned in the presente protocol have been previously tested and successfully tested by professor Raine Fenning in an already published experiment (N J Raine-Fenning et al. 2008a; N J Raine-Fenning et al. 2008b)

The BMF was based on a suspension of nylon particles (Orgasol™; 2001UDNAT1 Orgasol, ELF Atochem, Paris, France). The standard solution was made by mixing 1.82% 5-μm Orgasol particles with 83.86% pure water, 10.06% glycerol, 3.36% Sigma D4876 dextran 185 kDa (Sigma Ltd, Poole, UK) and 0.9% ICI synperonic N surfactant by weight (Merck Ltd, Glasgow, UK). This solution was mixed thoroughly for 2 h and then poured through a 32-μm sieve. The resulting solution has been shown to be stable, with backscatter properties that approximate real blood, and to be within International Electrotechnical Commission requirements.

All data were acquired with a Medison Accuvix V-20 prestige with a Medison 3D4-8ET 3D volumetric probe (Samsung Medical Co, Hoofddorp, Nz).. The probe was held in position at 90° to the surface of each ultrasound test tank, and in contact with the TMM, by a clamp attached to a retort stand to ensure that there were no inappropriate movements of the probe during data acquisition. The 'flow phantom' was commenced and after a steady flow rate had been achieved, for a minimum of 30 seconds, a central 2D view of the vessel(s) was obtained by moving the clamp stand. Power Doppler was then applied and the volume mode activated to generate a truncated sector defining the area of interest. The angle was set to 40° to ensure that a complete volume was obtained and a 3D-STIC dataset was acquired using the medium sweep mode, as is used in the clinical setting. The acquired volume was stored to a magnetic optical disk and subsequently sent to a personal computer via a dedicated DICOM (Digital Imaging and Communications in Medicine) link. Medison-Sonoview® (Samsung Medical Co, Hoofddorp, Nz) software was used by the personal computer to receive and store the volume datasets and for part of the subsequent data analysis.

The power Doppler settings were specifically maintained for all experiments as follows: medium central frequency, quality 9, density 8, reject 82, signal rise 0.4, signal persistence 0, frame rate 12.9, wall motion

filter 70 Hz, pulse repetition frequency 1.6 kHz, power 4 dB and color gain 36.8. All the image filters provided by the machine were de-activated (MR image, speckle reduction and cross beam reduction) The STIC setting were established as sweep angle 25º, acquisition time 7 seconds, frame rate 35 fps. These settings were chosen as they reflected those used in the clinical setting and allowed the best possible registration of the signal.

In order to achieve quantification in a repeatable way, we used part of the tools in the Sonoview® software provided by the machine. Two plug-in named “Oblique view” ® and “OVIX” ® which allowed us to, in order to maintain the same degree of consistency, generating a 3D ‘rectangular sampling box’ that was applied over the midpoint of the vessel. As indicated by a central point on the screen, and by maintaining a constant magnification of 1.1; this VOI was found to fit perfectly such that the vessel and its wall were just enclosed. This allowed the user to define an orthogonal VOI, with a 2mm length cylinder included whose dimensions may be modified manually relative to the object of interest but were always set at 2mm. To ensure that a consistent VOI was selected for each dataset, predetermined criteria were set according to the experiment under consideration All datasets were stored, transferred and subsequently measured in the same manner with no manipulation of the display. Because the relationship between the transducer and test tank was

maintained at 90°, the vessel was always located centrally and horizontally within the final dataset.

The power Doppler signal within each dataset was evaluated by applying the histogram facility in a volume defined by Virtual Organ Computer-aided AnaLysis (VOCAL: Samsung Medical Co, Hoofddorp, Nz). VOCAL allows the user to automatically define a sphere of variable size that can be applied within any 3D dataset to sample the Doppler signal within it. For these experiments a spherical volume of 0.9 cm^3, defined by a diameter of 1 cm as estimated from the sphere volume ($\pi D^3/6$, where D = diameter), was used to serially sample each dataset from the proximal to the more distal part. The fixed size of the sphere allowed assessment of the gain adjustment from the surface, at depths of 0–1 cm, to the more distant aspect of the dataset Owing to the nature of the experiments and the different designs employed we decided to report only the VFI, which is representative of both the VI and FI. The relationship between the VFI and the different settings within each flow-free phantom and with each transducer were represented as plot graphs. The results were plotted for: Bland- Altman intra e interobserver variability, and Intra-Class correlation coefficient with 95% Confidence Interval was calculated.

Offline Analysis of volume datasets: all stored volumes were then analyzed, as previously described, by using the image analysis software provided by Mathematica ® and the voxels intensity information was kept as a matrix of data. The actual velocity profile measurement was stored independently for a further plotting against the estimated calculations. The matrix of color deconvolution values was then inserted into a Matlab suite ® algorithm denominated “least-squares curve fitting“, used for adjusting complex matrix data in linear equations.

The data delivered by the machine was a function whose values were related to relative vectorial velocity values within the VOI and had the form:

$$\min_x \frac{1}{2}\|C \cdot x - d\|_2^2 \text{ such that } \begin{cases} Aeq \cdot x = beq, \end{cases} \tag{29}$$

Where

C Matrix

d Vector

Aineq Matrix for linear inequality constraints

bineq Vector for linear inequality constraints

Aeq Matrix for linear equality constraints

beq Vector for linear equality constraints

lb Vector of lower bounds

ub Vector of upper bounds

x0 Initial point for x

And the VPI is

(Xt -Xo/ Xx)

X value as its maximum register

Xo value is the initial (minimum) point for X

Xx value is the mean value for this vector

As dividing by two, for the example purposes, we are cutting in a half a 2cc cylinder and expressing the VPI value normalized by 1 cc

The results were plotted for: Bland- Altman intra e interobserver variability, and the Intra-Class correlation coefficient with 95% Confidence Interval was calculated. A Cochran Q- test was employed for comparing repeatability between the two techniques

All the measurements were stored in an Excel spreadsheet (Microsoft Corporation, Silicon Valley, Ca). Transferred into dedicate databases for statistical analysis by using Medcalc Software (Medcalc Corporation, Mariakerke, Belgium) and the Statistical Package for Social Sciences version 19 (SPSS Corp- IBM Company Armonk, New York)

3.1.4. The *in-vivo* test: Designing the animal model

This was an experimental animal model, carried out in eight, accurately time-dated, pregnant sheep carrying single fetuses. The posterior limbs of the fetuses were intervened and evaluated throughout this study. The research protocol was approved by the Committee for Animal Research of the Universitat Autònoma de Barcelona (UAB). All animals received care in compliance with the "principles of Laboratory Animal Care" formulated by the National Society for Medical Research and the "Guide for Care and Use of Laboratory Animals" prepared by the National Institute of Health (NIH publication Nr. 6380-2, revised 2004: http://www3.od.nih.gov/oma/manualchapters/contracts/6380-2/) and the Spanish law for protection of experimental animals (RD 223-1988).

A total of eight fetuses from near term pregnant sheeps (125-140 days) were gathered from the animal welfare house of the Vall d'Hebron Research Institute. Fetal vitality was previously assessed and, then, a cesarean section under general anesthesia All pregnant sheep were endotracheally intubated and underwent general anesthesia with isofluorane (Aerrane, Baxter Co, One Baxter parkway Deerfield, IL). The uterus was then exteriorized through a lower midline laparotomy, the fetuses were exposed via hysterotomy and the umbilical cord was exteriorized through the section. Afterwards, a modified central catheter

was inserted via umbilical vein and under direct echographic vision. An arterial line was also inserted in one of the umbilical arteries. Both transducers from the catheters were connected to a PICCO monitor for invasive testing (PULSION Medical Inc. Irving TX, USA). Continuous measurement of combined cardiac output was then registered as long as the experiment was carried out, meanwhile one of the authors (JB-M), recorded several volume datasets synchronizing the register of the data set with data obtained by monitorization.. Ultrasound and Doppler assessment was performed using a Samsung Accuvix V-20 Prestige machine with a 3-6 MHz multi-frequency 3D matrix array probe (Samsung-Medison Europe B.V. Parellaan 10, 2132WS, Hoofddorp, The Netherlands). All the scans were performed in synchronization with the invasive measurements.

The power Doppler settings were specifically maintained for all experiments as follows: medium central frequency, quality 9, density 8, reject 82, signal rise 0.4, signal persistence 0, frame rate 12.9, wall motion filter 70 Hz, pulse repetition frequency 1.6 kHz, power 4 dB and color gain 36.8. All the image filters provided by the machine were de-activated (MR image, speckle reduction and cross beam reduction) The STIC setting were established as sweep angle 25º, acquisition time 7 seconds, frame

rate 35 fps. These settings were chosen as they reflected those used in the clinical setting and allowed the best possible registration of the signal.
In order to achieve quantification in a repeatable way, we used part of the tools in the Sonoview® software provided by the machine. Two plug-in named “Oblique view” ® and “OVIX” ® which allowed us to, in order to maintain the same degree of consistency, generating a 3D ‘rectangular sampling box’ that was applied over the midpoint of the vessel. As indicated by a central point on the screen, and by maintaining a constant magnification of 1.1; this VOI was found to fit perfectly such that the vessel and its wall were just enclosed. This allowed the user to define an orthogonal VOI, with a 2mm length cylinder included whose dimensions may be modified manually relative to the object of interest but were always set at 2mm. To ensure that a consistent VOI was selected for each dataset, predetermined criteria were set according to the experiment under consideration All datasets were stored, transferred and subsequently measured in the same manner with no manipulation of the display. Because the relationship between the transducer and test tank was maintained at 90°, the vessel was always located centrally and horizontally within the final dataset.

The power Doppler signal within each dataset was evaluated by applying the histogram facility in a volume defined by Virtual Organ Computer-aided

AnaLysis (VOCAL: Samsung Medical Co, Hoofddorp, Nz). VOCAL allows the user to automatically define a sphere of variable size that can be applied within any 3D dataset to sample the Doppler signal within it. For these experiments a spherical volume of 0.9 cm^3, defined by a diameter of 1 cm as estimated from the sphere volume ($\pi D^3/6$, where D = diameter), was used to serially sample each dataset from the proximal to the more distal part. The fixed size of the sphere allowed assessment of the gain adjustment from the surface, at depths of 0–1 cm, to the more distant aspect of the dataset Owing to the nature of the experiments and the different designs employed we decided to report only the VFI, which is representative of both the VI and FI. The relationship between the VFI and the different settings within each flow-free phantom and with the transducer were represented as plot graphs. The results were plotted for: Bland- Altman intra e interobserver variability, and Intra-Class correlation coefficient with 95% Confidence Interval was calculated.

VPI Offline Analysis of volume datasets: all stored volumes were then analyzed, as previously described, by using the image analysis software provided by Mathematica ® and the voxels intensity information was kept as a matrix of data. The actual velocity profile measurement was stored independently for a further plotting against the estimated calculations. The matrix of color deconvolution values was then inserted into a Matlab suite

® algorithm denominated “least-squares curve fitting“, used for adjusting complex matrix data in linear equations.

The algorithms employed for the *in vivo* test were the same used in the *in-vitro* one, already described

The results were plotted for: Bland- Altman intra e interobserver variability, and Intra-Class correlation coefficient with 95% Confidence Interval was calculated. A Cochran Q- test was employed for comparing repeatability between the two techniques

All the measurements were stored in an Excel spreadsheet (Microsoft Corporation, Silicon Valley, Ca). Transferred into dedicate databases for statistical analysis by using Medcalc Software (Medcalc Corporation, Mariakerke, Belgium) and the Statistical Package for Social Sciences version 19 (SPSS Corp- IBM Company Armonk, New York)

Chapter 4. Results

4.1 Flow quantification
4.1.1 In vitro testing
4.1.1.1. Internal Validity

A total of 136 measurements were achieved during the experiment, always under similar conditions of pulse, flow, velocity and machine settings. All the registers were successfully analyzed offline and the VPI was calculated in all cases. With the same volume dataset an offline analysis of volumes using the VOCAL® software was attempted, successfully in all the cases.

While the graphic of estimated velocity depicts a “pulse-like” graphic (figure 21). The graphic of the VFI showed a stable value throughout the entire experiment. . When comparing the vectorial velocity values, as delivered by the Matlab® algorithm, the correlation was very high with a R^2 value of 0.67 ($p<0.05$) and a Pearson’s correlation index (95% CI) of 0.88 (0.58-0.97). When plotting the VFI values and the velocity values no correlation was found (R^2 value 0.034), and the Pearson’s correlation index (95%CI) was -0.34(-0.31-0.44) . (Figure 22 and 23).

When tested in-vitro, both techniques showed a good repeatability. Intra-Observer Intraclass Correlation Coefficient (ICC; 95% CI) was similar for

VPI (0.95; 0.91-0.99) and VFI (0.9; 0.88-0.92). Inter-Observer ICC was also alike for VPI (0.90; 0.87-0.99) and VFI (0.88; 0.84-0.91).

The Bland Altamn plot showed also a low disagreement between two observations by the same observer (Figures 24 and 25) and by two different observers (Figures 26 and 27)

When plotting VPI against actual flow calculation the Pearson's correlation Index (95% CI) was 0.88 (0.58-0.97) for VPI and 0.34 (0.31-0.44) for VFI. (Fig 28)

Table 3 summarizes the repeatability tests for both tools.

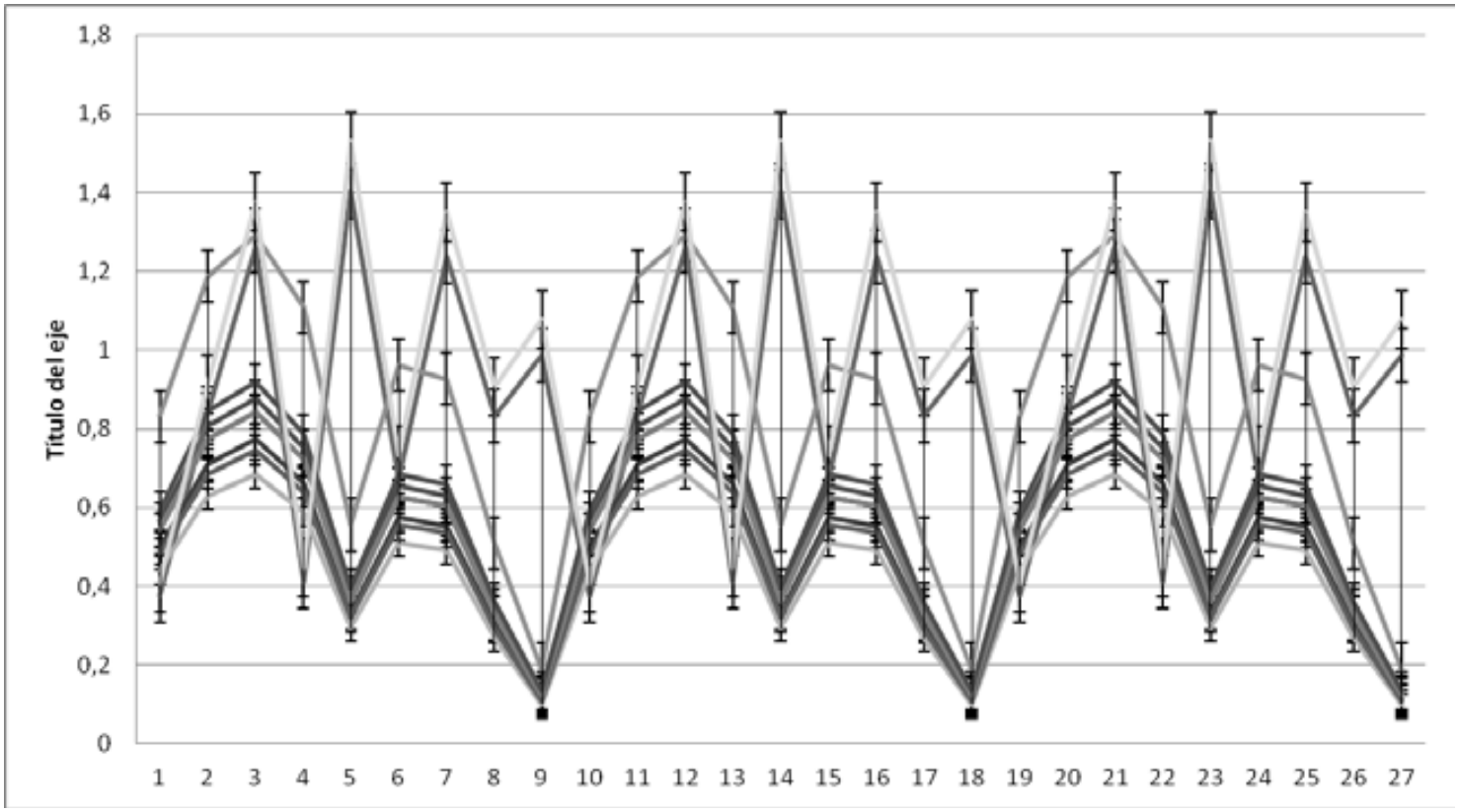

Figure 21 Linear plot from obtained vectorial velocity values as rendered by the matlab ® linear minimum squares algorithm. It can be seen how likely the graphic depicts a pulsatile fluctuation of the values.

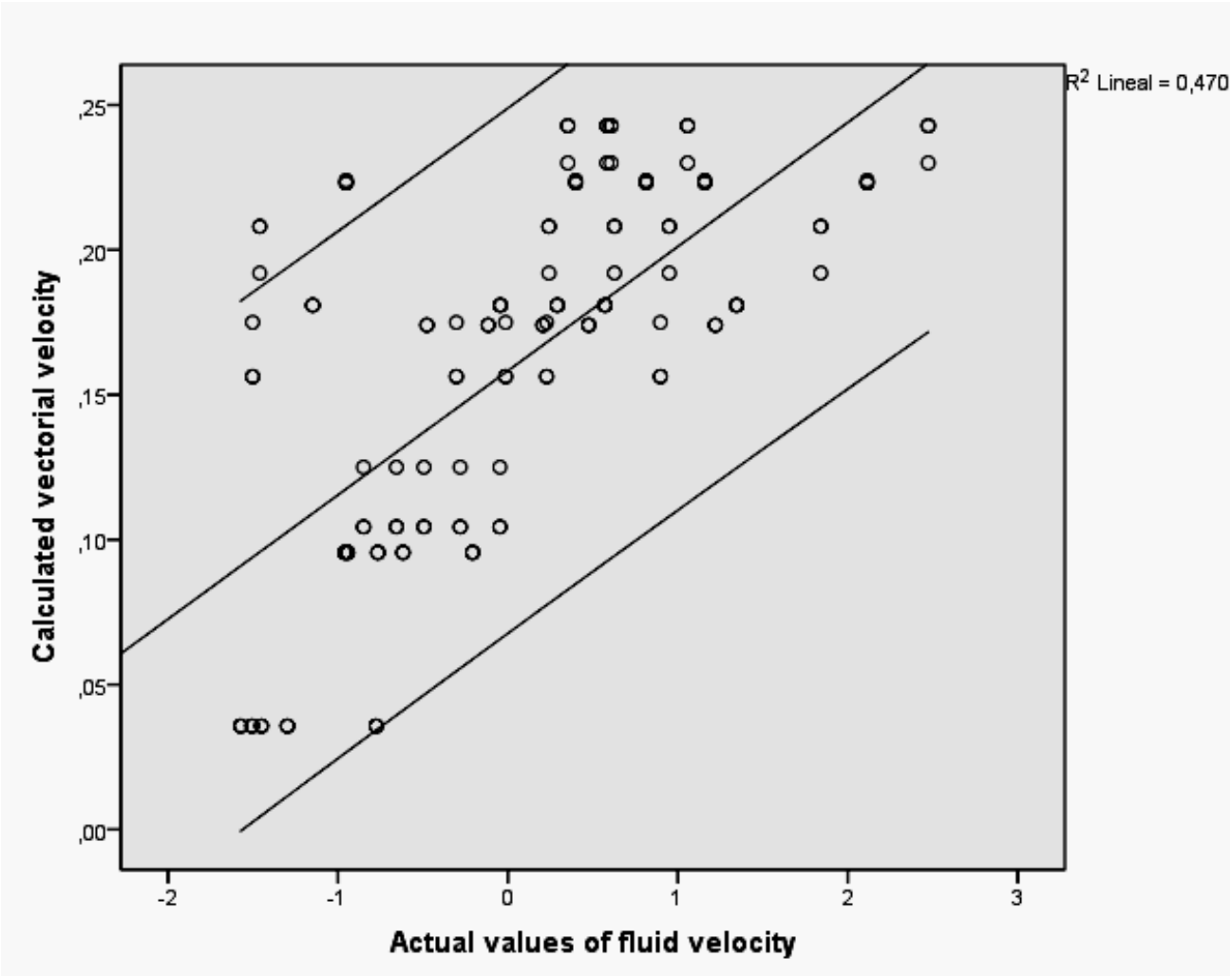

Figure 22 Linear regression plot from obtained vectorial velocity values as rendered by the Matlab ® linear minimum squares algorithm when compared to actual velocities as registered by the pump

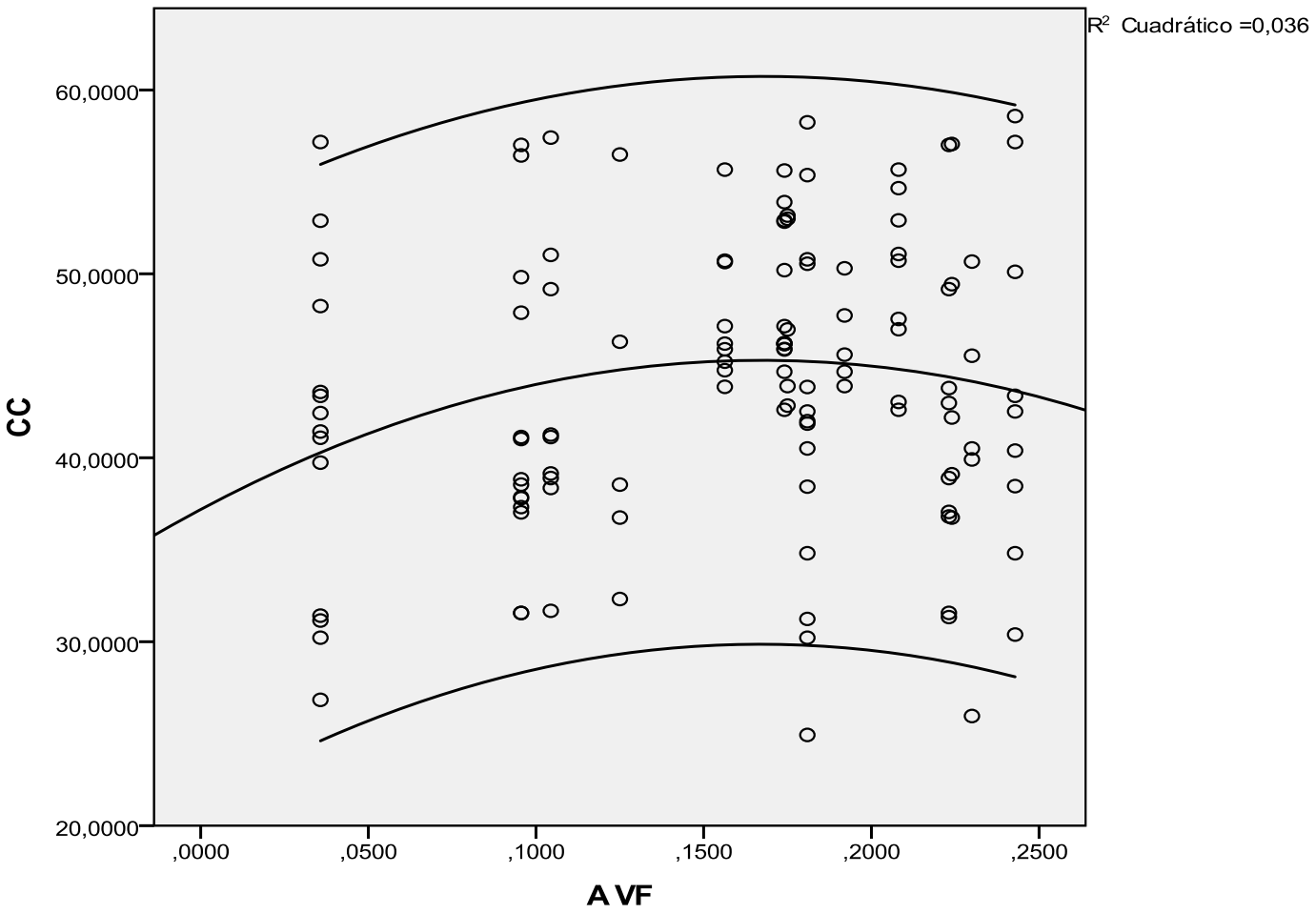

Figure 23 Quadratic regression plot of VFI when compared to actual velocities as registered by the pump

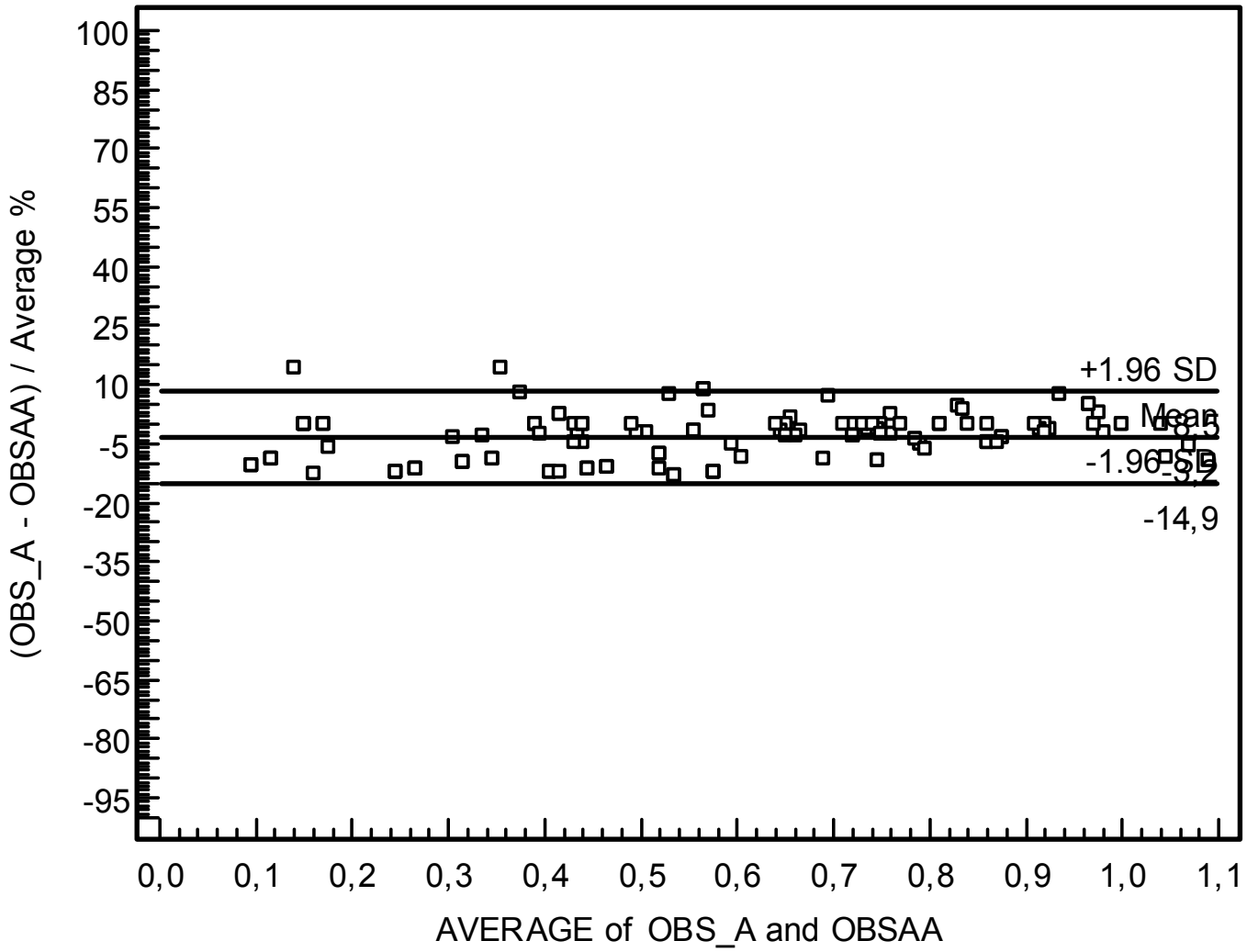

Figure 24 **Bland-Altman plot** showing the intra-observer disagreement of the Volume Perfusion Index as tested in-vitro.

B-A DA [%] (95% CI): 2,6 (-14.9-8.5)

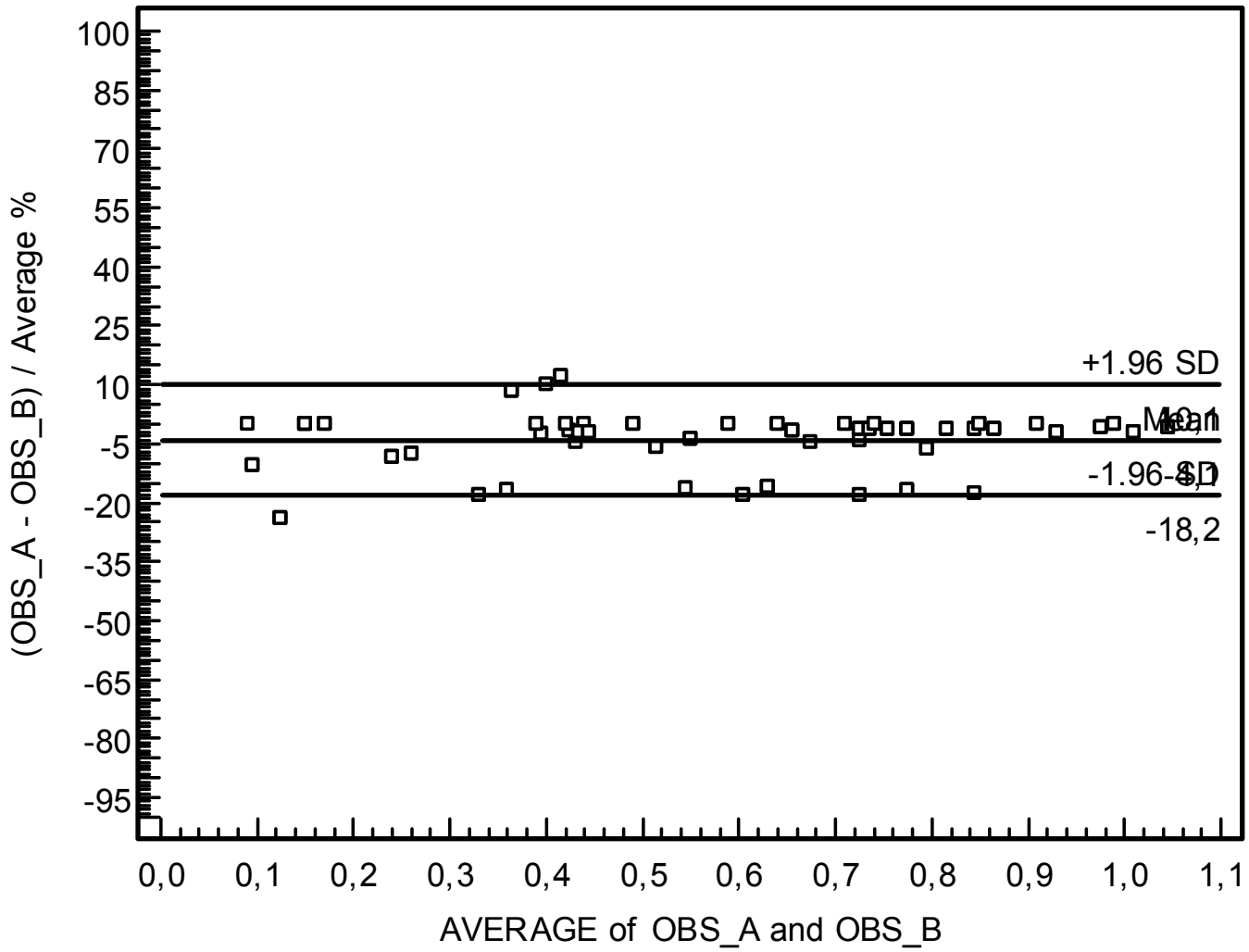

Figure 25 **Bland-Altman plot** showing the inter-observer disagreement of the Volume Perfusion Index as tested in-vitro

B-A DA [%] (95% CI): -1.4 (-18.2-10.0)

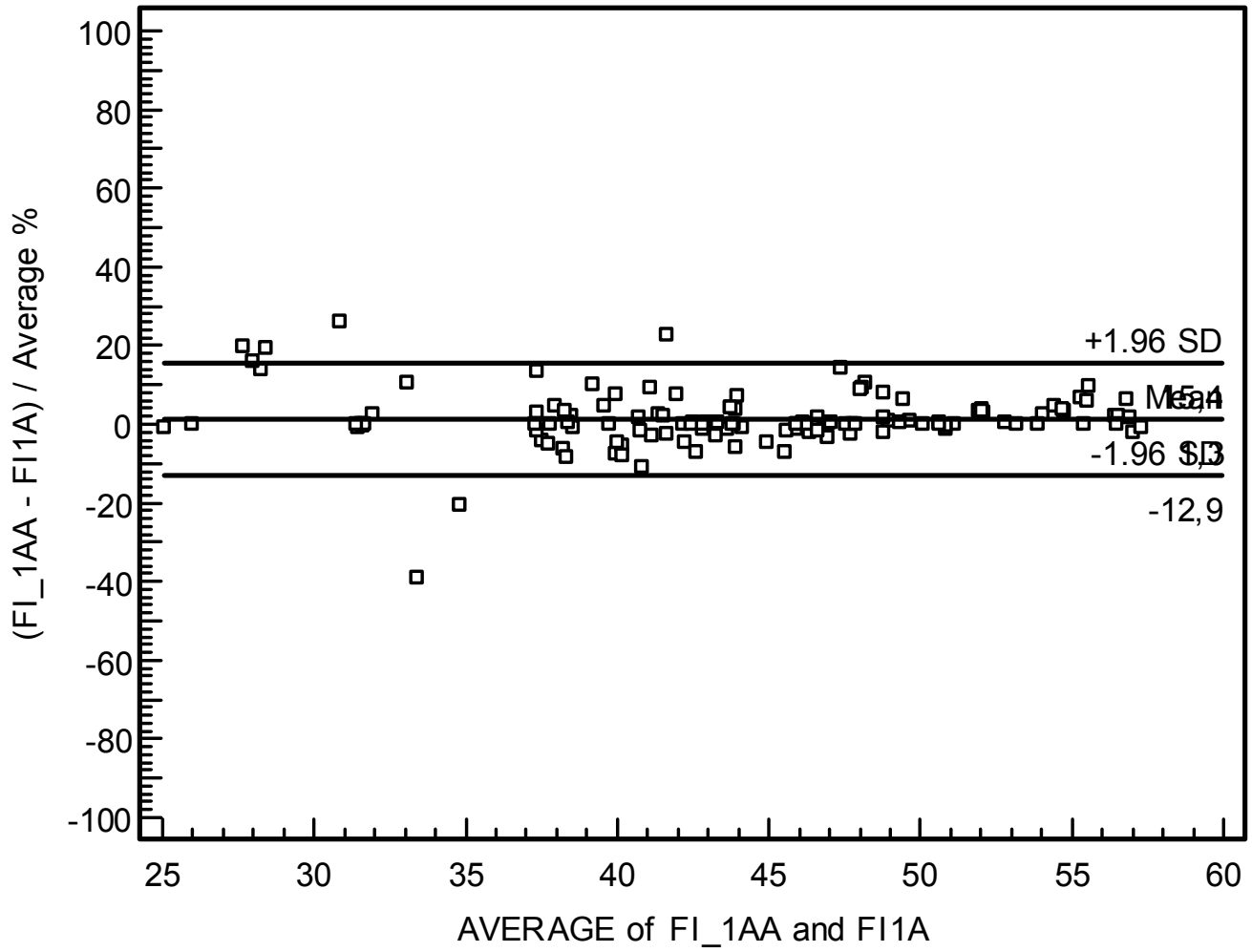

Figure 26 **Bland-Altman plot** showing the intra-observer disagreement of the Vascularization Flow Index (VFI) as tested in-vitro.

B-A DA [%] (95% CI): 1.3 (-12.9-15.5)

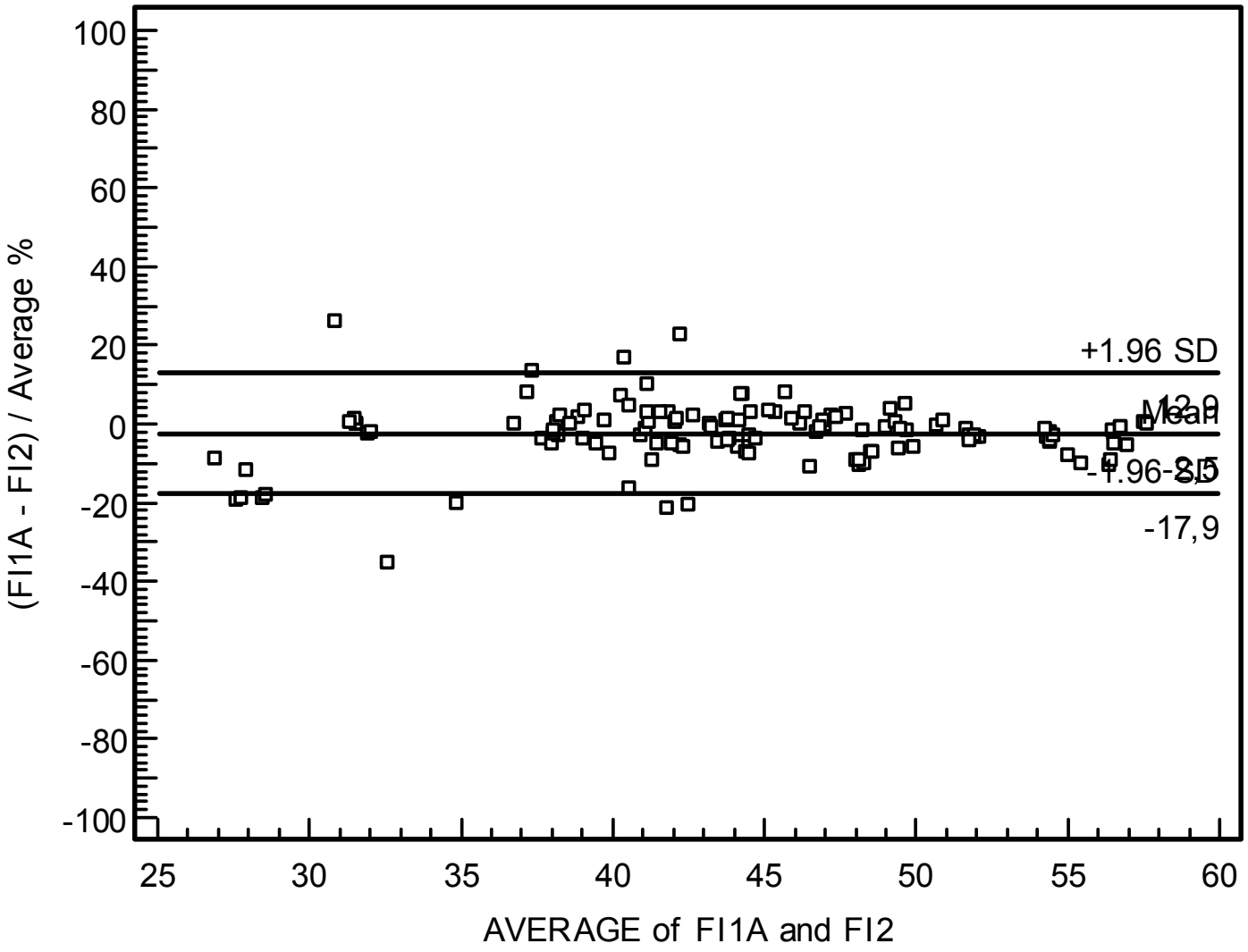

Figure 27 **Bland-Altman plot** showing the inter-observer disagreement of the Vascularization Flow Index (VFI) as tested in-vitro.

B-A DA [%] (95% CI): -2.5 (-17.9-12.8)

		BA D	95% CI	P(*)	ICC	95% CI	p
VPI	INTRA OBSERVER	2.6	-14.9-8.5	0.6	0.95	0.91-0.99	<0.01
	INTER OBSERVER	1.4	-18.2-10.0	0.6	0.90	0.87-0.99	<0.01
VFI	INTRA OBSERVER	1.3	-12.9-15.5	*	0.90	0.88-0.92	<0.01
	INTER OBSERVER	2.5	-17.9-12.8	*	0.88	0.84-0.91	<0.01

Table 3 Summarized results of intra and inter observer variability between the Volume Perfusion Index (VPI) and the Vascularization Flow Index (VFI) from in-vitro measurements

(*) p obtained by a Wilcoxon Sum rank test.

4.1.1.2. Standard Validation

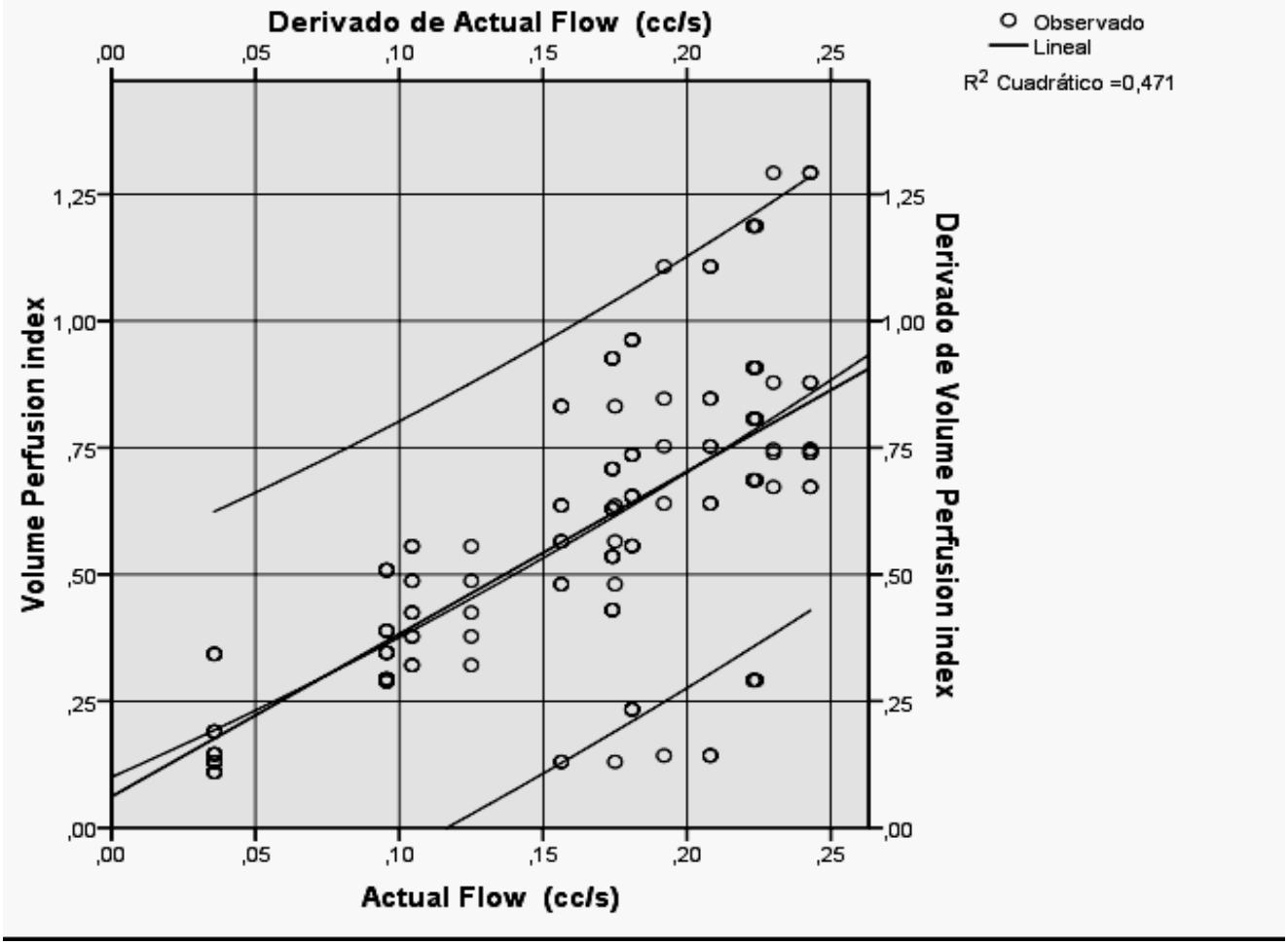

Figure 28 Linear regresion plot of Volume Perfusion Index when compared to actual flow as measured by direct monitorization (see description).

	R value	CC	95% CI	P(*)	RCC	95% CI	p
VPI	0.92	0.88	0.58-0.97	<0.01	0.69	0.68-0.89	<0.01
VFI	0.15	-0.34	-0.31-0.44	0.57	0.18	-0.1-0.35	0.61

Table 4 Summarized Pearsons' and Tau Rank correlation coefficient between the Volume Perfusion Index (VPI) and the Vascularization Flow Index (VFI) when compared to actual flow measurements as recorded by the autor throughout the experimet

4.1.2. In vivo testing
4.1.2.1. Internal Validity

A total of 128 measurements from eight subjects were achieved during the experiment (equivalent to 16 cardiac cycles each one), always under similar conditions of temperature, pulse, clinical status of the mother, gestational age and machine settings. In all cases, invasive monitorization was successful through umbilical vein and artery for pulse, flow, output and pressures. All the data form invasive monitoring were stored. In all cases the volume datasets were successfully achieved All the registers were successfully analyzed offline and the VPI was calculated in all cases. With the same volume dataset an offline analysis of volumes using the VOCAL® software was attempted, successfully in all the cases.

While the graphic of estimated velocity depicted a “pulse-like” graphic (figure 29). The graphic of the VFI showed a stable value throughout the entire experiment. When comparing the vectorial velocity values, as delivered by the Matlab® algorithm, the correlation was very high with a R^2 value of 0.77 ($p<0.05$) and a Pearson’s correlation index (95% CI) of 0.68 (0.58-0.77). When plotting the VFI values and the velocity values no correlation was found (R^2 value 0.034), and the Pearson’s correlation index (95%CI) was -0.24(-0.31-0.44) . (Figure 30).

When tested in-vivo the VPI exhibited an Intra-Observer ICC(95% CI) of 0.9(0.88-0.99) and the VFI 0.79(0.75-0.92) (Figure 31 and 32); and an Inter-Observer ICC (955 CI) of 0.88 (0.87-0.99) for VPI and 0.78 (0.74-0.91) for VFI (Figures 33 and 34).

Table 5 summarizes the repatibility tests for both tools.

The flow measurement in the animal model correlated significantly better in VPI than in VFI with a Perason's Correlation Index (95% CI) of 0.88(0.58-0.97) Vs -0.34 (-0.31-0.44). $p< 0.001$ (Figures 35 and 36).

Table 6 summarizes the correlation measurements for both techniques.

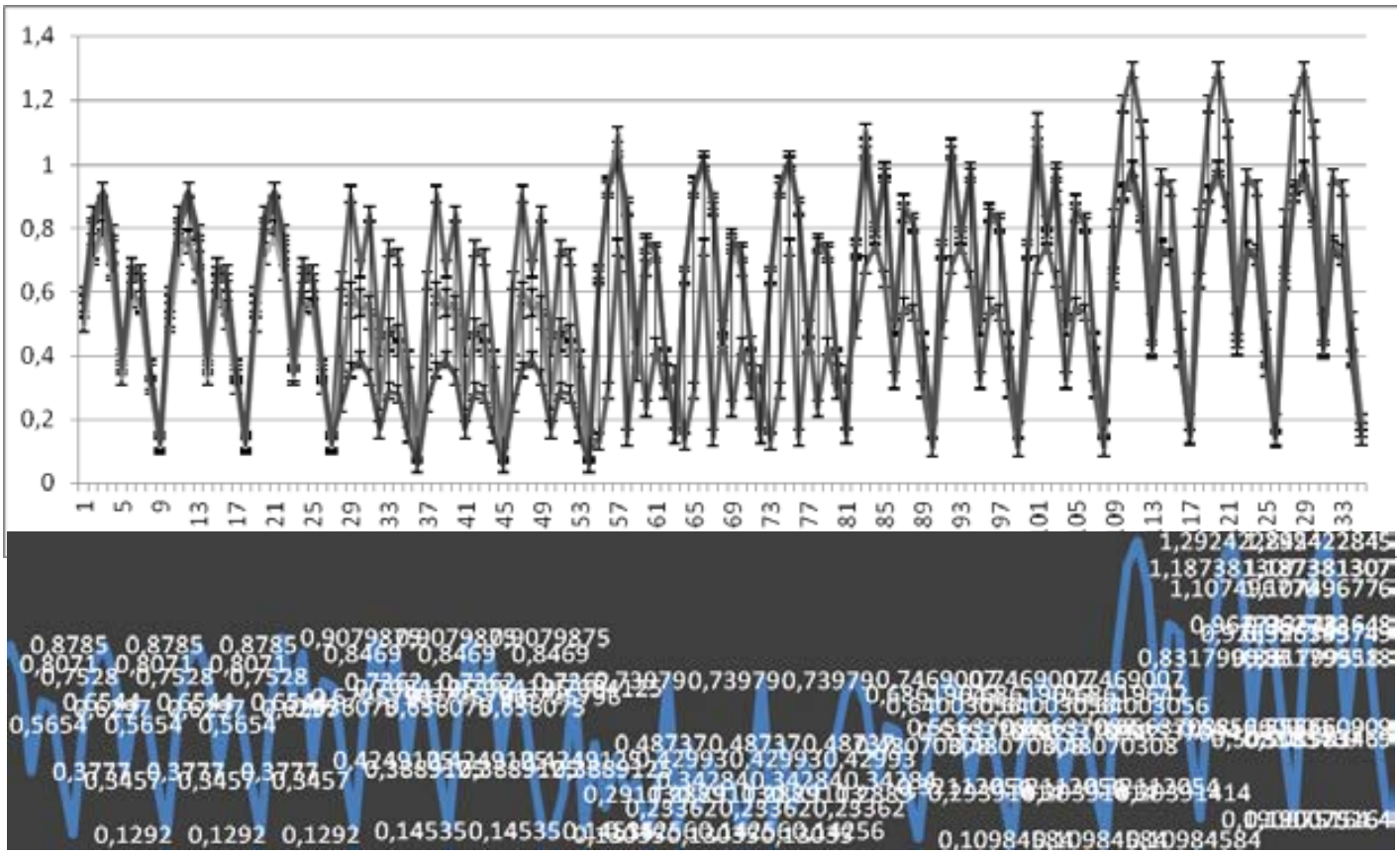

Figure 29 Linear plot from obtained vectorial velocity values as rendered by the matlab ® linear minimum squares algorithm. It can be seen how likely the graphic depicts a pulsatile register from the PICCO monitor

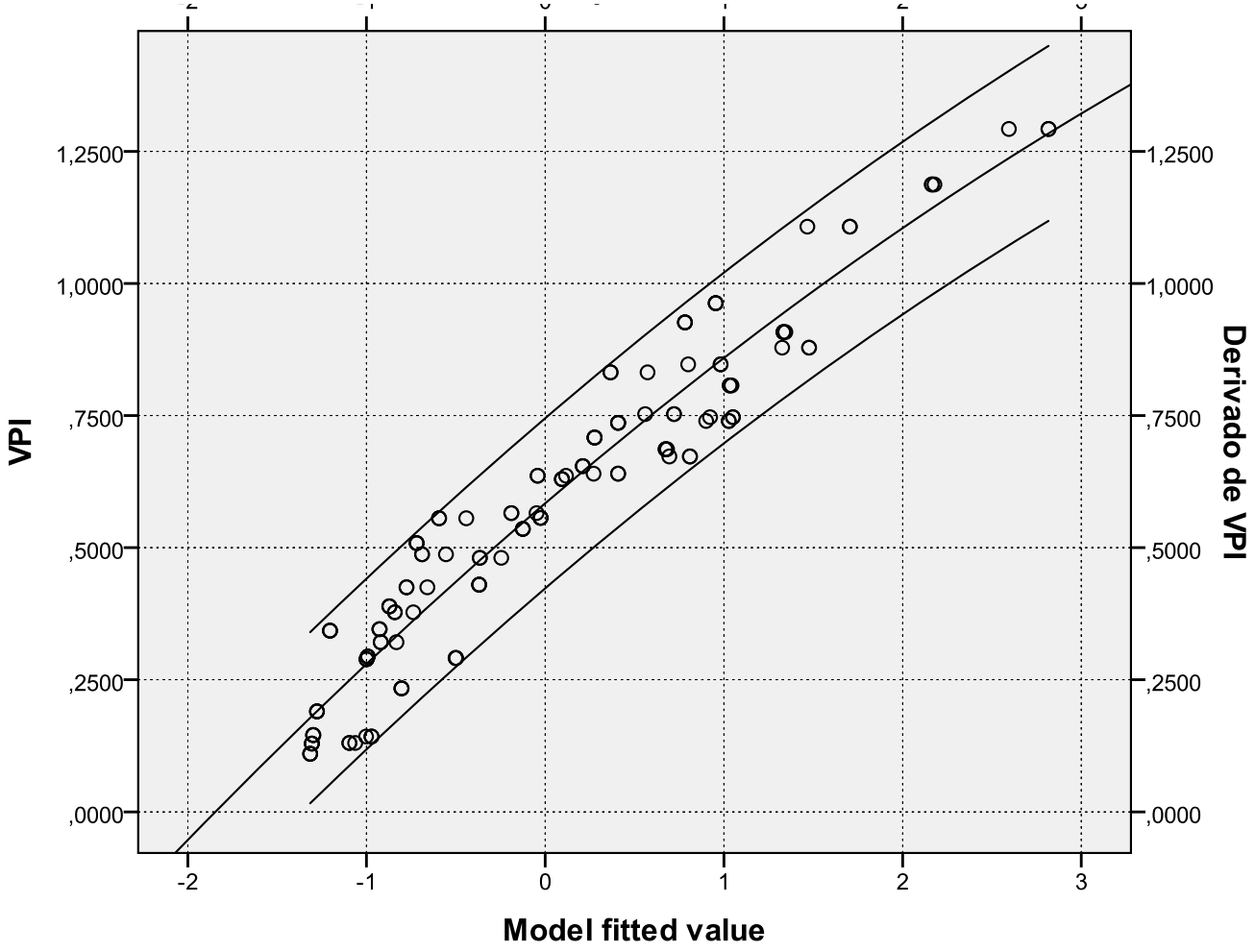

Figure 30 Cuadratic regression plot from obtained Volume Perfusion Index as rendered by the Matlab ® linear minimum squares algorithm when compared to a model fitted values of actual flow as obtained by direct monitorization

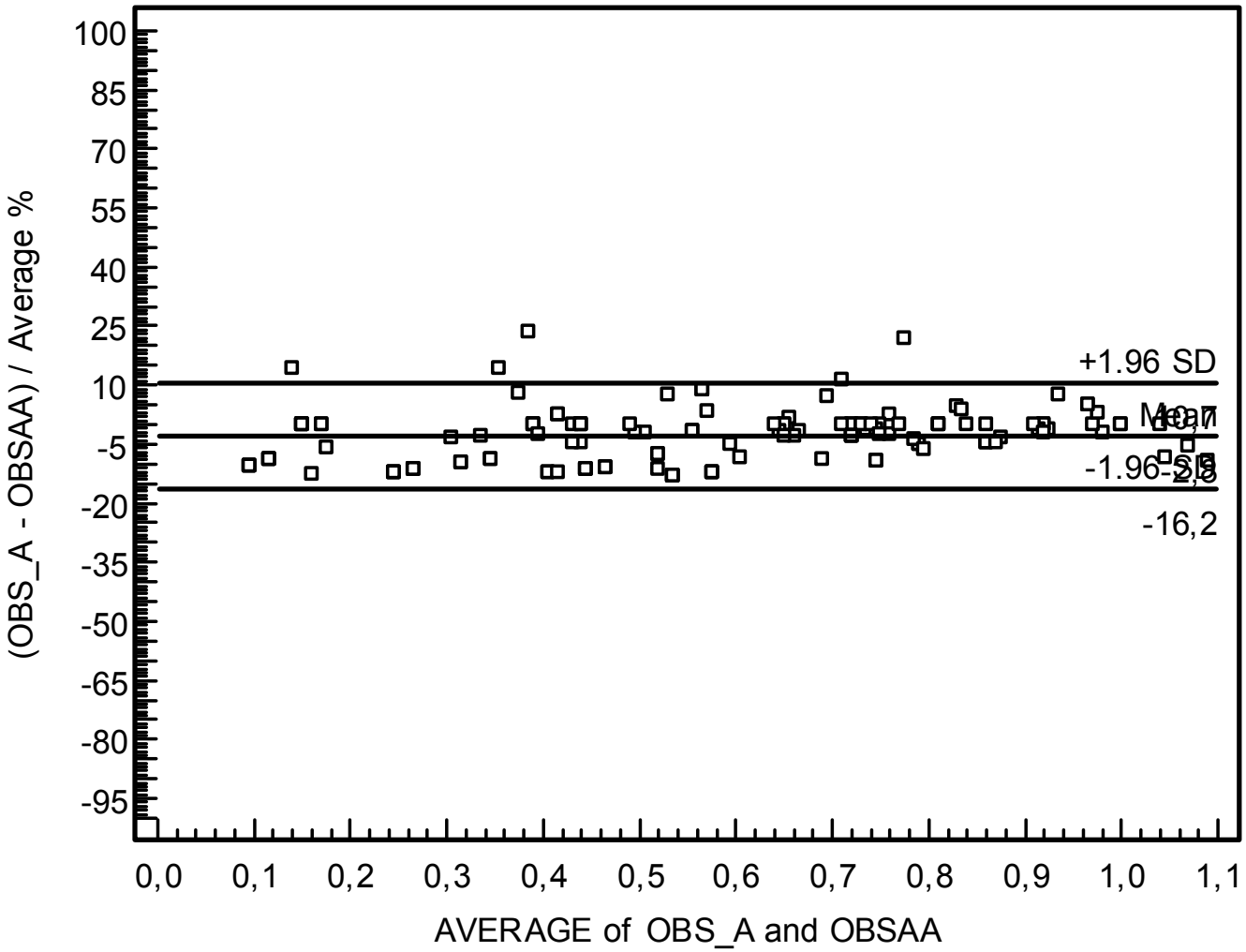

Figure 31 **Bland-Altman plot** showing the intra-observer disagreement of the Volume Perfusion Index as tested in a sheep model.

B-A DA [%] (95% CI): -4,6 (-16.2-10.7)

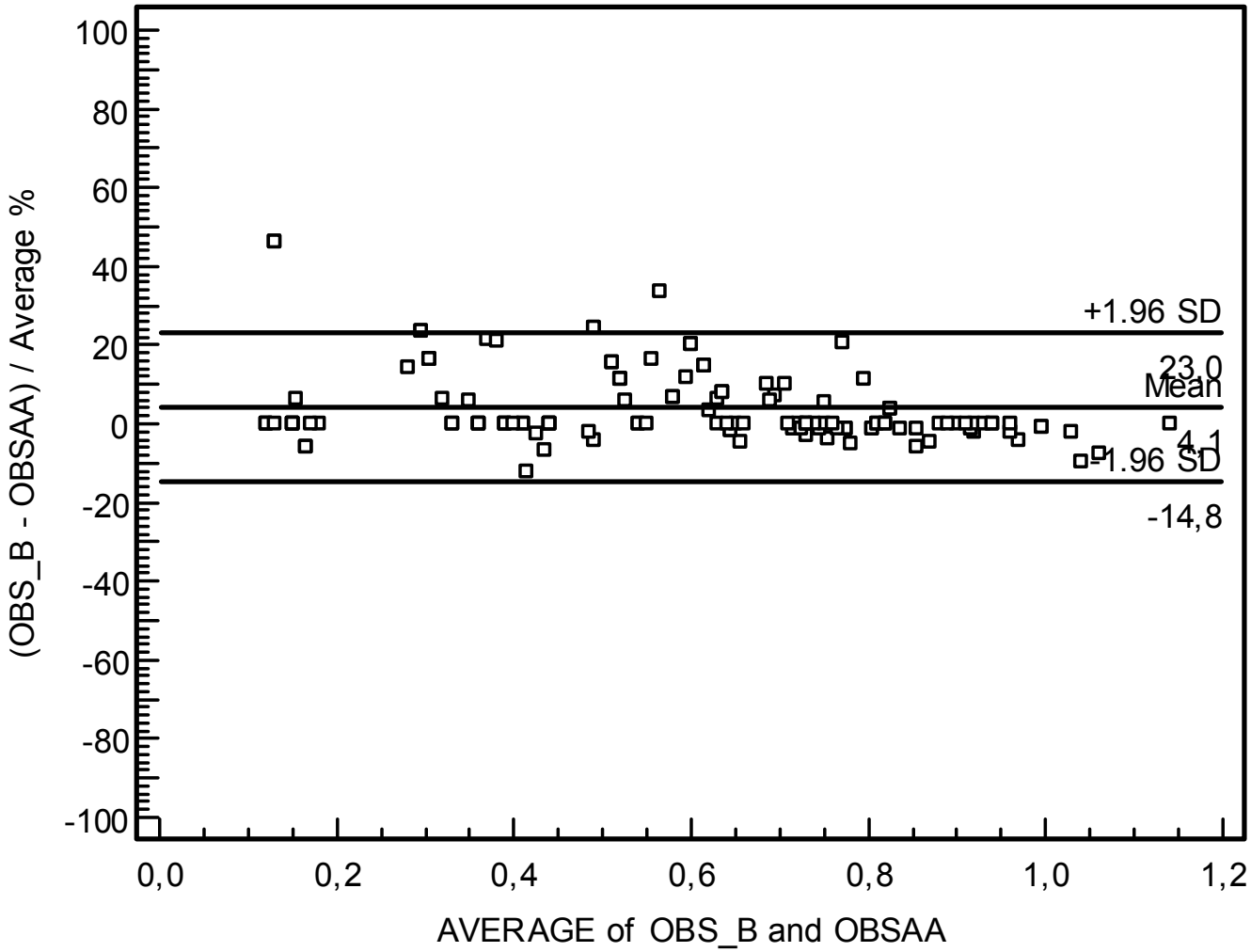

Figure 32 **Bland-Altman plot** showing the inter-observer disagreement of the Volume Perfusion Index as tested in a sheep model.

B-A DA [%] (95% CI): 4.1 (-14.8-23.0)

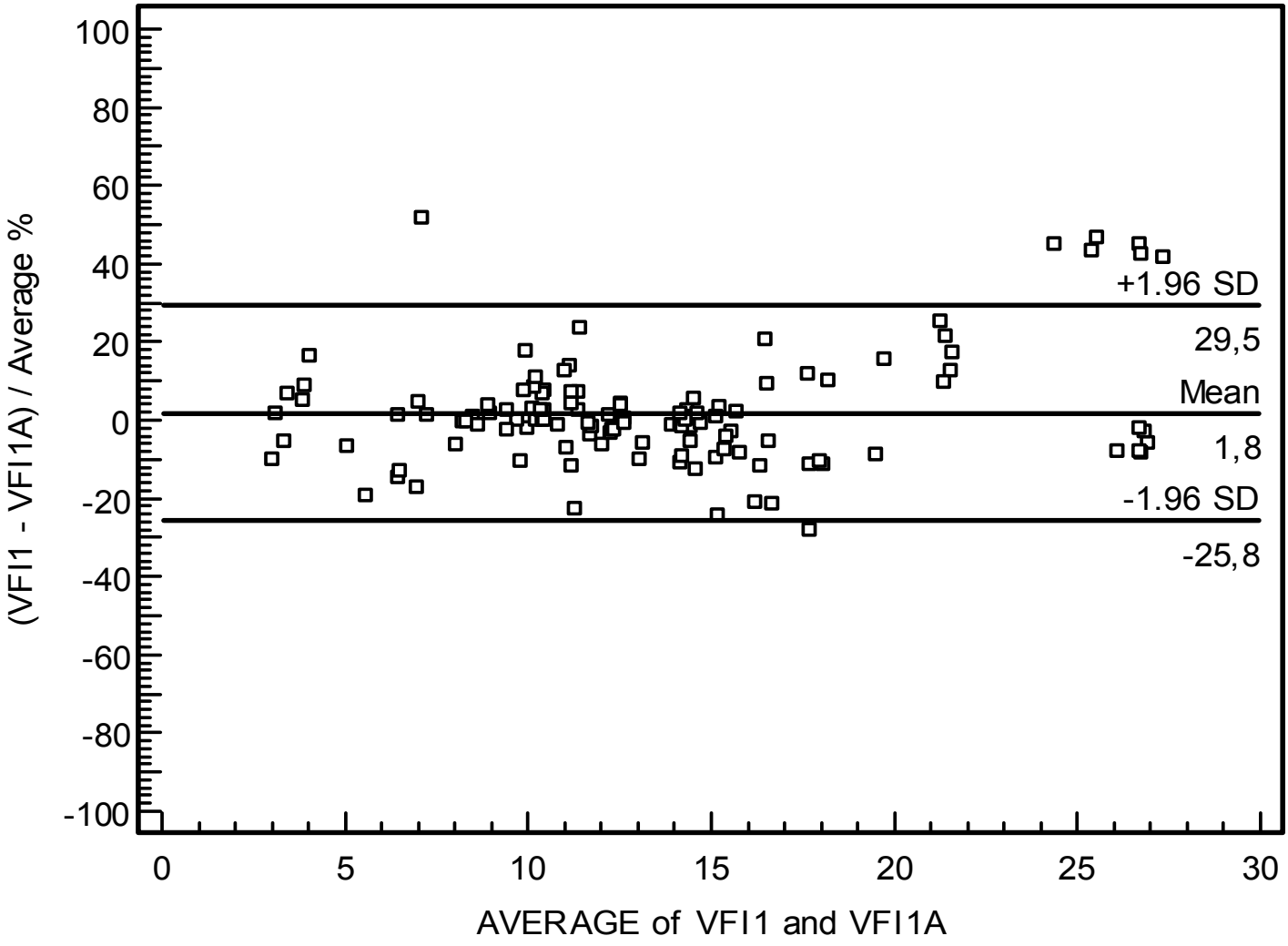

Figure 33 **Bland-Altman plot** showing the intra-observer disagreement of the Vascularization Flow Index (VFI) as tested in a sheep model.

B-A DA [%] (95% CI): 1.8 (-25.8-29.5)

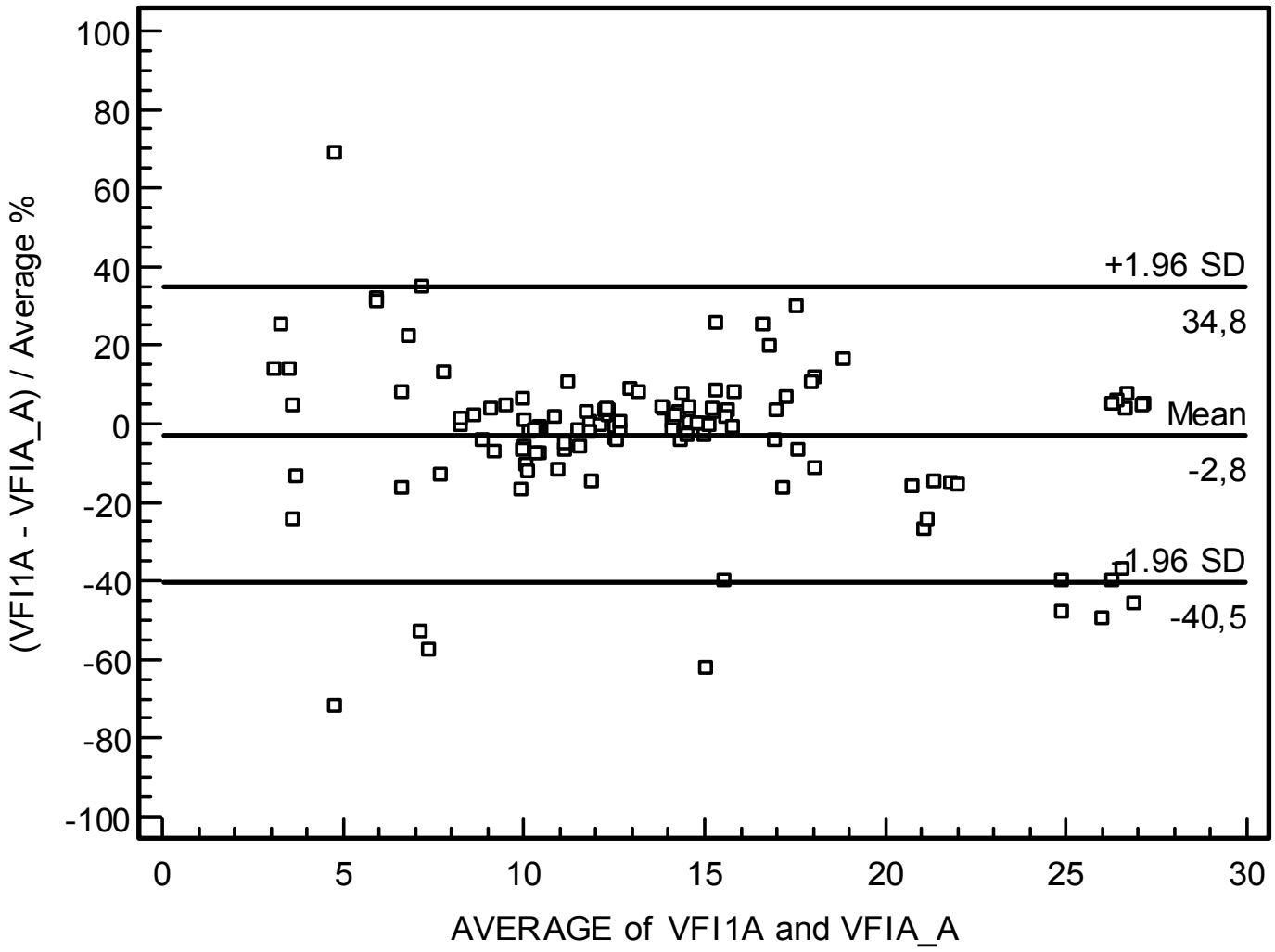

Figure 34 **Bland-Altman plot** showing the inter-observer disagreement of the Vascularization Flow Index (VFI) as tested in a sheep model.

B-A DA [%] (95% CI): -2.8 (-40.5-34.8)

		BA D	95% CI	P(*)	ICC	95% CI	p
VPI	INTRA OBSERVER	2.6	-16.2-10.7	0.2	0.90	0.88-0.99	<0.01
	INTER OBSERVER	4.1	-14.8-23	<0.1	0.88	0.87-0.99	<0.01
VFI	INTRA OBSERVER	1.8	-25.8-29.5	*	0.79	0.75-0.92	<0.01
	INTER OBSERVER	-2.8	-40.5-34.8	*	0.78	0.74-0.91	<0.01

Table 5 Summarized results of intra and inter observer variability between the Volume Perfusion Index (VPI) and the Vascularization Flow Index (VFI) as obtained from a sheep model

(*) p obtained by a Wilcoxon Sum rank test.

4.1.2.2. Standard Validation

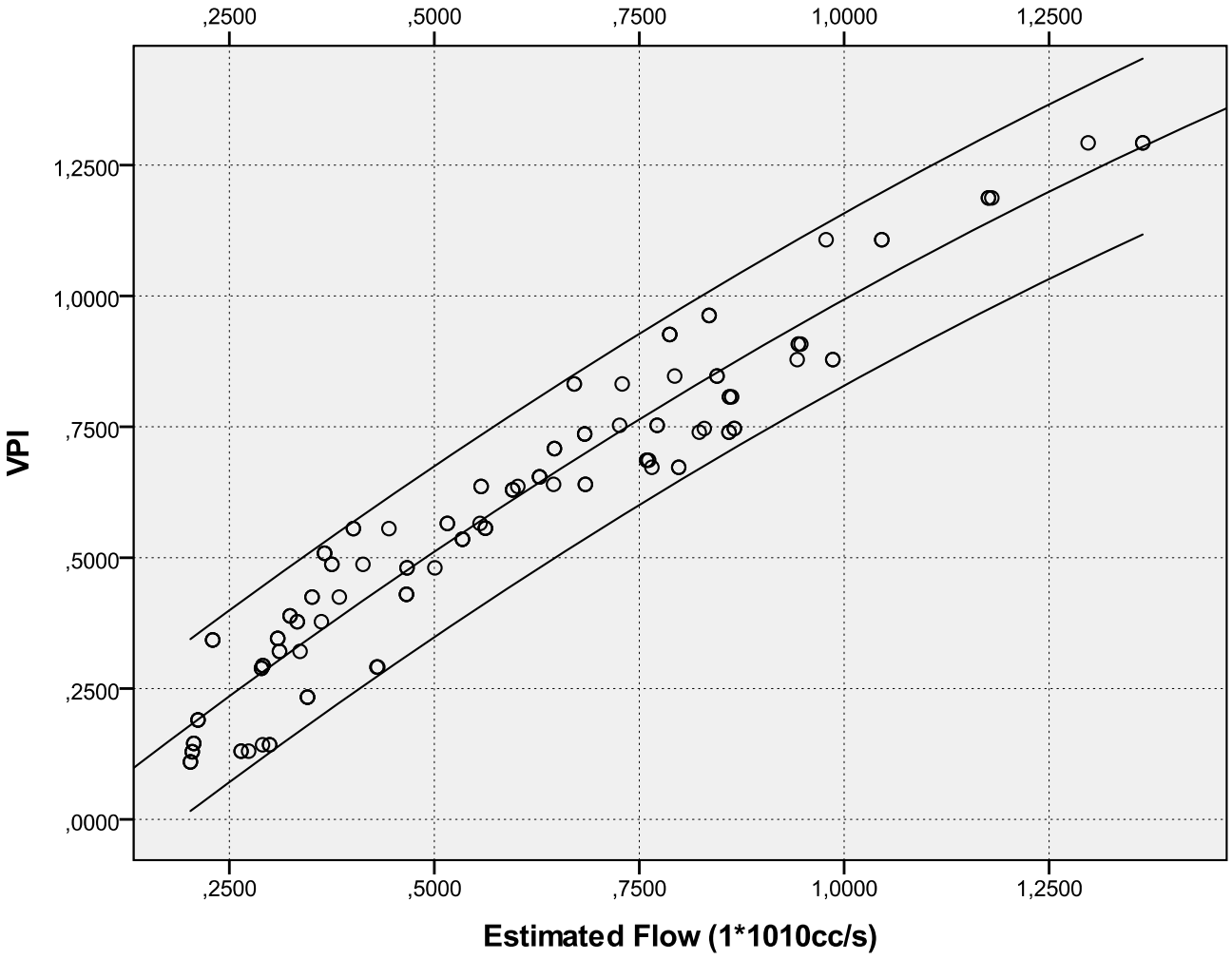

Figure 35 Linear correlation plot of Volume Perfusion Index when compared to actual flow as measured by invasive monitorization (see description). R^2 value 0.874

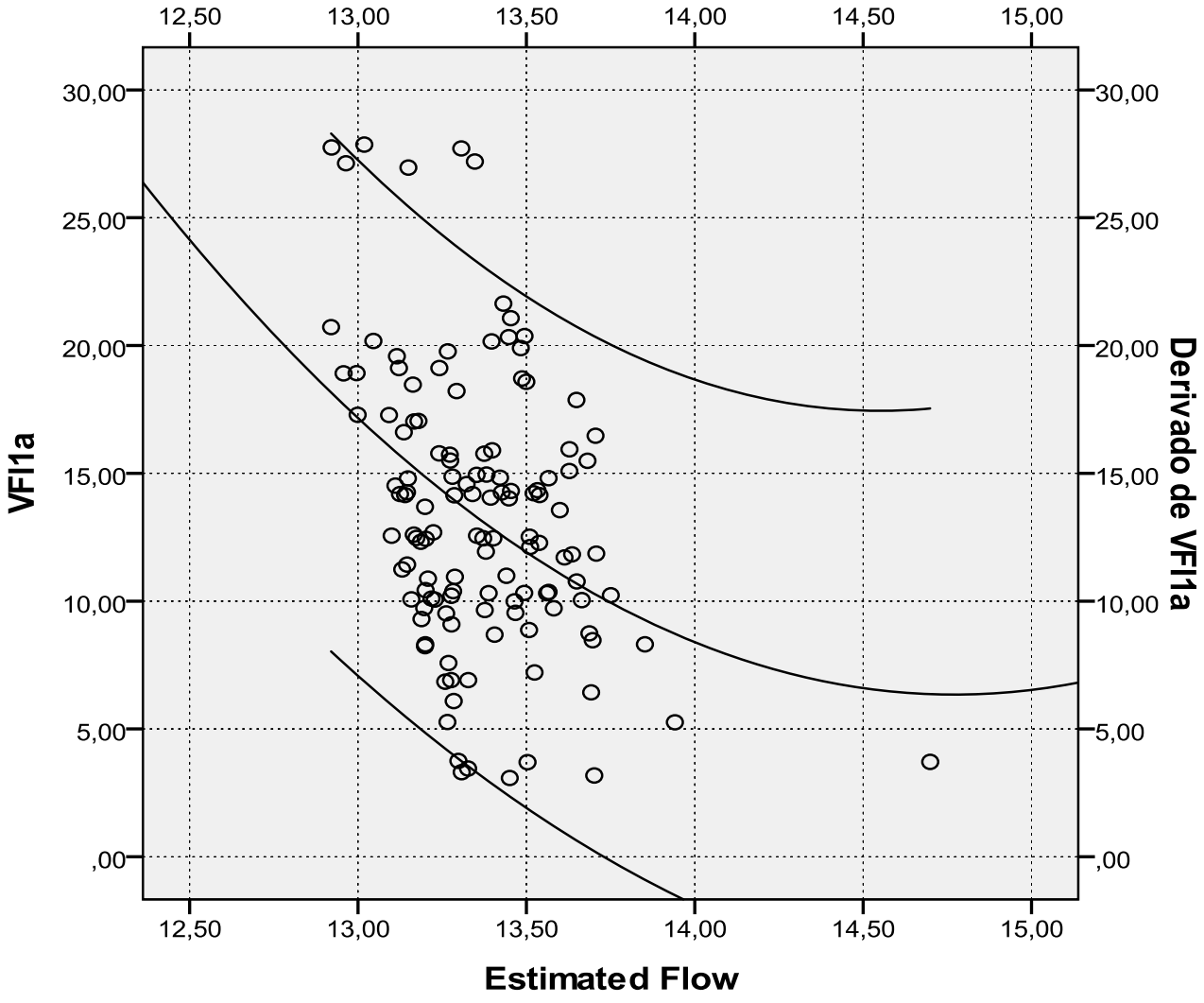

Figure 36 Linear correlation plot of Vascularization Flow Index when compared to actual flow as measured by invasive monitorization (see description). R^2 value 0.154

	CC	95% CI	P(*)	RCC	95% CI	p
VPI	0.68	0.58-0.77	<0.01	0.54	0.38-0.89	<0.01
VFI	-0.24	-0.31-0.44	0.63	0.28	0.08-0.31	0.31

Table 6 Summarized Pearsons' and Tau Rank correlation coefficient between the Volume Perfusion Index (VPI) and the Vascularization Flow Index (VFI) when compared to actual flow measurements as recorded by the autor throughout the experiment.

Chapter 5. Discussion

5.1 How much of a Breakthrough

The possibility of registering , in a reliable manner, the fetal blood flow, represents a milestone in the evaluation of certain fetal conditons whose circulatory changes make an essential impact in the prognosis and are fundamental for clinical decision making (Sifa Turan et al. 2008; A A Baschat 2006). Particular conditions like monochorionic twin pregnancy complications (Chmait et al. 2009; Hack et al. 2009; N. A. Smith et al. 2010), fetal growth restriction (R Cruz-Martinez, F Figueras, Benavides-Serralde, et al. 2011; Apel-Sarid et al. 2009; E Hernandez-Andrade et al. 2008), small for gestational age fetuses without **demonstrable** signs of hemodynamic compromise (Rogelio Cruz-Martinez et al. 2009; R Cruz-Martinez, F Figueras, E Hernandez-Andrade, et al. 2011; R Cruz-Martinez, F Figueras, E Hernandez-Andrade, et al. 2011), fetuses with cardiac anomalies and compromise of the upper body circulation (Simioni, Nardozza, Araujo Júnior, Liliam Cristine Rolo, et al. 2011; Smolich et al. 2012; Wald et al. 2012; K Flo, T Wilsgaard, Vårtun, et al. 2010). Since this point, several research teams are involved in evaluating in many different ways this phenomenon. However, the clinical variability of these

measurement in any living being makes nearly impossible to get a replicable measurement without direct evaluation or invasive measures (unavailable in fetal medicine nowadays).

The promise underneath this technique is the possibility of achieving a tool, accurate enough as for depicting such changes under any condition and circulatory territory (A. W. Welsh et al. 2005; Lai et al. 2010; Collins et al. 2011; Heck et al. 2012). It is quite likely that, this addition to the technique could be a new surpassed frontier and a step forward in the way for the actual registering of fetal circulation. (Bello-Munoz JC et al. 2012)

5.1.1. Further Adjustements

Despite the promising results described in the present thesis, the author sincerely thinks that further adjustments should be done to the tool before considering its clinical applicability. In its actual form it depicts quite accurately the pulsatile flow but, as far as we have tested, it is not possible to assume it is going to be able to detect subtle variations on this magnitude secondary to, either, physiological or pathological conditions. Further research addressing this particular issue should and will be attempted in the near future before launching any clinical application of this algorithm. We assume that five years from this point is a reasonable and achievable timeline for testing the tool and implementing it in a clinical setting.

5.2 Potential future uses

5.2.1. Prospective for new applications

As the tool can register any vascular territory with pulsatile flow the possibilities for evaluating regional flow are quite a number, In a pre-clinical way, our group is developing some protocols for registering such a regional flow in brain, kidneys, hepato-portal circulation, and heart. In order to withdraw a map of the regional vascularity and circulatory changes in the physiological condition of fetal growth and in certain pathological conditions like fetal growth restriction. This research is online with the state of the art in fetal circulation (Kari Flo, Tom Wilsgaard & Ganesh Acharya 2010; Cathrine Ebbing et al. 2009; Milani et al. 2011; Limperopoulos 2009; Clouchoux et al. 2011; Jordan-Young 2011)

A copy of the current protocol for such volume taking (in Spanish) is attached to the Annex 5.

5.4 Conclusion

The Volume Perfussion Index may be a significant advance in the way we observe and measure circulatory changes in the normal and compromised fetus as well. The VPI shows, under experimental conditions, significantly better repeatability and accuracy than the currently used tools for power Doppler quantification.

.

5.5 Disclosures

Author acknowledges the cooperation and support provided by Samsung Medical Co. during the experiment, but declares that has no commercial relationship whatsoever with that or any other company producing Ultrasound equipment. The techniques and results consigned here are subject of a confidentiality agreement between the author, the Vall d'Hebron Institute of Research and Samsung Medison Medical Company

6. References

3. *Acharya, G et al., 2005. Reference ranges for serial measurements of blood velocity and pulsatility index at the intra-abdominal portion, and fetal and placental ends of the umbilical artery. Ultrasound in Obstetrics & Gynecology: The Official Journal of the International Society of Ultrasound in Obstetrics and Gynecology, 26(2), pp.162–169.*
4. *Acharya, Ganesh et al., 2008. Metabolic acidosis decreases fetal myocardial isovolumic velocities in a chronic sheep model of increased placental vascular resistance. American journal of physiology. Heart and circulatory physiology, 294(1), pp.H498–504.*
5. *Acharya, Ganesh et al., 2004. Relationships among Doppler-derived umbilical artery absolute velocities, cardiac function, and placental volume blood flow and resistance in fetal sheep. American Journal of Physiology. Heart and Circulatory Physiology, 286(4), pp.H1266–1272.*
6. *Acharya, Ganesh & Sitras, V., 2009. Oxygen uptake of the human fetus at term. Acta Obstetricia Et Gynecologica Scandinavica, 88(1), pp.104–109.*
7. *Alcázar, J L, 2008. Three-dimensional power Doppler derived vascular indices: what are we measuring and how are we doing it? Ultrasound in Obstetrics & Gynecology: The Official Journal of the*

International Society of Ultrasound in Obstetrics and Gynecology, 32(4), pp.485–487.

8. *Alcázar, Juan Luis & Jurado, M., 2011. Three-dimensional ultrasound for assessing women with gynecological cancer: a systematic review. Gynecologic Oncology, 120(3), pp.340–346.*
9. *al-Ghazali, W. et al., 1989. Evidence of redistribution of cardiac output in asymmetrical growth retardation. British journal of obstetrics and gynaecology, 96(6), pp.697–704.*
10. *Angiolini, E et al., 2006. Regulation of placental efficiency for nutrient transport by imprinted genes. Placenta, 27 Suppl A, pp.S98–102.*
11. *Apel-Sarid, L. et al., 2009. Placental pathologies associated with intra-uterine fetal growth restriction complicated with and without oligohydramnios. Archives of Gynecology and Obstetrics, 280(4), pp.549–552.*
12. *Baez, E. et al., 2005. Ductus venosus blood flow velocity waveforms as a predictor for fetal outcome in isolated congenital heart disease. Fetal diagnosis and therapy, 20(5), pp.383–389.*
13. *Bartha, J.L., Moya, E.M. & Hervías-Vivancos, B., 2009. Three-dimensional power Doppler analysis of cerebral circulation in normal and growth-restricted fetuses. Journal of Cerebral Blood Flow and Metabolism: Official Journal of the International Society of Cerebral Blood Flow and Metabolism, 29(9), pp.1609–1618.*

14. *Baschat, A. A. et al., 2002. Demonstration of fetal coronary blood flow by Doppler ultrasound in relation to arterial and venous flow velocity waveforms and perinatal outcome – the 'heart-sparing effect'. Ultrasound in Obstetrics & Gynecology, 9(3), pp.162–172.*
15. *Baschat, A A, 2006. The fetal circulation and essential organs-a new twist to an old tale. Ultrasound in Obstetrics & Gynecology: The Official Journal of the International Society of Ultrasound in Obstetrics and Gynecology, 27(4), pp.349–354.*
16. *Baschat, A A, Turan, O.M. & Turan, S, 2012. Ductus venosus blood-flow patterns: more than meets the eye? Ultrasound in obstetrics & gynecology: the official journal of the International Society of Ultrasound in Obstetrics and Gynecology, 39(5), pp.598–599.*
17. *Behrman, R.E. et al., 1970. Distribution of the circulation in the normal and asphyxiated fetal primate. American journal of obstetrics and gynecology, 108(6), pp.956–969.*
18. *Bello-Munoz JC et al., 2012. Future Uses of Three/Four Dimensional Power Doppler Signal in Fetal Medicine. En Sonography. InTech web, pp. 249–272. Available at: http://www.intechopen.com/source/pdfs/27897/InTech-Future_uses_of_three_four_dimensional_power_doppler_signal_in_fetal_medicine.pdf.*

19. *Bello-Muñoz, J. et al., 2010. OC26.01: Fetal cardiac output: measurement by four dimensional power Doppler and artificial neural networks. Results from a sheep model. Ultrasound in Obstetrics & Gynecology, 36(S1), pp.46–46.*
20. *Bello-Muñoz, J. et al., 2009. OP23.05: A three-dimensional power Doppler algorithm for ductus venosus shunting evaluation in normal and growth restricted fetuses. Ultrasound in Obstetrics & Gynecology, 34(S1), pp.136–137.*
21. *Bellotti, M, Pennati, G & Ferrazzi, E, 2007. Re: ductus venosus shunting in growth-restricted fetuses and the effect of umbilical circulatory compromise. Ultrasound in Obstetrics & Gynecology: The Official Journal of the International Society of Ultrasound in Obstetrics and Gynecology, 29(1), pp.100–101; author reply 101–102.*
22. *Bellotti, M et al., 2000. Role of ductus venosus in distribution of umbilical blood flow in human fetuses during second half of pregnancy. American Journal of Physiology. Heart and Circulatory Physiology, 279(3), pp.H1256–1263.*
23. *Bellotti, Maria et al., 2004. Simultaneous measurements of umbilical venous, fetal hepatic, and ductus venosus blood flow in growth-restricted human fetuses. American Journal of Obstetrics and Gynecology, 190(5), pp.1347–1358.*

24. *Bendick, P.J. et al., 1998. Three-dimensional vascular imaging using Doppler ultrasound. American Journal of Surgery, 176(2), pp.183–187.*
25. *Berg, S. et al., 2000. Volumetric blood flow measurement with the use of dynamic 3-dimensional ultrasound color flow imaging. Journal of the American Society of Echocardiography: Official Publication of the American Society of Echocardiography, 13(5), pp.393–402.*
26. *Borrell, A. et al., 2003. Ductus venosus assessment at the time of nuchal translucency measurement in the detection of fetal aneuploidy. Prenatal diagnosis, 23(11), pp.921–926.*
27. *Bozkurt, N. et al., 2010. Correlations of fetal-maternal outcomes and first trimester 3-D placental volume/3-D power Doppler calculations. Clinical and Experimental Obstetrics & Gynecology, 37(1), pp.26–28.*
28. *Bracci, R., Perrone, S. & Buonocore, G., 2006. The timing of neonatal brain damage. Biology of the Neonate, 90(3), pp.145–155.*
29. *Burns, P.N., 1992. Measuring volume flow with Doppler ultrasound-an old nut. Ultrasound in Obstetrics & Gynecology: The Official Journal of the International Society of Ultrasound in Obstetrics and Gynecology, 2(4), pp.238–241.*
30. *van Cappellen, A.M. et al., 1999. Hypoxia, the subsequent systemic metabolic acidosis, and their relationship with cerebral metabolite concentrations: An in vivo study in fetal lambs with proton magnetic*

resonance spectroscopy. American Journal of Obstetrics and Gynecology, 181(6), pp.1537–1545.

31. *Cerf, M.E. et al., 2010. Gestational 30% and 40% fat diets increase brain GLUT2 and neuropeptide Y immunoreactivity in neonatal Wistar rats. International Journal of Developmental Neuroscience: The Official Journal of the International Society for Developmental Neuroscience, 28(7), pp.625–630.*
32. *Clouchoux, C. et al., 2011. Normative fetal brain growth by quantitative in vivo magnetic resonance imaging. American Journal of Obstetrics and Gynecology. Available at: http://www.ncbi.nlm.nih.gov/pubmed/22055336 [Accedido noviembre 20, 2011].*
33. *Coceani, F. & Olley, P.M., 1988. The control of cardiovascular shunts in the fetal and perinatal period. Canadian journal of physiology and pharmacology, 66(8), pp.1129–1134.*
34. *Collins, S. et al., 2011. Influence of power Doppler gain setting on Virtual Organ Computer AnaLysis (VOCAL) indices in vivo: Can use of the individual sub-noisegain (SNG) level optimise information? Ultrasound in Obstetrics & Gynecology: The Official Journal of the International Society of Ultrasound in Obstetrics and Gynecology. Available at: http://www.ncbi.nlm.nih.gov/pubmed/22009687 [Accedido mayo 14, 2012].*

35. *Crispi, Fatima & Gratacós, E., 2012. Fetal Cardiac Function: Technical Considerations and Potential Research and Clinical Applications. Fetal diagnosis and therapy. Available at: http://www.ncbi.nlm.nih.gov/pubmed/22614129 [Accedido junio 7, 2012].*
36. *Cruz-Martinez, R, Figueras, F, Hernandez-Andrade, E, et al., 2011. Normal reference ranges of fetal regional cerebral blood perfusion as measured by fractional moving blood volume. Ultrasound in Obstetrics & Gynecology: The Official Journal of the International Society of Ultrasound in Obstetrics and Gynecology, 37(2), pp.196–201.*
37. *Cruz-Martinez, R, Figueras, F, Benavides-Serralde, A., et al., 2011. Sequence of changes in myocardial performance index in relation to aortic isthmus and ductus venosus Doppler in fetuses with early-onset intrauterine growth restriction. Ultrasound in obstetrics & gynecology: the official journal of the International Society of Ultrasound in Obstetrics and Gynecology, 38(2), pp.179–184.*
38. *Cruz-Martinez, Rogelio et al., 2009. Cerebral blood perfusion and neurobehavioral performance in full-term small-for-gestational-age fetuses. American Journal of Obstetrics and Gynecology, 201(5), pp.474.e1–7.*

39. *Chang, C.-H. et al., 2003. Assessment of normal fetal liver blood flow using quantitative three-dimensional power Doppler ultrasound. Ultrasound in Medicine & Biology, 29(7), pp.943–949.*
40. *Chaoui, R. & Heling, K.S., 2005. New developments in fetal heart scanning: three- and four-dimensional fetal echocardiography. Seminars in Fetal & Neonatal Medicine, 10(6), pp.567–577.*
41. *Chaoui, R. & Kalache, K.D., 2001. Three-dimensional power Doppler ultrasound of the fetal great vessels. Ultrasound in Obstetrics & Gynecology: The Official Journal of the International Society of Ultrasound in Obstetrics and Gynecology, 17(5), pp.455–456.*
42. *Chmait, R., Kontopoulos, E. & Quintero, R., 2009. Fetoscopic management of complicated monochorionic twins. Clinical Obstetrics and Gynecology, 52(4), pp.647–653.*
43. *Dar, P. et al., 2010. First-trimester 3-dimensional power Doppler of the uteroplacental circulation space: a potential screening method for preeclampsia. American Journal of Obstetrics and Gynecology, 203(3), pp.238.e1–7.*
44. *DeVore, G.R. et al., 2003. Spatio-temporal image correlation (STIC): new technology for evaluation of the fetal heart. Ultrasound in Obstetrics & Gynecology: The Official Journal of the International Society of Ultrasound in Obstetrics and Gynecology, 22(4), pp.380–387.*

45. *Dong, F.Q. et al., 2011. Evaluation of normal fetal pulmonary veins from the early second trimester by enhanced-flow (e-flow) echocardiography. Ultrasound in obstetrics & gynecology: the official journal of the International Society of Ultrasound in Obstetrics and Gynecology, 38(6), pp.652–657.*
46. *Dubiel, M. et al., 2005. Computer analysis of three-dimensional power angiography images of foetal cerebral, lung and placental circulation in normal and high-risk pregnancy. Ultrasound in Medicine & Biology, 31(3), pp.321–327.*
47. *Ebbing, C, Rasmussen, S & Kiserud, T, 2011. Fetal hemodynamic development in macrosomic growth. Ultrasound in obstetrics & gynecology: the official journal of the International Society of Ultrasound in Obstetrics and Gynecology, 38(3), pp.303–308.*
48. *Ebbing, Cathrine et al., 2009. Redistribution pattern of fetal liver circulation in intrauterine growth restriction. Acta obstetricia et gynecologica Scandinavica, 88(10), pp.1118–1123.*
49. *Edelstone, D.I. & Rudolph, A.M., 1979. Preferential streaming of ductus venosus blood to the brain and heart in fetal lambs. The American journal of physiology, 237(6), pp.H724–729.*
50. *Eik-Nes, S.H. et al., 1982. Ultrasonic measurement of human fetal blood flow. Journal of Biomedical Engineering, 4(1), pp.28–36.*

51. *Erkinaro, T. et al., 2009. Placental and fetal hemodynamics after labetalol or pindolol in a sheep model of increased placental vascular resistance and maternal hypertension. Reproductive Sciences (Thousand Oaks, Calif.), 16(8), pp.749–757.*
52. *Fasouliotis, S.J. et al., 2002. The human fetal venous system: normal embryologic, anatomic, and physiologic characteristics and developmental abnormalities. Journal of Ultrasound in Medicine: Official Journal of the American Institute of Ultrasound in Medicine, 21(10), pp.1145–1158.*
53. *Fenster, A. et al., 1998. Three-dimensional ultrasound imaging of the vasculature. Ultrasonics, 36(1-5), pp.629–633.*
54. *Flo, K, Wilsgaard, T, Vårtun, A., et al., 2010. A longitudinal study of the relationship between maternal cardiac output measured by impedance cardiography and uterine artery blood flow in the second half of pregnancy. BJOG: An International Journal of Obstetrics and Gynaecology, 117(7), pp.837–844.*
55. *Flo, K, Wilsgaard, T & Acharya, G, 2010. Longitudinal reference ranges for umbilical vein blood flow at a free loop of the umbilical cord. Ultrasound in Obstetrics & Gynecology: The Official Journal of the International Society of Ultrasound in Obstetrics and Gynecology, 36(5), pp.567–572.*

56. *Flo, Kari, Wilsgaard, Tom & Acharya, Ganesh, 2010. Relation between utero-placental and feto-placental circulations: a longitudinal study. Acta obstetricia et gynecologica Scandinavica, 89(10), pp.1270–1275.*
57. *Forsberg, F. et al., 1995. Volume flow estimation using time domain correlation and ultrasonic flowmetry. Ultrasound in Medicine & Biology, 21(8), pp.1037–1045.*
58. *Fouron, J.C. et al., 2001. Correlation between prenatal velocity waveforms in the aortic isthmus and neurodevelopmental outcome between the ages of 2 and 4 years. American journal of obstetrics and gynecology, 184(4), pp.630–636.*
59. *Fouron, J.-C. et al., 2009. Feasibility and reliability of Doppler flow recordings in the fetal aortic isthmus: a multicenter evaluation. Ultrasound in obstetrics & gynecology: the official journal of the International Society of Ultrasound in Obstetrics and Gynecology, 33(6), pp.690–693.*
60. *Fugelseth, D. et al., 1998. Postnatal closure of ductus venosus in preterm infants < or = 32 weeks. An ultrasonographic study. Early human development, 53(2), pp.163–169.*
61. *Galan, H.L. et al., 2005. Fetal hypertension and abnormal Doppler velocimetry in an ovine model of intrauterine growth restriction. American journal of obstetrics and gynecology, 192(1), pp.272–279.*

62. *Gill, R.W., 1979. Pulsed Doppler with B-mode imaging for quantitative blood flow measurement. Ultrasound in Medicine & Biology, 5(3), pp.223–235.*

63. *Godfrey, K.M., 2002. The role of the placenta in fetal programming-a review. Placenta, 23 Suppl A, pp.S20–27.*

64. *Grosse-Wortmann, L., Bindl, L. & Seghaye, M.-C., 2006. Multiple types of cardiac arrhythmias in a child with head injury and raised intracranial pressure. Pediatric Cardiology, 27(2), pp.286–288.*

65. *Guimarães Filho, H.A. et al., 2011. Reproducibility of three-dimensional power Doppler placental vascular indices in pregnancies between 26 and 35 weeks. Archives of Gynecology and Obstetrics, 283(2), pp.213–217.*

66. *Guo, Z. et al., 1998. In vitro evaluation of multiple arterial stenoses using three-dimensional power Doppler angiography. Journal of Vascular Surgery: Official Publication, the Society for Vascular Surgery [and] International Society for Cardiovascular Surgery, North American Chapter, 27(4), pp.681–688.*

67. *Guo, Z. & Fenster, A., 1996. Three-dimensional power Doppler imaging: a phantom study to quantify vessel stenosis. Ultrasound in Medicine & Biology, 22(8), pp.1059–1069.*

68. *Hack, K.E.A. et al., 2009. Long-term neurodevelopmental outcome of monochorionic and matched dichorionic twins. PloS One, 4(8), p.e6815.*

69. *Hamill, N. et al., 2011. Fetal cardiac ventricular volume, cardiac output, and ejection fraction determined with 4-dimensional ultrasound using spatiotemporal image correlation and virtual organ computer-aided analysis. American Journal of Obstetrics and Gynecology. Available at: http://www.ncbi.nlm.nih.gov/pubmed/21531373 [Accedido julio 17, 2011].*

70. *Harrington, K., Deane, C. & Campbell, S., 1996. Measurement of volume flow with time domain and M-mode imaging: in vitro and in vivo validation studies. Journal of Ultrasound in Medicine: Official Journal of the American Institute of Ultrasound in Medicine, 15(10), pp.715–720.*

71. *Hashima, J.N. et al., 2010. Fetal ventricular diastolic filling characteristics in a primate model: the role of fetal heart rate and pulmonary vascular impedance. Reproductive sciences (Thousand Oaks, Calif.), 17(8), pp.760–766.*

72. *Haugen, G. et al., 2005. Fetal liver-sparing cardiovascular adaptations linked to mother's slimness and diet. Circulation research, 96(1), pp.12–14.*

73. *Hayashi, T. et al., 1998. Three-dimensional reconstruction of the power flow Doppler imaging of intracranial vascular structures in the neonate. Journal of Neuroimaging: Official Journal of the American Society of Neuroimaging, 8(2), pp.94–96.*
74. *Heck, S. et al., 2012. Evaluation of Neonatal Regional Cerebral Perfusion Using Power Doppler and the Index Fractional Moving Blood Volume. Neonatology, 101(4), pp.254–259.*
75. *Heling, K.S., Chaoui, R. & Bollmann, R., 2000. Prenatal depiction of the angioarchitecture of an aneurysm of the vein of Galen with three-dimensional color power angiography. Ultrasound in Obstetrics & Gynecology: The Official Journal of the International Society of Ultrasound in Obstetrics and Gynecology, 15(4), p.345.*
76. *Hernandez-Andrade, E et al., 2008. Changes in regional fetal cerebral blood flow perfusion in relation to hemodynamic deterioration in severely growth-restricted fetuses. Ultrasound in Obstetrics & Gynecology: The Official Journal of the International Society of Ultrasound in Obstetrics and Gynecology, 32(1), pp.71–76.*
77. *Hernandez-Andrade, E, Thuring-Jönsson, A., et al., 2004. Fractional moving blood volume estimation in the fetal lung using power Doppler ultrasound: a reproducibility study. Ultrasound in Obstetrics & Gynecology: The Official Journal of the International Society of Ultrasound in Obstetrics and Gynecology, 23(4), pp.369–373.*

78. *Hernandez-Andrade, E, Jansson, T, et al., 2004. Validation of fractional moving blood volume measurement with power Doppler ultrasound in an experimental sheep model. Ultrasound in Obstetrics & Gynecology: The Official Journal of the International Society of Ultrasound in Obstetrics and Gynecology, 23(4), pp.363–368.*
79. *Ishida, H. et al., 2011. Clinical features of the complete closure of the ductus arteriosus prenatally. Congenital heart disease, 6(1), pp.51–56.*
80. *Jansson, Thomas & Powell, T.L., 2007. Role of the placenta in fetal programming: underlying mechanisms and potential interventional approaches. Clinical science (London, England: 1979), 113(1), pp.1–13.*
81. *Jansson, Tomas et al., 2003. Estimation of fractional moving blood volume in fetal lung using Power Doppler ultrasound, methodological aspects. Ultrasound in Medicine & Biology, 29(11), pp.1551–1559.*
82. *Johnson, P., 2000. Intracardiac pressures in the human fetus. Heart, 84(1), pp.59–63.*
83. *Jones, M.G., Shipley, J.A. & Robinson, T.M., 2003. Visualisation of 4-D colour and power Doppler data. Ultrasound in Medicine & Biology, 29(12), pp.1735–1747.*
84. *Jones, N W et al., 2009. In vitro dual perfusion of human placental lobules as a flow phantom to investigate the relationship between*

fetoplacental flow and quantitative 3D power doppler angiography. Placenta, 30(2), pp.130–135.

85. *Jones, Nia W et al., 2011. Evaluating the intra- and interobserver reliability of three-dimensional ultrasound and power Doppler angiography (3D-PDA) for assessment of placental volume and vascularity in the second trimester of pregnancy. Ultrasound in Medicine & Biology, 37(3), pp.376–385.*
86. *Jordan-Young, R.M., 2011. Hormones, context, and «Brain Gender»: A review of evidence from congenital adrenal hyperplasia. Social Science & Medicine (1982). Available at: http://www.ncbi.nlm.nih.gov/pubmed/21962724 [Accedido octubre 4, 2011].*
87. *Kaji, T. et al., 2012. Simultaneous recordings of pulsed wave Doppler signals in hepatic vein and descending aorta using dual Doppler: a novel method for evaluating fetal arrhythmias. Ultrasound in obstetrics & gynecology: the official journal of the International Society of Ultrasound in Obstetrics and Gynecology, 39(3), pp.357–359.*
88. *Kessler, Jörg et al., 2009. Fetal growth restriction is associated with prioritization of umbilical blood flow to the left hepatic lobe at the expense of the right lobe. Pediatric research, 66(1), pp.113–117.*

89. *Kessler, Jörg et al., 2008. Longitudinal study of umbilical and portal venous blood flow to the fetal liver: low pregnancy weight gain is associated with preferential supply to the fetal left liver lobe. Pediatric research, 63(3), pp.315–320.*
90. *Kilavuz, O. et al., 2003. The left portal vein is the watershed of the fetal venous system. Journal of Perinatal Medicine, 31(2), pp.184–187.*
91. *Kiserud, T et al., 1992. Foramen ovale: an ultrasonographic study of its relation to the inferior vena cava, ductus venosus and hepatic veins. Ultrasound in obstetrics & gynecology: the official journal of the International Society of Ultrasound in Obstetrics and Gynecology, 2(6), pp.389–396.*
92. *Kiserud, T et al., 2006. Ductus venosus shunting in growth-restricted fetuses and the effect of umbilical circulatory compromise. Ultrasound in Obstetrics & Gynecology: The Official Journal of the International Society of Ultrasound in Obstetrics and Gynecology, 28(2), pp.143–149.*
93. *Kiserud, T. et al., 1994. Estimation of the pressure gradient across the fetal ductus venosus based on doppler velocimetry. Ultrasound in Medicine & Biology, 20(3), pp.225–232.*
94. *Kiserud, T, 2001. The ductus venosus. Seminars in Perinatology, 25(1), pp.11–20.*

95. *Kiserud, Torvid & Acharya, Ganesh, 2004. The fetal circulation. Prenatal Diagnosis, 24(13), pp.1049–1059.*

96. *Kok, R.D. et al., 2002. Maturation of the human fetal brain as observed by 1H MR spectroscopy. Magnetic Resonance in Medicine: Official Journal of the Society of Magnetic Resonance in Medicine / Society of Magnetic Resonance in Medicine, 48(4), pp.611–616.*

97. *Kripfgans, O.D. et al., 2006. Measurement of volumetric flow. Journal of Ultrasound in Medicine: Official Journal of the American Institute of Ultrasound in Medicine, 25(10), pp.1305–1311.*

98. *Kupesic, S. & Kurjak, A., 2000. Contrast-enhanced, three-dimensional power Doppler sonography for differentiation of adnexal masses. Obstetrics and Gynecology, 96(3), pp.452–458.*

99. *Kurjak, A. et al., 1998. The assessment of ovarian tumor angiogenesis: what does three-dimensional power Doppler add? Ultrasound in Obstetrics & Gynecology: The Official Journal of the International Society of Ultrasound in Obstetrics and Gynecology, 12(2), pp.136–146.*

100. *Lai, P.K., Wang, Y.A. & Welsh, A.W., 2010. Reproducibility of regional placental vascularity/perfusion measurement using 3D power Doppler. Ultrasound in Obstetrics & Gynecology: The Official Journal of the International Society of Ultrasound in Obstetrics and Gynecology, 36(2), pp.202–209.*

101. Lewis, R.L. & Gutmann, L., 2002. Post-traumatic paradoxical embolism in patent foramen ovale. Neurology, 59(10), p.1611.

102. Li, H., Gudmundsson, S. & Olofsson, P., 2006. Acute centralization of blood flow in compromised human fetuses evoked by uterine contractions. Early human development, 82(11), pp.747–752.

103. Li, X. et al., 2005. A novel method for the assessment of the accuracy of computing laminar flow stroke volumes using a real-time 3D ultrasound system: In vitro studies. European Journal of Echocardiography: The Journal of the Working Group on Echocardiography of the European Society of Cardiology, 6(6), pp.396–404.

104. Licht, D.J. et al., 2009. Brain maturation is delayed in infants with complex congenital heart defects. The Journal of Thoracic and Cardiovascular Surgery, 137(3), pp.529–536; discussion 536–537.

105. Lim, K. et al., 2012. Third trimester fetal pulmonary artery Doppler blood flow velocity characteristics following prenatal selective serotonin reuptake inhibitor (SSRI) exposure. Early human development. Available at: http://www.ncbi.nlm.nih.gov/pubmed/22305713 [Accedido mayo 14, 2012].

106. Limperopoulos, C., 2009. Disorders of the fetal circulation and the fetal brain. Clinics in Perinatology, 36(3), pp.561–577.

107. Loberant, N. et al., 1999. Closure of the ductus venosus in premature infants: findings on real-time gray-scale, color-flow Doppler, and duplex Doppler sonography. AJR. American journal of roentgenology, 172(1), pp.227–229.

108. Mäkikallio, K., Jouppila, P. & Räsänen, J., 2003. Retrograde aortic isthmus net blood flow and human fetal cardiac function in placental insufficiency. Ultrasound in Obstetrics & Gynecology, 22(4), pp.351–357.

109. Marín, R.C. et al., 2010. Use of 3-dimensional sonography for prenatal evaluation and follow-up of fetal goitrous hypothyroidism. Journal of Ultrasound in Medicine: Official Journal of the American Institute of Ultrasound in Medicine, 29(9), pp.1339–1343.

110. Martins, W.P. & Raine-Fenning, N J, 2010. Analysis and acquisition reproducibility of 3D power Doppler. Ultrasound in Obstetrics & Gynecology: The Official Journal of the International Society of Ultrasound in Obstetrics and Gynecology, 36(3), pp.392–393; author reply 393–394.

111. Mess, A.M. & Ferner, K.J., 2010. Evolution and development of gas exchange structures in Mammalia: the placenta and the lung. Respiratory physiology & neurobiology, 173 Suppl, pp.S74–82.

112. Messing, B. et al., 2007. Fetal cardiac ventricle volumetry in the second half of gestation assessed by 4D ultrasound using STIC

combined with inversion mode. Ultrasound in Obstetrics & Gynecology: The Official Journal of the International Society of Ultrasound in Obstetrics and Gynecology, 30(2), pp.142–151.

113. *Milani, H.J.F. et al., 2011. Assessment of cerebral circulation in normal fetuses by three-dimensional power Doppler ultrasonography. European Journal of Radiology. Available at: http://www.ncbi.nlm.nih.gov/pubmed/21300496 [Accedido julio 17, 2011].*

114. *Molina, F.S. et al., 2008a. Heart stroke volume and cardiac output by four-dimensional ultrasound in normal fetuses. Ultrasound in Obstetrics & Gynecology: The Official Journal of the International Society of Ultrasound in Obstetrics and Gynecology, 32(2), pp.181–187.*

115. *Molina, F.S. et al., 2008b. Heart stroke volume and cardiac output by four-dimensional ultrasound in normal fetuses. Ultrasound in Obstetrics & Gynecology: The Official Journal of the International Society of Ultrasound in Obstetrics and Gynecology, 32(2), pp.181–187.*

116. *Momma, K. & Takao, A., 1989. Increased constriction of the ductus arteriosus with combined administration of indomethacin and betamethasone in fetal rats. Pediatric research, 25(1), pp.69–75.*

117. Morel, O. et al., 2010. Correlation between uteroplacental three-dimensional power Doppler indices and true uterine blood flow: evaluation in a pregnant sheep model. Ultrasound in Obstetrics & Gynecology: The Official Journal of the International Society of Ultrasound in Obstetrics and Gynecology, 36(5), pp.635–640.

118. Moskalik, A.P. et al., 2001. Analysis of three-dimensional Doppler ultrasonographic quantitative measures for the discrimination of prostate cancer. Journal of Ultrasound in Medicine: Official Journal of the American Institute of Ultrasound in Medicine, 20(7), pp.713–722.

119. Murphy, V.E. et al., 2006. Endocrine regulation of human fetal growth: the role of the mother, placenta, and fetus. Endocrine reviews, 27(2), pp.141–169.

120. Myatt, L., 2006. Placental adaptive responses and fetal programming. The Journal of physiology, 572(Pt 1), pp.25–30.

121. Nardozza, L.M.M. et al., 2009. Evolution of 3-D power Doppler indices of fetal brain in normal pregnancy. Ultrasound in Medicine & Biology, 35(4), pp.545–549.

122. Nathanielsz, P.W. & Hanson, M.A., 2003. The fetal dilemma: spare the brain and spoil the liver. The Journal of physiology, 548(Pt 2), p.333.

123. *Negrini, R. et al., 2011. Assessment of placental blood flow between 22 and 34 weeks of gestation by 3D-sonography power Doppler vascular indices. Archives of Gynecology and Obstetrics, 284(1), pp.53–57.*

124. *Odeh, M. et al., 2011. Placental volume and three-dimensional power Doppler analysis in prediction of pre-eclampsia and small for gestational age between Week 11 and 13 weeks and 6 days of gestation. Prenatal Diagnosis, 31(4), pp.367–371.*

125. *Odibo, A.O. et al., 2011. Placental volume and vascular flow assessed by 3D power Doppler and adverse pregnancy outcomes. Placenta, 32(3), pp.230–234.*

126. *Pairleitner, H. et al., 1999. Three-dimensional power Doppler sonography: imaging and quantifying blood flow and vascularization. Ultrasound in Obstetrics & Gynecology: The Official Journal of the International Society of Ultrasound in Obstetrics and Gynecology, 14(2), pp.139–143.*

127. *Pardi, G. & Cetin, I., 2006. Human fetal growth and organ development: 50 years of discoveries. American journal of obstetrics and gynecology, 194(4), pp.1088–1099.*

128. *Pemberton, J. et al., 2005. The use of live three-dimensional Doppler echocardiography in the measurement of cardiac output: an*

in vivo animal study. Journal of the American College of Cardiology, 45(3), pp.433–438.

129. Petersch, B. & Hönigmann, D., 2007. Blood flow in its context: combining 3D B-mode and color Doppler ultrasonic data. IEEE Transactions on Visualization and Computer Graphics, 13(4), pp.748–757.

130. Pomorski, M. et al., 2011. Comparative analysis of placental vasculature and placental volume in normal and IUGR pregnancies with the use of three-dimensional Power Doppler. Archives of Gynecology and Obstetrics. Available at: http://www.ncbi.nlm.nih.gov/pubmed/21744006 [Accedido julio 17, 2011].

131. Raine-Fenning, N J et al., 2008a. Determining the relationship between three-dimensional power Doppler data and true blood flow characteristics: an in-vitro flow phantom experiment. Ultrasound in Obstetrics & Gynecology: The Official Journal of the International Society of Ultrasound in Obstetrics and Gynecology, 32(4), pp.540–550.

132. Raine-Fenning, N J et al., 2008b. Evaluation of the effect of machine settings on quantitative three-dimensional power Doppler angiography: an in-vitro flow phantom experiment. Ultrasound in Obstetrics & Gynecology: The Official Journal of the International

Society of Ultrasound in Obstetrics and Gynecology, 32(4), pp.551–559.

133. *Ram, R. et al., 2011. New approaches in small animal echocardiography: imaging the sounds of silence. American journal of physiology. Heart and circulatory physiology, 301(5), pp.H1765–1780.*

134. *Rasanen, J et al., 1996. Role of the pulmonary circulation in the distribution of human fetal cardiac output during the second half of pregnancy. Circulation, 94(5), pp.1068–1073.*

135. *Reller, M.D. et al., 1987. Fetal lamb ventricles respond differently to filling and arterial pressures and to in utero ventilation. Pediatric research, 22(6), pp.621–626.*

136. *Richards, M.S. et al., 2009. Mean volume flow estimation in pulsatile flow conditions. Ultrasound in Medicine & Biology, 35(11), pp.1880–1891.*

137. *Rizzo, G. et al., 2009. First-trimester placental volume and vascularization measured by 3-dimensional power Doppler sonography in pregnancies with low serum pregnancy-associated plasma protein a levels. Journal of Ultrasound in Medicine: Official Journal of the American Institute of Ultrasound in Medicine, 28(12), pp.1615–1622.*

138. *Robb, R.A., Aharon, S. & Cameron, B.M., 1997. Patient-specific anatomic models from three dimensional medical image data for*

clinical applications in surgery and endoscopy. Journal of Digital Imaging: The Official Journal of the Society for Computer Applications in Radiology, 10(3 Suppl 1), pp.31–35.

139. Robinson, J. et al., 1995. Placental control of fetal growth. Reproduction, fertility, and development, 7(3), pp.333–344.

140. Ruano, R. et al., 2006. Quantitative analysis of fetal pulmonary vasculature by 3-dimensional power Doppler ultrasonography in isolated congenital diaphragmatic hernia. American Journal of Obstetrics and Gynecology, 195(6), pp.1720–1728.

141. Rubin, J M, 1999. Flow quantification. European Radiology, 9 Suppl 3, pp.S368–371.

142. Rubin, J M et al., 1997. Normalizing fractional moving blood volume estimates with power Doppler US: defining a stable intravascular point with the cumulative power distribution function. Radiology, 205(3), pp.757–765.

143. Rubin, J M et al., 1994. Power Doppler US: a potentially useful alternative to mean frequency-based color Doppler US. Radiology, 190(3), pp.853–856.

144. Rubin, J M, Tuthill, T.A. & Fowlkes, J B, 2001. Volume flow measurement using Doppler and grey-scale decorrelation. Ultrasound in Medicine & Biology, 27(1), pp.101–109.

145. *Rudolph, A.M., 1985. Distribution and regulation of blood flow in the fetal and neonatal lamb. Circulation research, 57(6), pp.811–821.*

146. *Sandovici, Ionel et al., 2012. Placental adaptations to the maternal-fetal environment: implications for fetal growth and developmental programming. Reproductive biomedicine online. Available at: http://www.ncbi.nlm.nih.gov/pubmed/22560117 [Accedido mayo 14, 2012].*

147. *Sauders, J.B., Wright, N. & Lewis, K.O., 1980. Measurement of human fetal blood flow. British Medical Journal, 280(6210), pp.283–284.*

148. *Schulten-Wijman, M.J. et al., 2011. Re: Three-dimensional power Doppler: validity and reliability. Ultrasound in Obstetrics & Gynecology: The Official Journal of the International Society of Ultrasound in Obstetrics and Gynecology, 37(5), pp.620–621.*

149. *Sibley, C.P. et al., 2010. Review: Adaptation in placental nutrient supply to meet fetal growth demand: implications for programming. Placenta, 31 Suppl, pp.S70–74.*

150. *Simioni, C., Nardozza, L.M.M., Araujo Júnior, E., Rolo, Liliam Cristine, et al., 2011. Fetal cardiac function assessed by spatio-temporal image correlation. Archives of Gynecology and Obstetrics, 284(1), pp.253–260.*

151. *Simioni, C., Nardozza, L.M.M., Araujo Júnior, E., Rolo, Líliam Cristine, et al., 2011. Heart stroke volume, cardiac output, and ejection fraction in 265 normal fetus in the second half of gestation assessed by 4D ultrasound using spatio-temporal image correlation. The Journal of Maternal-Fetal & Neonatal Medicine: The Official Journal of the European Association of Perinatal Medicine, the Federation of Asia and Oceania Perinatal Societies, the International Society of Perinatal Obstetricians. Available at: http://www.ncbi.nlm.nih.gov/pubmed/21250911 [Accedido julio 17, 2011].*

152. *Smith, G.C.S. & Cameron, A.D., 2003. Estimating human fetal blood volume on the basis of gestational age and fetal abdominal circumference. BJOG: An International Journal of Obstetrics & Gynaecology, 109(6), pp.721–722.*

153. *Smith, N.A. et al., 2010. Contemporary management of monochorionic diamniotic twins: outcomes and delivery recommendations revisited. American Journal of Obstetrics and Gynecology, 203(2), pp.133.e1–6.*

154. *Smolich, J.J., Penny, D.J. & Mynard, J.P., 2012. Enhanced central and conduit pulmonary arterial reservoir function offsets reduced ductal systolic outflow during constriction of the fetal ductus*

arteriosus. American journal of physiology. Regulatory, integrative and comparative physiology, 302(1), pp.R175–183.

155. Sohn, C., 1993. [Ultrasound--future developments]. Bildgebung = Imaging, 60(4), pp.301–309.

156. Staboulidou, I. et al., 2011. Prevalence and outcome of absence of ductus venosus at 11(+0) to 13(+6) weeks. Fetal diagnosis and therapy, 30(1), pp.35–40.

157. Staboulidou, I. et al., 2007. The significance of intracardiac Doppler sonography in terms of fetal growth retardation. Archives of gynecology and obstetrics, 276(1), pp.35–42.

158. Sun, Y. et al., 1995. Estimation of volume flow rate by surface integration of velocity vectors from color Doppler images. Journal of the American Society of Echocardiography: Official Publication of the American Society of Echocardiography, 8(6), pp.904–914.

159. Tchirikov, M, Schröder, H J & Hecher, K, 2006. Ductus venosus shunting in the fetal venous circulation: regulatory mechanisms, diagnostic methods and medical importance. Ultrasound in Obstetrics & Gynecology: The Official Journal of the International Society of Ultrasound in Obstetrics and Gynecology, 27(4), pp.452–461.

160. Tchirikov, Michael, Strohner, M. & Scholz, A., 2010. Cardiac output and blood flow volume redistribution during acute maternal

hypoxia in fetal sheep. Journal of perinatal medicine, 38(4), pp.387–392.

161. Tchirikov, Mikhail et al., 2005. Structural evidence for mechanisms to redistribute hepatic and ductus venosus blood flows in nonhuman primate fetuses. American journal of obstetrics and gynecology, 192(4), pp.1146–1152.

162. Thomas, J.T. et al., 2012. Absent ductus venosus - outcomes and implications from a tertiary centre. Prenatal diagnosis. Available at: http://www.ncbi.nlm.nih.gov/pubmed/22610967 [Accedido junio 4, 2012].

163. Turan, Sifa, Miller, J. & Baschat, Ahmet A, 2008. Integrated testing and management in fetal growth restriction. Seminars in Perinatology, 32(3), pp.194–200.

164. Tuuli, M.G. et al., 2010. Validation of placental vascular sonobiopsy for obtaining representative placental vascular indices by three-dimensional power Doppler ultrasonography. Placenta, 31(3), pp.192–196.

165. Uerpairojkit, B. et al., 2012. Are the cardiac dimensions spared in growth-restricted fetuses resulting from uteroplacental insufficiency? The journal of obstetrics and gynaecology research, 38(2), pp.390–395.

166. *Vallance, P., Collier, J. & Moncada, S., 1989. Effects of endothelium-derived nitric oxide on peripheral arteriolar tone in man. Lancet, 2(8670), pp.997–1000.*

167. *Volpe, P. et al., 2011. Fetal cardiac evaluation at 11-14 weeks by experienced obstetricians in a low-risk population. Prenatal diagnosis, 31(11), pp.1054–1061.*

168. *Volpe, P. et al., 2002. Prenatal diagnosis of ductus venosus agenesis and its association with cytogenetic/congenital anomalies. Prenatal diagnosis, 22(11), pp.995–1000.*

169. *Wald, N.J., Bestwick, J.P. & Borrell, A., 2012. Adding ductus venosus blood flow as a categorical variable to the Combined and Integrated tests in Down's syndrome screening. Journal of medical screening, 19(1), pp.49–50.*

170. *Wei, S. et al., 2011. Idiopathic occlusion of the fetal ductus arteriosus without lumen narrowing. Echocardiography (Mount Kisco, N.Y.), 28(4), pp.E85–88.*

171. *Weichert, J., Hartge, D.R. & Axt-Fliedner, R., 2010. The fetal ductus arteriosus and its abnormalities--a review. Congenital heart disease, 5(5), pp.398–408.*

172. *Welsh, A, 2004. Quantification of power Doppler and the index «fractional moving blood volume» (FMBV). Ultrasound in Obstetrics*

& Gynecology: The Official Journal of the International Society of Ultrasound in Obstetrics and Gynecology, 23(4), pp.323–326.

173. Welsh, A.W. et al., 2005. Standardization of power Doppler quantification of blood flow in the human fetus using the aorta and inferior vena cava. Ultrasound in Obstetrics & Gynecology: The Official Journal of the International Society of Ultrasound in Obstetrics and Gynecology, 26(1), pp.33–43.

174. Welsh, Aw et al., 2012. Inapplicability of the Fractional Moving Blood Volume (FMBV) technique to standardise VOCAL indices for quantified power Doppler. Ultrasound in Obstetrics & Gynecology: The Official Journal of the International Society of Ultrasound in Obstetrics and Gynecology. Available at: http://www.ncbi.nlm.nih.gov/pubmed/22344971 [Accedido mayo 14, 2012].

175. Williams, D.J. et al., 1997. Nitric oxide-mediated vasodilation in human pregnancy. The American Journal of Physiology, 272(2 Pt 2), pp.H748–752.

176. Wolfberg, A.J. et al., 2007. Identification of fetal cerebral lactate using magnetic resonance spectroscopy. American Journal of Obstetrics and Gynecology, 196(1), pp.e9–11.

177. Yagel, S et al., 2006. Rendering in fetal cardiac scanning: the intracardiac septa and the coronal atrioventricular valve planes.

Ultrasound in Obstetrics & Gynecology: The Official Journal of the International Society of Ultrasound in Obstetrics and Gynecology, 28(3), pp.266–274.

178. *Yamamura, J. et al., 2012. Cardiac MRI of the fetal heart using a novel triggering method: Initial results in an animal model. Journal of magnetic resonance imaging: JMRI, 35(5), pp.1071–1076.*

179. *Yigiter, A.B. et al., 2011. Placental volume and vascularization flow indices by 3D power Doppler US using VOCAL technique and correlation with IGF-1, free beta-hCG, PAPP-A, and uterine artery Doppler at 11-14 weeks of pregnancy. Journal of Perinatal Medicine, 39(2), pp.137–141.*

Annex 1 DISCLOSURES

1. *Confidentiality agreemetn with Samsung Medison*

NON DISCLOSURE AGREEMENT BETWEEN FUNDACIÓ HOSPITAL UNIVERSITARI VALL D'HEBRON INSTITUT DE RECERCA AND SAMSUNG MEDISON EUROPE

This Agreement is made effective as of the date of the last signature hereto by and between:

FUNDACIÓ HOSPITAL UNIVERSITARI VALL D'HEBRON INSTITUT DE RECERCA (hereinafter referred to as "**VHIR**"), a non-for-profit Spanish foundation with tax identification number G-60594009, based in Barcelona, Spain, Passeig Vall d'Hebron, 119-129, represented by Dr. Joan X. Comella Carnicé.

and

SA,SING MEDISON EUROPE B.V. (hereinafter "SMNL"), a Dutch company with tax identification number NL8151.86.368.B01 based in Parellaan 10, 2132WS, Hoofddorp, The Netherlands represented by Ms/Mr. SH Ko that acts in his/her capacity as a CEO

VHIR and Recipient are collectively referred to as the "**Parties**" and individually as a "**Party**".

RECITALS

I. VHIR is the owner of Confidential Information related to developments and research in the field of Doppler ultrasound blood

flow velocity conducted by Dr. Bello and Dr. Carreras as defined under this document.

II. VHIR considers the disclosure of Confidential Information to Recipient to be necessary and desirable for the purpose of facilitating discussion and evaluation of possible collaborative research, development activities, commercialization of technology and/or other related activities, etc. (hereinafter, the "**Purpose**") and unauthorised disclosure of such Confidential Information may cause irreparable damages to VHIR.

III. Such Confidential Information is not public knowledge and is being disclosed to Recipient only under the terms and conditions of the present document.

IV. This Agreement is being entered into by and between the Parties in order to protect the confidentiality and non-disclosure of Confidential Information by Recipient.

NOW THEREFORE, the Parties, mutually acknowledging their sufficient legal capacity to enter into and be bound by this Non-Disclosure Agreement (hereinafter, the "**Agreement**") agree as follows:

1. CONFIDENTIAL INFORMATION

1.1. For the purposes of this Agreement, "**Confidential Information**" means any business, commercial scientific or technical information that VHIR discloses to Recipient, including but not limited to, technical data, know-how, ideas, inventions, concepts, business plans, new products, agreements, projects, documents, mechanical or

electronic designs, logos, new technologies, planes, drawings, designs, instructions, recommendations and any other information of any nature regarding VHIR and its activity or which, under the circumstances surrounding disclosure ought to be treated as confidential by Recipient, that has been transferred by the VHIR to Recipient prior to the execution of this Agreement or that is transferred in the future, whether orally or in writing, or which is made available to the Recipient.

1.2. Recipient acknowledges and agrees that Confidential Information in his possession, whether currently or in the future, shall be deemed valuable information or information owned by VHIR.

2. USE OF CONFIDENTIAL INFORMATION

2.1. Recipient shall use Confidential Information only for the Purpose.

2.2. Recipient agrees to hold in confidence any and all Confidential Information disclosed, and further agrees not to disclose Confidential Information to third parties or to use Confidential Information, except for the Purpose or with the written permission from an authorized officer of IR-HUVH. **For Clarification, Samsung Medison, as a head office of Samsung Medison Europe B.V., located in Seoul , Korea, is not a third party.**

2.3. Recipient undertakes to use its best efforts to limit access to Confidential Information under its control solely to Recipient's employees whose access to Confidential Information is essential, provided that such employees have been specifically informed of the confidentiality of Confidential Information and have agreed to be bound by the terms of this Agreement or have entered into an agreement of similar scope and obligations with Recipient to protect the proprietary/confidential information of Recipient or the

proprietary/confidential information of third parties in Recipient's possession. Notwithstanding the above, Recipient shall remain liable for the compliance of the terms and conditions of the present Agreement by its employees.

2.4. Recipient shall use the same degree of care as Recipient uses to protect its own confidential information of a similar nature, but no less than reasonable care, to prevent the unauthorized use, disclosure or publication of Confidential Information.

2.5. In the event that VHIR provides any computer software and/or hardware to Recipient as Confidential Information, Recipient may not directly or indirectly, disassemble, decrypt, electronically scan, decompile or derive source code from Confidential Information, or otherwise attempt to reverse engineer the design and function of Confidential Information.

2.6. Recipient shall notify VHIR immediately upon discovery of any unauthorized use or disclosure of Confidential Information or any other breach of this Agreement by Recipient and its employees and consultants, and cooperate with VHIR in order to help VHIR regain possession of Confidential Information and prevent its further unauthorized use or disclosure.

2.7. Recipient shall, at VHIR's request, return all originals, copies, reproductions and summaries of Confidential Information and all other tangible materials and devices provided to the Recipient as Confidential Information, or at VHIR's option, certify destruction of the same.

2.8. Recipient shall fully comply with Spain's imperative Organic Law 15/1999 of Personal Data Protection, when Confidential Information includes personal data identifiable with any individual.

2.9. Should any of the Parties be interested in using any information regarding this Agreement, whether in total or in part, to any other third party, both Parties shall have to reach an agreement prior to any disclosure of such information establishing the terms and conditions of the disclosure of any such information.

3. OWNERSHIP OF CONFIDENTIAL INFORMATION

3.1. All Confidential Information is and shall remain the property of VHIR, and VHIR may use such Confidential Information for any purpose without obligation to Recipient. Neither the execution of this Agreement nor the furnishing of any Confidential Information hereunder shall be construed as an assignment or transmission, neither expressly nor by implication, of any intellectual and/or industrial property right now or hereinafter owned by or controlled by IR-HUVH.

3.2. Recipient covenants and undertakes not to use under its name (or register), nor shall it collaborate with any third party for said purpose, all or part of intellectual and/or industrial property rights, patents or trademarks owned by VHIR.

4. PERSONAL DATA PROTECTION

4.1. Recipient agrees to abide by applicable personal data protection laws. As a result, Recipient agrees to:

a) Use the data following the instructions of the owner of such data.

b) Only use the data for the purposes of this Agreement.

c) Not disclose to third parties nor copy any personal data, even for conservation purposes.

d) Apply all the reasonable security measures, and in any case those required by the Law, in order to preserve the integrity, confidentiality and the disposure/traffic of the data.

e) Destroy the personal data, including any documentation or format containing such information, or return it to the other party, upon termination of this Agreement.

5. LIMITATIONS ON CONFIDENTIALITY

Nothing in this Agreement shall be interpreted as placing any obligation of confidentiality and non-use by Recipient with respect to any information that:

(a) can be demonstrated to have been in the public domain as of the effective date of this Agreement, or legitimately comes into the public domain through no fault of the Recipient; or

(b) can be demonstrated to have been known by the Recipient prior to execution of this Agreement and that it has not been acquired, directly or indirectly, from VHIR or from a third party under a continuing obligation of confidentiality; or

(c) can be demonstrated to have been independently developed by personnel of the Recipient who had no substantive knowledge of any information provided by VHIR; or

(d) is required to be disclosed pursuant to law or court order, provided that Recipient provides prior notice to VHIR and

provides sufficient time to VHIR to assert any exclusions or privileges that may be available by law.

6. LIMITED WARRANTY AND LIABILITY

VHIR makes no warranties in respect of Confidential Information and provides all information "as is", without any express or implied warranty of any kind, including any warranty as to merchantability, fitness for a particular purpose, accuracy, completeness or violation of third party intellectual and/or property rights. In no event shall VHIR be liable for any special, incidental or consequential damages of any kind whatsoever resulting from the disclosure, use or receipt of Confidential Information.

7. REMEDIES

The Parties acknowledge that monetary damages may not be a sufficient remedy for unauthorized disclosure of Confidential Information and that VHIR shall be entitled, without waiving any other rights or remedies, to such injunctive or equitable relief as may be deemed proper by a court of competent jurisdiction.

8. TERM

8.1. The term of this Agreement is of [five] (5) years. Notwithstanding the referred term, this Agreement shall remain in full force and effect indefinitely for as long as Confidential Information is secret and confidential. In the event any Confidential Information should be under physical control of the Recipient before this Agreement is signed, the terms and provisions shall apply for such Confidential Information retroactively.

8.2. Upon expiration or termination of this Agreement, Recipient will immediately cease any and all disclosures or uses of Confidential Information and, upon request by VHIR, all such information obtained from VHIR and all copies thereof made by Recipient will be destroyed or returned to VHIR within fifteen (15) days.

9. MISCELLANEOUS

9.1. Any formal notice required or permitted by this Agreement must be delivered in writing and sent by certified mail, return receipt requested, addressed to the other Party at the address shown at the beginning of this Agreement or at such other address for which such Party gives notice hereunder.

9.2. Should any part, article, paragraph, sentence or clause of this Agreement be deemed vague, valid or inapplicable, such part shall be eliminated and the rest of the Agreement shall remain valid and in force.

9.3. The Agreement may not be changed, modified, or discharged, in whole or in part, except by a subsequent agreement in writing signed by authorized representatives of VHIR and Recipient.

9.4. This Agreement shall be construed according to the laws of Spain, except its provision on conflicts of law. Any dispute arising from the interpretation and/or implementation of this Agreement, which cannot be settled amicably, shall be brought before a competent court of the city of Barcelona.

IN WITNESS WHEREOF, the Parties have caused this Agreement to be executed by their duly authorized representatives.

SIGNATURES:

For and on behalf of **FUNDACIÓ'HOSPITAL UNIVERSITARI VALL D'HEBRON INSTITUT DE RECERCA**

NAME: DR. JOAN X. COMELLA CARNICÉ
TITLE: DIRECTOR
DATE: 28 JUNE 2011
SIGNATURE:

For and on behalf of **Samsung Medison Europe B.V.**
NAME: SUNGHO KO
TITLE: CEO
DATE: 28 JUNE 2011
SIGNATURE:

Annex II Patent application [Spanish]

FORMULARI DE SOL·LICITUD DE NOVA INVENCIÓ

Nom JUAN CARLOS BELLO MUÑOZ
Correu electrònic jcbello@vhebron.net
Telèfon 646488475

Dades de la tecnologia

1. Títol Volume Perfusion Index (VPI)

2. Inventors

Qui s'ha de considerar inventor: La qüestió a respondre és qui ha concebut la invenció. Si una persona no contribueix a la concepció de la invenció, no es inventor. Respecte a definir la inventoria, la reducció a la practica *per se* es irrellevant, així como la mera suggestió de la idea a aconseguir (la persona que suggereix una idea d'un resultat a aconseguir, en lloc dels medis per a aconseguir-lo, tampoc és inventor). S'ha de tenir en compte que no és essencial per a un inventor haver estat implicat personalment en les etapes del procés d'obtenció de la invenció, sempre que la implementació d'aquestes etapes no requereixi una activitat inventiva. Sota el mateix principi, no es pot considerar inventor la persona implicada en les etapes d'obtenció de la invenció on aquestes etapes no requereixin activitat inventiva per part d'aquesta persona.

Cal indicar a continuació el nom complert i el percentatge de participació de la invenció.

Nom i cognoms	Relació laboral	Entitat	Percentatge
JUAN CARLOS BELLO MUÑOZ	Contracte mercantil	HOSPITAL VALL D'HEBRON	50%
MAURICIO AYALA SANCHEZ	Estudiante de doctorado	Universitat de Barcelona	50%

3. Descripció

Desarrollo de un modelo matemático para evaluar la perfusión tisular fetal (Cerebral, Renal y Hepática).

4. Aplicacions de la invenció

En Medicina Fetal podría emplearse para mejorar la calidad de la evaluación hemodinámica en fetos con sospecha de insuficiencia placentaria

5. Model assistencial en el que incideix la invenció

Incide en el cuidado prenatal de alto riesgo

6. Millores i avantatges de la tecnologia sobre el model assistencial actual

1. El modelo asistencial actual se basa en el uso de Doppler pulsado para calcular indices que INDIRECTAMENTE miden la resistencia periférica al flujo (Anexo 1)

2. Las limitaciones del modelo actual consisten en su baja sensibilidad para detectar alteraciones en la perfusión de órganos. (Por ejemplo la oliguria fetal se instaura sin que se alteren estos índices en la circulación renal) (Anexo 2)

3. Se ha intentado medir flujo y perfusión con power Doppler 3D sin exito (Anexo 3)

4 Se han planteado modelos teóricos previos sin comprobación experimental hasta el momento (Anexo 4). El modelo propuesto permitirá aumentar la precisión de las determinaciones hemodinámicas fetales y potencialmente podría aumentar la calidad del seguimiento

7. Productes/processos competidors o alternatius

El Doppler color y Doppler pulsado y

Los índices de power Doppler tridimensional: cuyas limitaciones ya hemos discutido

8. Tipus d'usuaris de la tecnologia

Los usuarios potenciales serían los especialistas en Medicina Materno Fetal del mundo. También serían la población diana de cara a la difusión de resultados.

9. Tipus empreses potencials de la tecnologia (empreses diana, tipus de possibles llicenciataris)

Se han adelantado conversaciones preliminares con Samsung Corporation, propietarios de la marca de ecógrafos Medison

10. S'ha fet divulgació?

Mitjà de divulgació

Data divulgació

Se ha hecho divulgación de los procesos previos a esta solución (algunos también desarrollados por nosotros) en un capítulo del libro ***Ultrasonography*** (Anexo 5)

Se ha hecho divulgación de las etapas previas hasta el primer modelo animal (gasto cardiaco) en el Congreso Mundial de Ultrasonido en Obstetricia y Ginecología. (Anexo6)

11. Està prevista una pròxima divulgació?
Mitjà de divulgació
Data divulgació
No está prevista
SIN EMBARGO la tesis doctoral de JCBM menciona los procesos previos para llegar a esta solución (mencionados superficialmente en el capítulo del libro)

Finançament / Acords

1. Fons de finançament
Esta investigación se ha financiado con fondos propios de la unidad de Medicina Fetal, provenientes de cursos y demás actividades educativas.

2. Material adquirit?
Ampliar
No, los equipos empleados para la investigación se adquirieron para uso clínico

Estat

1. Estat de la invenció
La fórmula se ha ensayado en un modelo animal preliminar que permitía calcular el gasto cardiaco combinado (que es la medición de flujo mas gruesa que se puede intentar en el feto) y que demostró que el cálculo del flujo se puede inferir con certeza razonable.
El paso siguiente se resume en el anexo preparado por MAS (Anexo 7)

2. Hi ha plans de millora?
Ampliar
Se están iniciando estudios de validación clínica con fetos sanos de cara a establecer valores de normalidad, rangos de referencia y estadísticos necesarios para desarrollar su empleo en la práctica clínica.
Se inciará este año un estudio de evaluación de la perfusión cerebral en fetos con anomalías cardiacas congénitas.

3. Hi ha hagut mostres d'interès?
Ampliar
La mencionada empresa SAMSUNG –Medison ha suscrito un acuerdo de confidencialidad con el IR Vall d'Hebron de cara a compartir información para el desarrollo de la herramienta a nivel de la industría electromédica.

Annex 3 Matlab ® Code Line for generating the fitted value and the function for calculating the VPI

```
function [X,resnorm,residual,exitflag,output,lambda] =
lsqlin(C,d,A,b,Aeq,beq,lb,ub,X0,options,varargin)
%LSQLIN Constrained linear least squares.
%   X = LSQLIN(C,d,A,b) attempts to solve the least-squares
problem
%
%           min  0.5*(NORM(C*x-d)).^2       subject to    A*x <= b
%            x
%
%   where C is m-by-n.
%
%   X = LSQLIN(C,d,A,b,Aeq,beq) solves the least-squares
%   (with equality constraints) problem:
%
%           min  0.5*(NORM(C*x-d)).^2    subject to
%            x                               A*x <= b and Aeq*x =
beq
%
%   X = LSQLIN(C,d,A,b,Aeq,beq,LB,UB) defines a set of lower and
upper
%   bounds on the design variables, X, so that the solution
%   is in the range LB <= X <= UB. Use empty matrices for
%   LB and UB if no bounds exist. Set LB(i) = -Inf if X(i) is
unbounded
%   below; set UB(i) = Inf if X(i) is unbounded above.
%
%   X = LSQLIN(C,d,A,b,Aeq,beq,LB,UB,X0) sets the starting point
to X0.
%
%   X = LSQLIN(C,d,A,b,Aeq,beq,LB,UB,X0,OPTIONS) minimizes with
the default
%   optimization parameters replaced by values in the structure
OPTIONS, an
%   argument created with the OPTIMSET function. See OPTIMSET for
details.
%   Used options are Display, Diagnostics, TolFun, LargeScale,
MaxIter,
%   JacobMult, PrecondBandWidth, TypicalX, TolPCG, and MaxPCGIter.
%   Currently, only 'final' and 'off' are valid values for the
parameter
%   Display ('iter' is not available).
%
```

```
%   X = LSQLIN(PROBLEM) solves the least squares problem defined
in
%   PROBLEM. PROBLEM is a structure with the matrix 'C' in
PROBLEM.C, the
%   vector 'd' in PROBLEM.d, the linear inequality constraints in
%   PROBLEM.Aineq and PROBLEM.bineq, the linear equality
constraints in
%   PROBLEM.Aeq and PROBLEM.beq, the lower bounds in PROBLEM.lb,
the upper
%   bounds in PROBLEM.ub, the start point in PROBLEM.x0, the
options
%   structure in PROBLEM.options, and solver name 'lsqlin' in
%   PROBLEM.solver. Use this syntax to solve at the command line a
problem
%   exported from OPTIMTOOL. The structure PROBLEM must have all
the
%   fields.
%
%   [X,RESNORM] = LSQLIN(C,d,A,b) returns the value of the squared
2-norm
%   of the residual: norm(C*X-d)^2.
%
%   [X,RESNORM,RESIDUAL] = LSQLIN(C,d,A,b) returns the residual:
C*X-d.
%
%   [X,RESNORM,RESIDUAL,EXITFLAG] = LSQLIN(C,d,A,b) returns an
EXITFLAG
%   that describes the exit condition of LSQLIN. Possible values
of
%   EXITFLAG and the corresponding exit conditions are
%
%     1  LSQLIN converged to a solution X.
%     3  Change in the residual smaller that the specified
tolerance.
%     0  Maximum number of iterations exceeded.
%    -2  Problem is infeasible.
%    -4  Ill-conditioning prevents further optimization.
%    -7  Magnitude of search direction became too small; no
further
%         progress can be made. The problem is ill-posed or badly
%         conditioned.
%
%   [X,RESNORM,RESIDUAL,EXITFLAG,OUTPUT] = LSQLIN(C,d,A,b) returns
a
%   structure OUTPUT with the number of iterations taken in
%   OUTPUT.iterations, the type of algorithm used in
OUTPUT.algorithm, the
%   number of conjugate gradient iterations (if used) in
OUTPUT.cgiterations,
%   a measure of first order optimality (large-scale algorithm
only) in
%   OUTPUT.firstorderopt, and the exit message in OUTPUT.message.
%
```

```
%   [X,RESNORM,RESIDUAL,EXITFLAG,OUTPUT,LAMBDA] = LSQLIN(C,d,A,b)
returns
%   the set of Lagrangian multipliers LAMBDA, at the solution:
%   LAMBDA.ineqlin for the linear inequalities C, LAMBDA.eqlin for
the
%   linear equalities Ceq, LAMBDA.lower for LB, and LAMBDA.upper
for UB.
%
%   See also QUADPROG.

%   Copyright 1990-2011 The MathWorks, Inc.
%   $Revision: 1.1.6.3 $  $Date: 2011/05/09 01:16:16 $

defaultopt = struct( ...
    'Diagnostics','off', ...
    'Display','final', ...
    'JacobMult',[], ...
    'LargeScale','on', ...
    'MaxIter',200, ...
    'MaxPCGIter','max(1,floor(numberOfVariables/2))', ...
    'PrecondBandWidth',0, ...
    'TolFun',100*eps, ...
    'TolPCG',0.1, ...
    'TypicalX','ones(numberOfVariables,1)' ...
);


% If just 'defaults' passed in, return the default options in X
if nargin==1 && nargout <= 1 && isequal(C,'defaults')
   X = defaultopt;
   return
end

% Handle missing arguments
if nargin < 10
    options = [];
    if nargin < 9
        X0 = [];
        if nargin < 8
            ub = [];
            if nargin < 7
                lb = [];
                if nargin < 6
                    beq = [];
                    if nargin < 5
                        Aeq = [];
                        if nargin < 4
                            b = [];
                            if nargin < 3
                                A = [];
                            end
                        end
                    end
```

```
                end
            end
        end
    end
end

% Detect problem structure input
if nargin == 1
    if isa(C,'struct')
        [C,d,A,b,Aeq,beq,lb,ub,X0,options] =
separateOptimStruct(C);
    else % Single input and non-structure.
        error(message('optimlib:lsqlin:InputArg'));
    end
end

if nargin == 0
  error(message('optimlib:lsqlin:NotEnoughInputs'))
end

% Check for non-double inputs
% SUPERIORFLOAT errors when superior input is neither single nor
double;
% We use try-catch to override SUPERIORFLOAT's error message when
input
% data type is integer.
try
    dataType = superiorfloat(C,d,A,b,Aeq,beq,lb,ub,X0);
catch ME
    if strcmp(ME.identifier,'MATLAB:datatypes:superiorfloat')
        dataType = 'notDouble';
    end
end

if ~strcmp(dataType,'double')
    error(message('optimlib:lsqlin:NonDoubleInput'))
end

% Set up constant strings
medium =  'medium-scale: active-set';
large = 'large-scale: trust-region reflective Newton';
unconstrained = 'slash';
output.iterations = []; % initialize so that it will be the first
field

% Options setup
largescale =
strcmpi(optimget(options,'LargeScale',defaultopt,'fast'),'on');
diagnostics =
strcmpi(optimget(options,'Diagnostics',defaultopt,'fast'),'on');
mtxmpy = optimget(options,'JacobMult',defaultopt,'fast');
% Check if name clash
```

```
functionNameClashCheck('JacobMult',mtxmpy,'atamult','optimlib:lsql
in:JacobMultNameClash');

% Use internal Jacobian-multiply function if user does not provide
JacobMult function
if isempty(mtxmpy)
    mtxmpy = @atamult;
end

switch optimget(options,'Display',defaultopt,'fast')
case {'off','none'}
   verbosity = 0;
case {'iter','iter-detailed'}
   verbosity = 2;
case {'final','final-detailed'}
   verbosity = 1;
otherwise
   verbosity = 1;
end

% Set the constraints up: defaults and check size
[nineqcstr,numberOfVariables]=size(A);
neqcstr = size(Aeq,1);
ncstr = nineqcstr + neqcstr;

if isempty(C) || isempty(d)
   error(message('optimlib:lsqlin:FirstTwoArgsEmpty'))
else
   numberOfVariables = max([size(C,2),numberOfVariables]); % In
case C is empty
end

[rows,cols]=size(C);
if length(d) ~= rows
   error(message('optimlib:lsqlin:InvalidCAndD'))
end

if length(b) ~= size(A,1)
   error(message('optimlib:lsqlin:InvalidAAndB'))
end

if length(beq) ~= size(Aeq,1)
   error(message('optimlib:lsqlin:InvalidAeqAndBeq'))
end

if ( ~isempty(A)) && (size(A,2) ~= cols)
    error(message('optimlib:lsqlin:CAndA'))
end

if ( ~isempty(Aeq)) && (size(Aeq,2) ~= cols)
    error(message('optimlib:lsqlin:CAndAeq'))
end
```

```
if isempty(X0)
    % This zero-valued X0 will potentially be changed in sllsbox
or qpsub.
    % (This potentially temporary zero-valued x0 needed here for
backwards
    % compatibility because it's returned in output x if early
termination
    % occurs when bounds are inconsistent.)
    X0 = zeros(numberOfVariables,1);
    params.emptyInitialPoint = true;  % parameter passed to
sllsbox
else
    params.emptyInitialPoint = false; % parameter passed to
sllsbox
end
if isempty(A)
    A = zeros(0,numberOfVariables);
end
if isempty(b)
    b = zeros(0,1);
end
if isempty(Aeq)
    Aeq = zeros(0,numberOfVariables);
end
if isempty(beq)
    beq = zeros(0,1);
end

% Set d, b and X to be column vectors
d = d(:);
b = b(:);
beq = beq(:);
X0 = X0(:);

[X0,lb,ub,msg] = checkbounds(X0,lb,ub,numberOfVariables);
if ~isempty(msg)
   exitflag = -2;
   [resnorm,residual,lambda]=deal([]);
   output.iterations = 0;
   output.algorithm = ''; % not known at this stage
   output.firstorderopt=[];
   output.cgiterations =[];
   output.message = msg;
   X=X0;
   if verbosity > 0
      disp(msg)
   end
   return
end

% Test if C is all zeros or empty
if norm(C,'inf')==0 || isempty(C)
```

```
   C=0;
end

caller = 'lsqlin';

% Test for constraints
if isempty([Aeq;A]) && isempty([beq;b]) && all(isinf([lb;ub]))
    output.algorithm = unconstrained;
    % If interior-point chosen and no A,Aeq and C isn't short and
fat, then call sllsbox
elseif largescale && (isempty([A;Aeq])) && (rows >= cols)
    output.algorithm = large;
else
    if largescale
        if (rows < cols)
            warning(message('optimlib:lsqlin:MoreColsThanRows'))
        else % ~isempty([A;Aeq]))
            warning(message('optimlib:lsqlin:LinConstraints'))
        end
    end
    output.algorithm = medium;
end


if diagnostics
   % Do diagnostics on information so far
   gradflag = []; hessflag = []; constflag = false; gradconstflag
= false;
   non_eq=0;non_ineq=0; lin_eq=size(Aeq,1); lin_ineq=size(A,1);
   XOUT=ones(numberOfVariables,1); funfcn{1} = []; confcn{1}=[];
   msg =
diagnose('lsqlin',output,gradflag,hessflag,constflag,gradconstflag
,...
      XOUT,non_eq,non_ineq,lin_eq,lin_ineq,lb,ub,funfcn,confcn);
end


switch output.algorithm;
case 'slash'
   % Disable the warnings about conditioning for singular and
   % nearly singular matrices
   warningstate1 = warning('off', 'MATLAB:nearlySingularMatrix');
   warningstate2 = warning('off', 'MATLAB:singularMatrix');
   X = C\d;
   % Restore the warning states to their original settings
   warning(warningstate1)
   warning(warningstate2)
   residual = C*X-d;
   resnorm = sum(residual.*residual);
   exitflag = 1;
   lambda.lower = [];
   lambda.upper = [];
   lambda.ineqlin = [];
```

```
   lambda.eqlin = [];
   output.iterations = 0;
   output.algorithm = unconstrained;
   output.firstorderopt=[];
   output.cgiterations =[];
   output.message = '';
case 'large-scale: trust-region reflective Newton';
   params.verb = verbosity; % pack parameters together into struct

[X,resnorm,residual,firstorderopt,iterations,cgiterations,exitflag
,lambda,msg]=...

sllsbox(C,d,lb,ub,X0,params,options,defaultopt,mtxmpy,varargin{:})
;
   output.iterations = iterations;
   output.algorithm = large;
   output.firstorderopt = firstorderopt;
   output.cgiterations = cgiterations;
   output.message = msg;
case 'medium-scale: active-set'
   if largescale && ( issparse(A) || issparse(C) || issparse(Aeq)
)% asked for sparse
      warning(message('optimlib:lsqlin:ConvertToFull'))
   end

   % Create options structure for qpsub
   lsqlinoptions.MaxIter =
optimget(options,'MaxIter',defaultopt,'fast');
   % A fixed constraint tolerance (eps) is used for constraint
   % satisfaction; no need to specify any value
   lsqlinoptions.TolCon = [];

   [X,lambdaqp,exitflag,output,dum1,dum2,msg]= ...

qpsub(full(C),d,[full(Aeq);full(A)],[beq;b],lb,ub,X0,neqcstr,verbo
sity,caller,ncstr,numberOfVariables,lsqlinoptions);
   output.algorithm = medium; % qpsub overwrites output with
output.iterations
   residual = C*X-d;
   resnorm = sum(residual.*residual);
end

if isequal(output.algorithm , medium)
   llb = length(lb);
   lub = length(ub);
   lambda.lower = zeros(llb,1);
   lambda.upper = zeros(lub,1);
   arglb = ~isinf(lb); lenarglb = nnz(arglb);
   argub = ~isinf(ub); lenargub = nnz(argub);
   lambda.eqlin = lambdaqp(1:neqcstr,1);
   lambda.ineqlin = lambdaqp(neqcstr+1:neqcstr+nineqcstr,1);
   lambda.lower(arglb) =
lambdaqp(neqcstr+nineqcstr+1:neqcstr+nineqcstr+lenarglb);
```

```
   lambda.upper(argub) =
lambdaqp(neqcstr+nineqcstr+lenarglb+1:neqcstr+nineqcstr+lenarglb+l
enargub);
   output.firstorderopt=[];
   output.cgiterations =[];
   output.message = msg;

   if exitflag == 1 % qpsub terminated successfully
     normalTerminationMsg = sprintf('Optimization terminated.');
     if verbosity > 0
       disp(normalTerminationMsg)
     end
     if isempty(msg)
       output.message = normalTerminationMsg;
     else
       % append normal termination msg to current output msg
       output.message =
sprintf('%s\n%s',msg,normalTerminationMsg);
     end
   else
     output.message = msg;
   end
end
```

Annex 4 Abstract of a preliminary report on the current work as accepted to the XX World Congress of the International Society of Ultrasound In Obstetrics and Gynecology (and nominee for the Alfred Kratochwil medal) Volume 36, Issue S1, October 2010, Page: 46

OC26: CARDIAC FUNCTION IN SPECIFIC CONDITIONS

OC26.01
Fetal cardiac output: measurement by four dimensional power Doppler and artificial neural networks. Results from a sheep model

J. Bello-Muñoz[1,2], J. Peiró[3], P. Oliveros Orozco[1,2], F. Soldado[1], E. Carreras Moratonas[1], L. Cabero[1]

[1]Fetal Medicine, Hospital Vall d'Hebron, Barcelona, Spain; [2]Obstetricia i Ginecologia, Universidad Autónoma de Barcelona, Bellaterra, Spain; [3]Pediatric Surgery, Hospital Vall d'Hebron, Barcelona, Spain

Objectives: Non invasive measurement of fetal vascular flow remains an elusive matter, accuracy of current tools is very limited and relies mainly in operator skills. The aim of our study was to develop a tool for indirect flow measurement, accurate and repeatable, by using power Doppler signal, Real time three dimensional ultrasound (4DPD) and mathematical image data simulation and adjustment tools based on artificial neural networks (ANN).

Methods: Six pregnant sheep with adequately controlled gestational age of 125 days (near term) were surgically instrumented to access fetal ascending aorta by transventricular catheterization. Cardiac output was measured by Fick thermodilution, as well as by pulsed Doppler. Several sets of 4DPD volumes were taken during the procedure. Measurements were stored in an electronic datasheet. Pearson's correlation coefficient and simple linear regression were obtained. Linear equation matrix were generated and obtained data was evaluated through an error adjustment process by employing an artificial neural network software (ANN).

Results: A total of 30 sets of measurements in controlled conditions were collected during the study period. A mean of six measurements by cardiac cycle were digitally obtained from the velocity curve. A six by six matrix of data was designed for every measurement. Mean velocity at every time was calculated and compared to actual data, intraclass correlation coefficient (95% CI) was 0.9 (0.73–0.99). ANN predicted calculated measurements in 99% of cases.

Conclusions: 4DPD might be a reliable, accurate, non invasive tool for fetal vascular flow measurement.

Annex 5

Protocol for volume taking as it is already implemented in our Fetal Medicine Unit

Vall d'Hebron
Hospital Materno-infantil

UAB
Universitat Autònoma de Barcelona

Corazón STIC Color

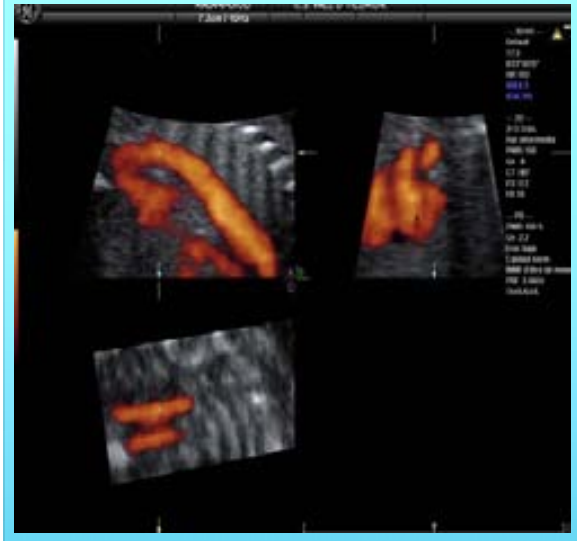

- **Ajustes del 2D**
  - Ajustes de imagen:
  - Ángulo 30º-FPR 30
  - Ganancia muy baja (-6).
  - Contraste (rango dinámico) 5.
  - NO SRI 5/ CRI 2
- **Ajustes del 3D**
  - Calidad Máxima
  - Volumen (ángulo):
    - 20-24 sem : 40º
    - 24-28 sem : 50º
    - 28-32 sem : 60º
  - Dorso posterior o lateral derecho (feto cefálico) o izquierdo (podálico)
- **Ajustes del 4D**
  - Tiempo de toma
    - 20-24 sem : 7,5"
    - 24-28 sem : 10"
    - 28-32 sem : 12"
  - No sirven volúmenes parciales
  - No sirven otros planos de toma
  - No sirven volúmenes con movimiento